Optimizing Shoreface Nourishment Design using the concept of Equilibrium Beach Profiles

A Case Study At Nags Head

R. (Ruben) Visser

Cover image: An aerial view toward the northeast over the Outer Banks from Cape Lookout toward Ocracoke. (Photo by Richard H. Verdier, 2017)

Optimizing Shoreface Nourishment Design using the concept of Equilibrium Beach Profiles

A Case Study At Nags Head

by

R. Visser

in partial fulfilment of the requirements for the degree of

Master of Science
in Civil Engineering

to be defended publicly on Thursday 10 July 2018 at 14.00

Graduation Committee

Prof. dr. ir. S.G.J. Aarninkhof	TU Delft, supervisor
Dr. ir. A.J.H.M. Reniers	TU Delft
Dr. ir. M.A. de Schipper	TU Delft
Dr. ir. D.J.R. Walstra	Deltares, TU Delft
T.W. Kana, PhD	Coastal Science and Engineering

High Value Services
Sustainable Solutions
CSE
COASTAL SCIENCE & ENGINEERING

TU Delft
Delft University of Technology

The river is within us, the sea is all about us;
The sea is the land's edge also, the granite
Into which it reaches, the beaches where it tosses
Its hints of earlier and other creation

T. S. Eliot

Preface

This thesis concludes the final step of my Master of Science program in Hydraulic Engineering at Delft University of Technology, the Netherlands. Over the course of the past months, I've greatly expanded my skillset and learned a great deal about academic research. Many people have contributed to this thesis. I would like to take the opportunity to thank them:

During the period of March '17 - March '18, I was lucky enough to be part of an exceptional coastal engineering firm. The team at CSE made sure that this graduation process was everything except the usual. By offering and encouraging the possibilities to do my own field work and actively include me in the world of academic research, I've really been able to strengthen my passion for this field. Many thanks to everybody at CSE who helped me get involved for these opportunities. Special thanks to my daily supervisor Tim, who didn't just helped me at my day-to-day tasks at the job, but who also helped me making South Carolina my second home. I'll definitely stop by in the near future.

I would like to thank all my supervisors for guidance during this thesis process. I very much appreciate the efforts to remain in close contact, to ensure that everything stays on tracks. Finally, many thanks to all my fellow student for the help during the entire study.

R. Visser
Columbia, SC, USA
March 2018

Summary

Introduction and Problem Description: The autonomous nearshore morphodynamics along the Nags Head shoreline are characterized by consistent erosional behavior. The use of shoreface nourishments to counteract this erosion along shorelines has received considerable attention in the past, having the advantage of reduced cost compared to beach nourishments. Although shoreface nourishments are thus an increasingly interesting option for coastal managers, their design is often highly empirical and based on guidelines. A better understanding of the way a shoreface nourishment interacts with the antecedent bathymetry and respective forcing agents (i.e. - waves and tides) may help to reduce the degree of empiricism and possibly optimizing nourishment design in terms of longevity and shoreline sedimentation. Rather than using design guidelines, the present research aims to relate nourishment design to beach profile shaping parameters like wave climate and sediment characteristics.
Representation of beach profiles based on local wave dissipation, wave reflection and sediment characteristics have previously been studied in the form of equilibrium beach profiles (EBP). Recently major improvement in beach profile representations are made by including wave reflection in the energy balance, resulting in a two-sectioned EBP. After local site-specific parameter calibration, the vertical deviation between the initial profile and analogous calibrated EBP ($z_{ebp} - z_{ini}$) should indicate where a scarcity of sediment along the cross-shore profile is. Shoreface nourishments are then designed by filling in the vertical gaps between these two profiles. A hypothesis was postulated stating that the optimal form for a shoreface nourishment follows the equilibrium beach profile the best. The differences in impact conventional nourishment designs (based on guidelines) have on either cross-shore and longshore transport rates are computed and compared to an EBP-based design in two separate modeling studies.

Effects on cross-shore transport: Beach profile morphology and the response to shoreface nourishments are modeled in the 1D cross-shore profile model UNIBEST-TC. Three distinct conventional designs which have found recent applications are selected and based on either; extension of the outer bar, creating a new outer bar or filling in the trough shoreward of the outer bar. Analysis of the model results show that all four nourishment designs are incorporated well in the cross-shore morphodynamics as compared to the situation prior to construction. The EBP-design shows strongest reduction of offshore directed transport, followed by designs based on filling in the trough, creating a new outer bar or extending the existing outer bar. Therefore the model simulations suggest that a nourishment design with the largest vertical deviations from the EBP may be the least effective to counteract coastal erosion. This partially confirms the postulated hypothesis that cross-shore transport rates are lowered most efficient while using the concept of EBP to design shoreface nourishments.

Effects on longshore transport: The coastal area flow model Delft3D was utilized for a series of numerical modeling simulations to examine the potential dependencies between nourishment design and post-dredging longshore transport rates and local gradients. Model results show a similar outcome as the cross-shore profile model, where the EBP-design results in the lowest longshore transport rates. Closer examination of the simulations, especially concerning the local gradients and longshore transport rates, show that the EBP-design reduces longshore gradients by a factor two up to four compared to conventional nourishment designs. The EBP-design therefore shows less sediment transport and local gradients because of a divergence of non-linear local sediment transport rates over the coastal zone. Confirming earlier studies that local longshore gradients

dominate coastal change at the scale of nourishments and the hypothesis that shoreface nourishment design based on the concept of EBP is a more efficient way compared to conventional designs.

Practical applications: The results and theory demonstrate how the incoming wave climate and sediment characteristics are responsible for both the EBP shape and sediment transport. Since the erosion rates at the project site show local longshore variability, and the EBP shape remains constant even though using the same characteristics, the deviation between the initial- and EBP profile should indicate a gradient in longshore transport rates as well. Knowing this, the overall longshore gradient can be estimated using only one survey dataset. This could lead to a preliminary nourishment design, based on only one bathymetry survey and project budget. Approximation of longshore transport gradients could strongly improve the nourishment lifetime, especially in remote locations.
The constant longshore shape of the EBP with respect to MSL is furthermore efficient in reducing the local longshore transport gradients. Since the EBP-model is used as a template to fill in the vertical deviations between the initial profile and EBP, the longshore variabilities are spread out over the project site creating a less obstructive flow, thereby reducing longshore transport rates as well. Whereas conventional nourishment designs follow the original longshore variabilities and only enhance them, resulting in strong 3D bathymetrical features corresponding to coastal erosion as well.

Nomenclature

Acronyms

CSE	- Coastal Science and Engineering
DOC	- Depth of Closure
EBP	- Equilibrium Beach Profile
FEMA	- Federal Emergency Management Agency
FRF	- Field Research Facility
GLM	- Generalized Lagrangian Mean
MHW	- Mean Higher High Water
MLLW	- Mean Lower Low Water
MorFac	- Morphological acceleration Factor
MSL	- Mean Sea Level
NAVD-88	- North American Vertical Datum of 1988
NDBC	- National Data Buoy Center
NOAA	- National Oceanic and Atmospheric Administration
SWAN	- Simulating WAves Nearshore
WIS	- Wave Information Studies
UNIBEST-TC	- UNIform Beach Sediment Transport Time dependent Cross-shore
USACE	- United States Army Corps of Engineers

Terminology

Some sources in this study use the U.S. imperial units while others the customary metric system. Even though the consistency of this study is endeavored throughout the report, provision of the U.S. imperial units is sometimes inevitable. Therefore conversion between different units is as follows:

1 mile	=	1609.3 meter
1 feet	=	0.3048 meter
1 inch	=	0.0254 meter

The vertical datum used throughout the report is 'NAVD-88' (North American Vertical Datum of 1988). It is sometimes inevitable, due to the source, to denote water levels with respect to MLLW or MSL. All depth and bathymetry files therefore have an offset with respect to MSL. For further applicability of the data, the relation between MSL and NAVD-88 is:

Mean Higher High Water (MHHW)	NAVD-88 +0.264 m
Mean Sea Level (MSL)	NAVD-88 +0.108 m
Mean Lower-Low Water (MLLW)	NAVD-88 -0.074 m

List of Symbols

Symbol	Unit	Description
a	m	bed-load layer thickness
c	kgm^{-3}	sediment concentration averaged over space and time at height z above the seabed
c_a	kgm^{-3}	reference sediment concentration at height a
$\tilde{c}$	kgm^{-3}	oscillating concentration component, including turbulence
c_f	-	friction coefficient
d_{50}	m	geometric mean sediment diameter; grain size diameter such that 50% of the grains by mass are smaller than $d = d_{50}$
d_{90}	m	grain size diameter such that 90% of the grains by mass are smaller than $d = d_{90}$
D^*	Wm^{-2}	wave energy dissipation rate corresponding to a stable cross-shore profile with a net cross-shore transport rate of zero
D_*	-	non-dimensional sediment grain size
D_b	Wm^{-2}	incident wave energy per unit volume turbulence dissipation
D_f	Wm^{-2}	dissipation by bottom friction per unit area
D_V	m^2/s	vertical eddy diffusivity
D_H	m^2/s	horizontal eddy diffusivity
dx	m	distance increment
dx	m	distance increment
F_I	Wm^{-2}	onshore directed indicent energy flux
F_R	Wm^{-2}	offshore directed reflection energy flux
F_T	Wm^{-2}	total energy flux
f_{BED}	-	user-defined calibration factor
f'_{cw}	-	weighted friction factor, accounting both current and wave friction
f_{SUS}	-	user-defined calibration factor
f_{SUSW}	-	user-defined calibration factor
g	ms^{-2}	gravity acceleration
H_{rms}	m	root mean square wave height
H_s	m	significant wave height
H_{sa}	m	corresponding wave height reaching the depth h_a
h	m	local water depth
h_a	m	maximum profile depth in which the shallow-water assumptions can be satisfied
K	-	empirical calibration parameter
k_{as}	m/s	phase lag coefficient, resulting from a delay of sediment response to orbital velocities
k'	$-$	shoaling profile reflection coefficient
k	$\circ/m$	wave number, in which $\frac{2\pi}{L} = \frac{360^\circ}{L}$
L	m	tidal wave length
L_T	kgm^{-3}	suspended sediment load
M	-	sediment mobility number driven by currents and waves
M_e	-	excess sediment mobility number
n	-	empirical calibration parameter
p	-	porosity
q	m^3s^{-1}	cross-shore sediment transport

Symbol	Unit	Description
q_b	m^3/ms	bed-load transport rate in volume per unit width and time including pores
$q_{s,c}$	m^3/ms	suspended sediment transport met unit width and time, including pores
$\bar{q}_s$	kgm^{-3}	suspended transport rate averaged over space and time
s	-	relative density, $s = \frac{\rho_s}{\rho_w}$
T	-	dimensionless bed shear stress parameter
T_p	s	wave period
$\bar{u}$	m/s	depth-averaged velocity
u_b	m/s	time dependent, intra wave, near bottom horizontal velocity vector of the combined wave-current motion
u_{off}	m/s	near-bed peak orbital velocity, offshore directed
u_{on}	m/s	near-bed peak orbital velocity, onshore directed
v	m/s	Fluid velocity averaged over space and time at height z above the seabed
v_{eff}	m/s	effective velocity due to currents and waves
v_{cr}	m/s	critical velocity
$\tilde{v}$	m/s	oscillating velocity component, including turbulence
w	m/s	sediment fall velocity
$w_{s,m}s$	m/s	fall velocity of the suspended sediment in a fluid sediment mixture
x	m	horizontal cross-shore coordinate
x_o	m	distance between the virtual origin of the shoaling profile and the beginning of the surf profile
x_r	m	distance between the mean sea level and the discontinuity point
z	m	height above the bed
z_a	m	reference height
$z_{b,c}$	m	computed bed level
$z_{b,m}$	m	measured bed level
$z_{b,o}$	m	observed bed level
α	-	wave dissipation calibration coefficient
β	-	wave breaker slope calibration parameter in roller model
Δ	-	relative density, $\Delta = (\rho_s - \rho_w)/\rho_w$
ϵ	Wm^{-2}	energy dissipation
ϵ_b	Wm^{-2}	wave breaking induced turbulence dissipation
$\epsilon_{s,cw}$	m^2/s	sediment mixing coefficient for combined action of waves and current
η	m	free surface elevation above the reference plane (at $z = 0$)
γ	-	wave breaker calibration parameter
$\hat{\eta}$	m	amplitude of the surface elevation
Ω	-	dimensionless fall velocity
ω	$\circ/hr$	angular velocity or frequency, $\omega = \frac{360\circ}{T(hour)}$
Φ_{bd}	-	non-dimensional bed-load transport vector
ϕ	-	damping factor dependent on the concentration
ρ_s	kg/m^{-3}	sediment density
ρ_w	kg/m^{-3}	water density
$\tau_{b,cr}$	Nm^{-2}	time averaged critical bed shear stress, according to Shields
$\tau_{b,cw}$	Nm^{-2}	time averaged effective bed shear stress
Θ'	-	dimensionless effective shear stress
Θ'_{cr}	-	dimensionless critical shear stress

Contents

1

Introduction

Coastal areas around the globe host about two-thirds of the world population. Besides their economic and social value, coastal areas are also extremely valuable from an ecological point of view. Nevertheless, those areas are also extremely vulnerable. Coastal erosion and associated loss of land is the most evident sign of this vulnerability.

Adequate solutions counteracting coastal erosion require knowledge of the underlying morphodynamics and ecological processes. The Dutch experience shows that an effective and sustainable way to deal with coastal erosion is to work with nature. In case of sandy coasts, the most appropriate material for restoring, raising or building out sandy coasts is sand. Sand nourishments have lately become a common practice around the world. Nourishment can be divided into backshore nourishment, beach nourishment and shoreface nourishment, in which the latter is the supply of sand to the outer offshore part of the coastal profile. An inventory and comparison of different nourishment practices around Europe is given for example in Hanson et al. (2002)

Of these types of nourishments, shoreface nourishments have the advantage of reduced cost: natural forces are assumed to redistribute the sediment shoreward, therefore there is no need to scrape the beach. The use of the beach is also not hindered while the nourishment is placed and there is no need to distribute sediment (generally mined offshore) directly on land. Any reduction in costs is desirable as shoreface nourishments, like all shore nourishments, are expensive and in general are an ongoing commitment, incurring monitoring expenses as well as those of repeated nourishment.

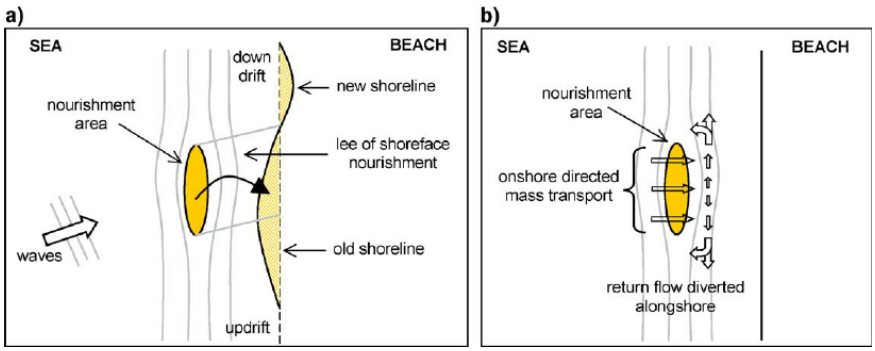

Figure 1.1: Top view of expected effects to occur after nourishing the shoreface to mitigate coastal erosion. *a:* Reduction of longshore transport rates by offshore wave breaking (Lee effect). *b:* Increase of onshore directed transport after offshore wave breaking (Feeder effect). [after Van Duin et al. (2004)]

Shoreface Nourishments Shoreface nourishments (also known as feeder berms) are used in regions of rather wide and high dunes (relatively safe coastal regions) to maintain or increase the sand volume in the nearshore zone by natural processes (Van Rijn, 2011). Those processes can be described by an increase of net onshore transport (feeder effect) and a reduction of longshore transport behind the nourishment (lee effect), see Figure 1.1 (Ojeda et al., 2008; Van der Werf et al., 2010).

Equilibrium Beach Profiles (EBP) Another approach in shoreface nourishment designs is using the concept of equilibrium beach profiles (EBP), see Figure 1.2. The concept of an equilibrium shape of the beach profile has proven to be fruitful in a variety of applications in coastal science and engineering, such as beach nourishment design and studies concerned with morphological evolution in the nearshore. Under this concept, if the incident waves and water level remain constant, the beach profile is expected to evolve toward a stable shape for which the net cross-shore sediment transport rate across the profile approaches zero.

Dean and Dalrymple (2004) propose three avenues of research for possible development of a theory to determine the equilibrium beach profile. These are:

- Kinematic approximation: an attempt is made to predict the movements of the sand particles by describing the forces acting on them (Eagleson et al., 1963).
- Dynamic approximation: a macroscopic balance of constructive and destructive forces is considered.
- Empirical approximation: a purely descriptive approximation representing the attempt to adjust static beach profiles to the most common forms found in nature, using parameters determined by means of adjustment or dimensional adjustment techniques.

As there have been lots of studies regarding these equilibrium beach profiles, Aragonés et al. (2016) worked on a development of a new methodology to increase the accuracy of the existing equilibrium beach profile models, providing an improvement to the inputs used in such models and in the fitting of the formulae used to obtain seabed shape. This study concluded that an empirical approximation using a potential function to describe a profile shape fits best. These time invariant static profiles furthermore indicate interesting morphological phenomena when comparing the static EBP to the initial bed, a feature dynamic approximations lack. The remainder of this report will therefore focus on equilibrium beach profiles approximated using a potential function to design shoreface nourishments. Justification upon this choice and the introduction to the underlying morphological phenomena of the static EBP is presented in detail in Chapter 4 - Equilibrium Beach Profiles.

Equilibrium beach profiles have been tested in a laboratory study using SUPERTANK data (Wang and Kraus, 2005). This has shown that significant net cross-shore sediment transport and beach profile change occurred at locations where the rate of wave energy dissipation deviated substantially from the equilibrium rate. Indicating that the largest changes in beach morphology are at the location where the beach differs the most from the equilibrium beach profile.

The test was also performed using a profile without bars. This test has shown that the highest amount of wave energy dissipation was found at the location of the possible bars. Again, since these bars are currently not present, this is also the location at which the profile is furthest from equilibrium. This conclusion gives options in reshaping cross-shore beach profiles using nourishment towards a profile where the wave dissipation rates and net cross-shore transport rates will lower, and will thoroughly be explored in the following chapters.

1.1 Problem Description

Despite their wide use, the design and implementation of nourishments is often carried out based on practical experience. Guidelines for the construction of nourishments can be found in (Van der Spek et al., 2007) and (Van Rijn, 2011). These guidelines are based on the current understandings on nourishment effects. These understandings are hypotheses which are derived from the available observations and monitoring. This guideline based approach is mainly because detailed modeling of the physical processes in the shoreface and foreshore is still a complex task and the processes playing a role are either not fully understood or difficult to model. In particular, the resulting sediment transport is the result of a delicate balance between onshore and offshore transport which can result in different morphodynamic development of the profile under different conditions.

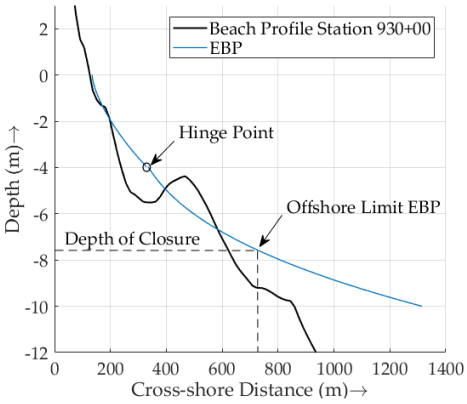

Figure 1.2: Example of an Equilibrium Beach Profile plotted over an cross-shore beach profile.

Although the interaction between shoreface nourishments and the initial surroundings are complex, recent studies lowered the degree of empiricism for designing such nourishments. Ojeda et al. (2008) concluded that apparently, cross-shore displacement of nourished sand is strongly dependent on the location of the nourishment within the active profile. A study by Grunnet and Ruessink (2005) examined a shoreface nourishment placed in the trough between the inner and outer storm bar. Results concluded that the beach tried to reshape to its original two barred cross-shore shape, directly after placing the nourishment. Therefore the gradual reappearance of the pre-nourishment bar-trough morphology is shown to return the cross-shore distribution of sediment transport rates to pre-nourishment rates, indicating an inefficient nourishment placement. However, the driving forces for this cross-shore distribution are still unclear.

Nourishment Efficiency In this thesis the optimal shoreface nourishment is defined as the design that reduces the coastal erosion for the longest time using the least amount of sediment (i.e. - morphological optimization). The time a nourishment is counteracting coastal erosion is expressed in the longevity of the nourishment and the amount of sediment in volume (m^3/m). A shoreface nourishment with the highest efficiency thus has the greatest longevity using the lowest amount of volume.

Knowledge Gap While comparing conclusions of different studies, it is shown that:

- The highest amount of sediment transport and wave energy dissipation is located at the locations where the bed elevation is the furthest from the equilibrium profile (Wang and Kraus, 2005)
- Cross-shore displacement of nourished sand depends greatly on the location of the nourishment within the active profile (Ojeda et al., 2008)
- The gradual reappearance of the pre-nourishment bar-trough morphology is shown to return the cross-shore distribution of sediment transport rates to pre-nourishment rates (Grunnet and Ruessink, 2005)

Combining these conclusions, it is hypothesized that the optimal form for a shoreface nourishment follows the equilibrium beach profile the best.

After the nourishment, the beach profile tries to reshape back to the form in which its most efficient for wave dissipation. With increased vertical deviation from the equilibrium profile due to the shoreface nourishment, the shoreface locally dissipated more wave energy than it previously had to. Wave dissipation over the beach profile remains constant, but is now more concentrated over the nourishment. Due to the increase in wave energy dissipation, more sediment is mobilized compared to the pre-nourishment profile. An increase in suspended sediment induces an increase in longshore sediment transport, thereby lowering the nourishment efficiency and longevity as more sediment gets washed away. When the shoreface nourishment follows the contours of the EBP, the wave energy dissipation is lowest as well, thereby reducing the longshore sediment transport.

1.2 Study Objective

To optimize the shoreface nourishment design and to maximize the nourishment efficiency, detailed knowledge in the morphological behavior of the beach profile with and without a shoreface nourishment needs to be obtained. The main research question is therefore:

How does a shoreface nourishment affect the beach morphological behavior and is it possible to optimize the shoreface nourishment design using the concept of an EBP?

To conclude on the abovementioned objective and the earlier proposed hypothesis, the study is divided in several research questions which are treated in the following section. The combined answer of these research questions will fill the knowledge gap in order to conclude on the study objective. A case study in the town of Nags Head, NC, USA is applied to help answering several research questions. This project site will be introduced in detail in the following chapter.

1.3 Research Questions

In order to know how a shoreface nourishment can be designed using the concept of an EBP, its first necessary to know how the forcing agents (i.e. - waves and tide) shape this EBP profile. Given a constant wave climate, the beach profile approaches the EBP. However, as the time scale of the hydrodynamic changes are smaller than the morphodynamic changes of the beach, this equilibrium is never reached (Dean, 1977). Nonetheless if the relation between the EBP shape and the wave climate is known, a possible correlation between the EBP shape and the morphological changes of the initial beach profile can be drafted. To do so, the first research question is as follows:

1. *How is the EBP shape determined and how can its concept be used for shoreface nourishment design?*

Wang and Kraus (2005) concluded that significant net cross-shore sediment transport and beach profile change occurred at locations where the rate of wave energy dissipation deviated substantially from the equilibrium rate. They also found that wave energy dissipation in a profile without bars is highest where the EBP differs the most from the profile. That's why the profile tries to reshape into a barred system due to the forcing agents. To confirm that this conclusion also holds for existing barred beach profiles, the second research question is:

2. *How do cross-shore transport rates lower while reshaping the cross-shore profile towards an EBP using nourishments compared with conventional nourishment designs?*

From Van Duin et al. (2004), it is known that shoreface nourishment will reduce coastal erosion by lowering the longshore transport rates. Furthermore, Ruggiero et al. (2009) suggest that longshore variability in sediment transport dominate coastal change at the scale of nourishments. Ideally a shoreface nourishment would not only lower the longshore transport rates but also lower its gradients. To check this the third research question is formulated as:

3. *How do longshore transports and local gradients in sediment transport lower by using the concept of EBP during nourishment design?*

Finally, accurate nourishment design is currently based to match the longshore variability in erosion rates and sediment transport. This way, the nourishment lifetime is constant along a project site, forestalling costly local renourishment. Accurate erosion rates could be acquired by comparing different survey datasets and historical aerial photography. Which could become troublesome due to scarcity of accurate field data, especially at remote sites where no accurate data is available. This problem might be solved using the concept of EBP. As the relationships between the dimensionless fall velocity, profile morphology and the calibration coefficients are integrated in the proposed EBP, its possible to compute the EBP of any morphological beach state by any given beach. This possibly makes the proposed EBP useful for predictions of the beach longshore transport gradients as a response of the forcing agents, which could be used to determine the longshore distribution of nourishment volume. The fourth and final Research Question is therefore:

4. *Is the proposed EBP useful for predictions of the overall longshore transport gradient and longshore fill density design?*

1.4 Scope

According to Van Duin et al. (2004) shoreface nourishments can either be divided in cross-shore and longshore effects. Each of these effects is treated in a different chapter with a different methodology and scope. In Research Question 2, while focusing on the cross-shore effects, longshore variability such as crescentic shapes and rip channels, are averaged out and considered as a noise term. Longshore variability is often thought to develop during low to moderate wave heights, when cross-shore sandbar migration is small (Wright and Short, 1984). The effects of longshore variability on cross-shore sandbar migration are therefore obscured by large longshore-uniform sandbar migration during high wave events. Shoreface nourishments furthermore tend to decrease the longshore variability, spreading out and evening the beach profile.

The nearshore, however, experiences strong longshore variability in the hydrodynamics and bathymetry (Van Enckevort et al., 2004). This longshore variability yield in gradients in longshore processes which in term is one of the dominant factors for coastal erosion (Grunnet and Ruessink, 2005). Research Question 3 will therefore explicitly focus on the effects that a shoreface nourishment has on longshore variabilities and sediment transport rates.

Throughout the report, the sediment characteristics are also considered uniform. Although changes in sediment characteristics influence the efficiency of the nourishment (Giardino et al., 2016), these changes are not taken into account in this scope of the study. This is done in order to highlight the shoreface nourishment effects due to changes in the cross-shore profile. There are beaches which, due to their location (near headlands) or protective measures implemented on them, are subject to diffraction or energy reduction phenomena. These types of beach has been omitted from this study due to its shape in planform and profile being different from the open beaches (Iglesias et al., 2009a,b). Therefore, the beach and shore profile can be represented by models defined from potential, exponential, logarithmic and rational functions.

The cost of a nourishment project can largely be affected by the use of certain types of dredges and the location of the nourishment among other factors. Depending on the site-specific requirements of the project, some nourishment alternatives might become financially unfeasible or even impossible. This study will purely focus on the theoretical aspect of differences in nourishment designs, therefore the financial aspect will largely be disregarded for now.

1.5 Tested Nourishment Design Scenarios

The efficiency of certain shoreface nourishment designs has been the subject of several previous studies, e.g. Giardino et al. (2009); Van der Werf et al. (2010). These studies compared the hydro- and morphodynamics of different designs with the initial profile, of which the nourishment designs were largely based on real life applications. In general, three different conventional nourishment alternatives are examined (Figure 1.3). The first alternative design is by nourishing the seaward slope of the outer bar at the same height as the peak of the outer bar. Second alternative is adding the nourishment in deeper water further offshore at the seaward side of the outer bar. The third and final conventional alternative is to construct the nourishment by filling up the trough between the outer and swash bar.

All designs are largely based on designs previous used in the study of Giardino et al. (2009), in which shoreface nourishment in Egmond aan Zee (NL) were analyzed. This study is chosen because of the strong agreement in cross-shore profiles between Egmond aan Zee and the study area. The current study will further explore these previously used designs and compare them with a fourth alternative design based on the concept of an EBP. The background of the design of this nourishment will be elaborated in Chapter 4 - Equilibrium Beach Profiles. Nourishment impact and efficiency is among others largely determined by its size. In order to be able to compare the nourishment impact results of each scenario, all design alternatives are rescaled to the same fill density of 175 cy/ft (435 m^3/m).

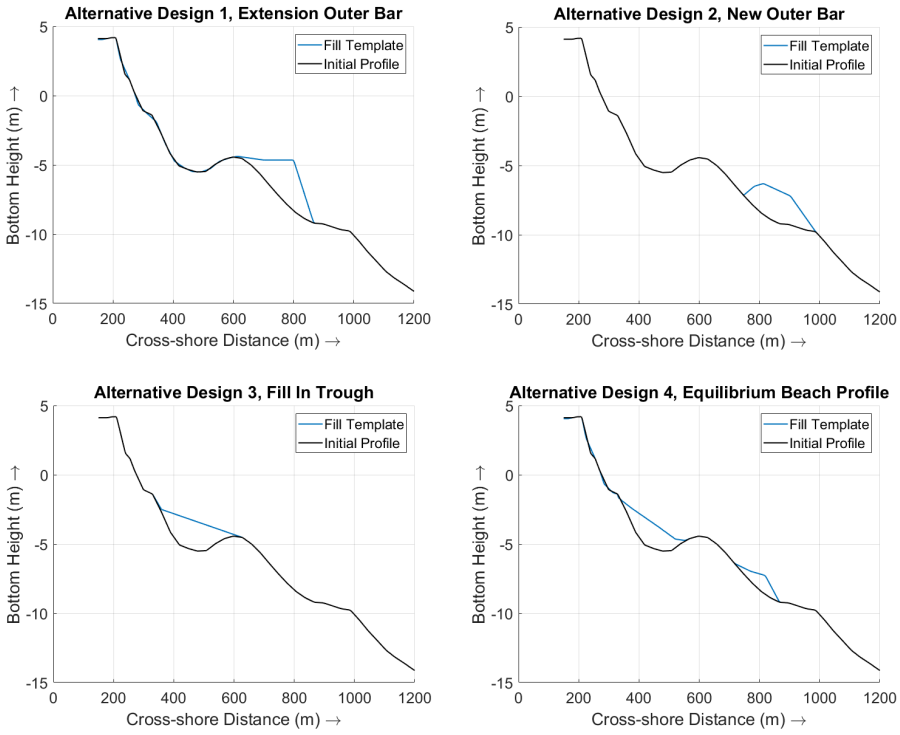

Figure 1.3: The four different shoreface nourishment alternatives used in this study. Bed levels are indicated with respect to MSL.

1.6 Report Layout

The report is divided in four different chapters, each treating one of the research questions. Depending on the goal per research question a different scientific background and methodology is proposed and the questions are concluded at the end of each chapter.

First a theoretical background on the coastal terminology and main processes around shoreline erosion and bar morphodynamics is summarized, together with a description of the study site. After which the different research questions are treated.

Research Question 1 will introduce the concept of equilibrium beach profiles and how to apply the concept for shoreface nourishments. Research Question 2 and 3 will respectively treat the cross-shore and longshore shoreface nourishment effects. Research Question 4 will apply the findings from the previous chapters and proposes applications for further beach restoration projects.

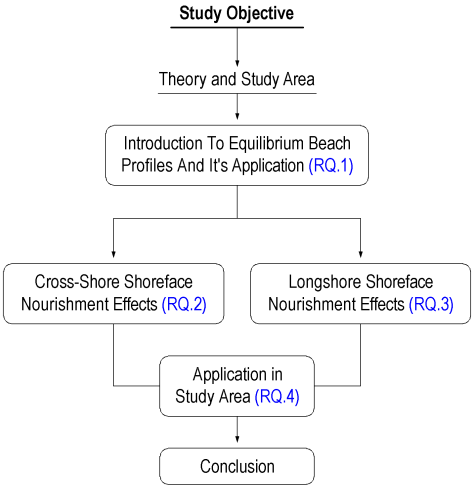

Figure 1.4: Report layout structure, four research questions are treated separately, after which the study objective is concluded

After all four research questions are answered, results will be summarized and the study objective is concluded, see Figure 1.4.

2
Theory

2.1 Coastal Terminology

Beach Profile[1]**:** It should be apparent that the shore can actually extend over a broad zone at the coast. At any point in time, the stillwater level (i.e. – the level in the absence of waves) can equal the average global sea level, be well below it at low tide, or be well above it at high tide. To understand the basic processes of coastal erosion, one must consider a set of boundaries. At the scale in the order of kilometers, the coastal width of interest is referred to as the *littoral zone*, see Figure 2.1. This zone is generally defined as the area over which waves in the presence of changing water levels dissipate most of their energy. In common practice, the littoral zone extends from the point of maximum yearly uprush of waves to some small distance seaward of the breakpoint if the largest yearly wave. Along sedimentary coasts, the continual exposure to wave breaking and fluctuating water levels rearranges sediment particles. This leads to development of slopes and morphologic feature balances for the particular waves striking the beach and distribution of sediment grain sizes. Viewed in cross-section (Figure 2.1), the littoral zone at a site develops a profile that is related primarily to sediment texture, wave climate, tide range, sediment supply and prevailing winds. Key elements of a profile include the following:

The *outer surf zone* is the gently sloping inshore area over which waves of all sizes begin to break and measurably redistribute sediment. It sometimes includes breakpoint or longshore bars (outer bar and more shoreward bars), which trigger wave breaking in storms, and troughs between bars. Bottom friction dissipation in this zone is dominant.

The *inner surf zone* is the area of complex topography between the normal point of wave breaking and usual limit of wave uprush along the beach face, sometimes encompassing an inner bar and trough. This zone experiences the greatest vertical changes and irregular bottom topography. Wave energy dissipation by breaking waves is dominant in this zone.

The *beach face* is that portion of the inner surf zone over which wave uprush and backrush (undertow) occur. It is generally an area of uniform slope that is balanced according to the local sediment grain size and wave climate. This is the final zone of wave energy dissipation and is sometimes referred to as the wet-sand beach over which tides migrate.

The *berm* is a nearly horizontal portion of the profile beginning at the upper beach face and extending landward to the base of the dune or backshore environment. Situated at the highest wave uprush level, the berm is dry for most of the tidal cycle and therefore is often referred to as the dry-beach zone.

Proper assessment of coastal erosion requires study of how the entire littoral zone responds to waves, tides, and currents over a period of time.

[1]For consistant use of the coastal terminology in this and previous reports, the used definitions are as found in (CSE, 2011b).

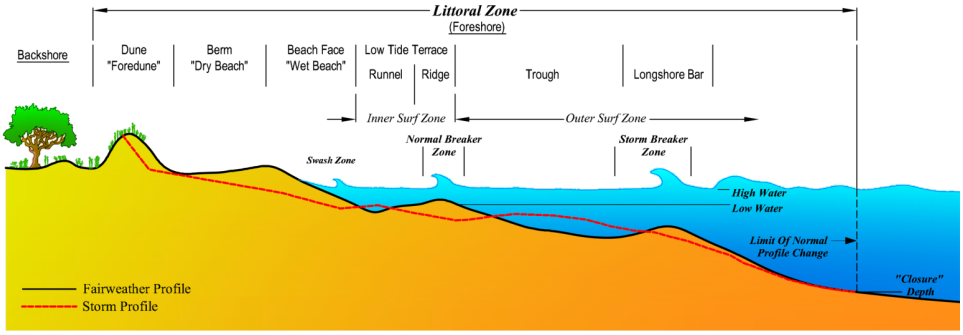

Figure 2.1: Terminology of the littoral zone, after Komar (1998).

Waves and Wave-Generated Currents: While tides and surges are the principal controls on water level at the coast, waves do most of the work of moving sediments. Waves arriving at the shore are transformed in shallow water, becoming steeper in the crest and flatter in the trough. As waves approach depths of water similar to their height (measured from crest to trough), they break. The form of the breaker varies from a gradual spilling over at the crest to a gentle up-and-down sloshing.

Wave-breaking generates oscillating currents as well as circulation currents parallel and perpendicular to the shore. If waves arrive straight to a shoreline, the principal motion is onshore-offshore. However, when waves arrive at an angle to the shore, the motion becomes saw-toothed. Wave-generated currents can be resolved into longshore components as well as cross-shore components. The current associated with the shore-parallel component is considered the longshore current carrying the longshore sediment transport. It gains its momentum during the process of breaking so, characteristically, it tends to be strongest between the initial wave breakpoint and the point where the undertow meets the next incoming wave.

2.2 Shoreface Nourishments

Shoreface nourishments are able to counteract coastal erosion by adding a surplus in the sediment budget in the littoral zone. The behavior of this effect is extensively studied along shoreface nourishments along European coasts (Hanson et al., 2002; Wijnberg et al., 2007) and is divided into several phases.

Behavior: After nourishment construction, the cross-shore profile is taken out of its natural pre-nourishment profile. The beach tries to re-shape back into a profile where the nourishment is better incorporated, into a profile with a bar with the shape and volumes per meter that are comparable to the bars in the original system. After construction, most nourishments follow the general trend of onshore migration in the following years, which is caused by an onshore directed larger sediment transport rate at the nourishment crest compared with the bottom, and wave asymmetry on top of the nourishment.

The nourishment tries to form an extra bar in the cross-shore profile, whereas the wave climate only allows the number of bars found in the pre-nourishment profile. To prevent the occurrence of an extra bar in the profile, the beach counteracts with onshore migration of all bars. The bar closest to the beach face is pushed onshore and incorporates with the beach face, thereby widening the beach and counteracting coastal erosion.

Effects: The morphological effects shoreface nourishments have on the beach profile is strongly related to the process of wave energy dissipation over the new bar (Van Duin et al., 2004). As the waves now break further offshore, the shoreface nourishment basically acts as an offshore submerged breakwater, causing a salient by trapping sediment shoreward of the nourishment.

Van Duin et al. (2004) further explored shoreface nourishment effects and divided it into cross-shore and longshore effects. This division of nourishment effects is also used as a guideline for this report. Therefore, the cross-shore effects are computed in Research Question 2, and the longshore effects in Research Question 3.

Longshore Effects: The larger incoming waves break further offshore on the seaward side of the shoreface nourishment. This reduces the approaching onshore directed wave energy, thereby reducing the longshore transport rates as well. As a result, a salient will form shoreward of the nourishment. To compensate this, downdrift erosion is found as well. The longshore effects are commonly referred to the lee effect and is described in Figure 1.1(a).

Cross-shore Effects: The larger incoming waves break further offshore on the seaward side of the shoreface nourishment. This reduces the approaching onshore directed wave energy, leaving shoaling waves with lower wave energy shoreward of the nourishment. This reduction of wave energy will lower sediment stirring which in term reduces the wave-induced transport carried by the undertow, and is referred to as the feeder effect, see Figure 1.1(b).

2.2.1 Shoreface Nourishment Effect Quantification

Shoreface nourishment effects have been studied extensive all over the world, with results showing that such nourishments can have fruitful applications in reducing the significant wave height and longshore transport rates, e.g. Dean et al. (1997). These effects are divided and quantified by either checking the feeder and lee effects. The feeder effect is described by an increase of net onshore transport, which can be checked by measuring the differences in net total cross-shore sediment transport rates. These effects will be further explained and explored in 5 - Cross-shore Nourishment Effects. The lee effect corresponds to a reduction of longshore sediment transport which in term is proportional to the significant wave height along the beach profile. A lowering of this wave height therefore lowers the longshore transport and the coastal erosion. Chapter 6 - Longshore Nourishment Effects will fully focus on these effects and is done by computing the longshore transport rates per nourishment scenario. A more detailed description of these effects and how they are quantified is given in the corresponding chapters.

3
Study Area

3.1 Activity Location

The Town of Nags Head is located in Dare County along the Atlantic coast of the North Carolina Outer Banks, a chain of barrier islands along the Atlantic Ocean, 145 kilometers south of Norfolk (VA). Figure 3.2 shows the proposed project location. The Town faces east to northeast and is bordered by the Town of Kill Devil Hills to the north and Cape Hatteras National Seashore to the south. Roanoke Sound borders the Town on the west, and the Atlantic Ocean bounds the Town on the east. Oregon Inlet, the closest inlet to Nags Head, is located 8 kilometer south of the Town line. The proposed nourishment location begins 1.5 kilometer from the Town's northern limit, near the Bonnett Street public beach access, and will extend south to the Town line bordering the Cape Hatteras National Seashore (Fig 3.3).

South Nags Head has sustained higher erosion rates than north Nags Head, where there are numerous historic buildings along the oceanfront dating to the early 1900s. NCDENR (1998) reports 50-year erosion rates along the northern half of Nags Head in the range of 2–3 ft/yr. While the official erosion rates for Nags Head vary widely from north to south (southern erosion rates are 2.5x as high in the north), it sustained erosion over many years at some level has left nearly all oceanfront properties vulnerable to damaging storms, as determined by (USACE, 2000), see Figure 3.1.

Figure 3.1: Nags Head beach in 2003. Severe consistent beach erosion is visible, from CSE (2011a)

3.2 Bathymetry and Beach Conditions Surveys

As part of the planning for the federal Dare County project (USACE, 2000), the Corps of Engineers established a baseline from the northern Kitty Hawk town line to Oregon Inlet. Stationing in engineering notation ranges from station 0+00 in Kitty Hawk to approximately station 1025+00 at the south Nags Head town line with a 500 ft distance between stations. The northern limit of Nags Head is situated around USACE station 436+83. Therefore, Nags Head encompasses 58,817 linear feet (~18km) of shoreline. The baseline was established in the early 1990s and included numerous turning points as it generally followed the oceanfront roads from Kitty Hawk to Nags Head. In August 1994, a contractor for the Corps of Engineers surveyed profiles at ~1,000-ft spacing along the baseline from the backshore to a distance of about 3,000 ft offshore. To the best of knowledge,

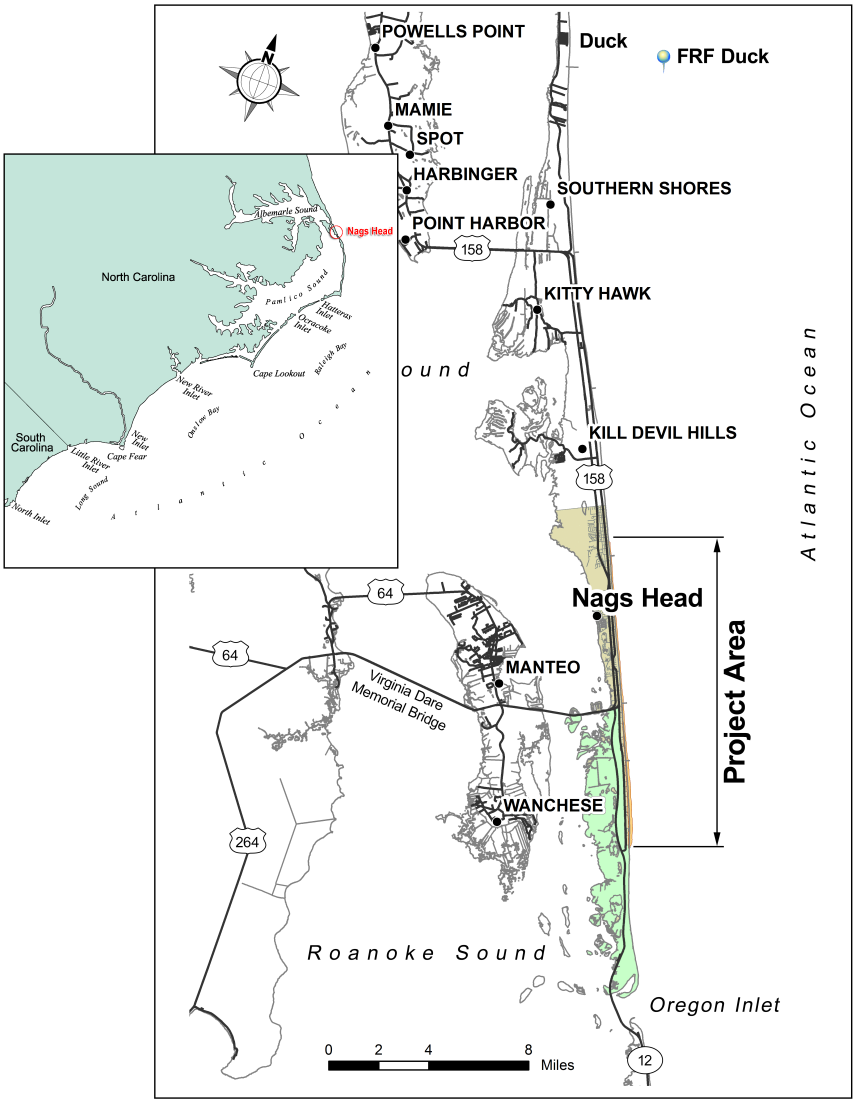

Figure 3.2: Nags Head (NC) project vicinity map.

this was the first comprehensive survey of offshore profiles along Nags Head. Data collection methodology and the development of the beach profile in the last 6 years are summarized in A - Data Collection Methodology. Survey data uses the USACE baseline to resurvey profiles at 1,000-ft spacing along nearly the same alignments as the 1994 survey. Surveys typically extend from the foredune to 750 m offshore (CSE, 2011a). Profiles from 1994, 2004, 2005, 2006, and yearly data from 2009 until 2017 were then overlaid and compared to get a high-accuracy bathymetry dataset and to compute sand losses and gains.

Figure 3.3 shows the location of available profiles along with Town boundaries and the road grid for Nags Head. Five shoreline segments ("reaches") are referenced in Figure 3.3, with strong variations in coastal erosion and longshore transport rates between the reaches. Additional profiles were surveyed in Kill Devil Hills (410+00 to 430+00) and along the National Seashore to Oregon Inlet (1030+00 to 1290+00). The USACE 1994 survey terminated at profile 1010+00; therefore, no comparative data are available in the National Seashore.

3.3 Reference Contours and Boundaries for the Project Area

Volume variations along the Nags Head project area were estimated using standard methods (average-end-area method) and common cross-shore boundaries and contour datums. Three lenses (i.e. – volumes between particular reference contours) were used in the present analysis for purposes of evaluating levels of dune protection, beach, and the underwater zone. Figure 3.4 illustrates the cross-sectional areas of these three lenses for Nags Head. Emphasis was on the overall volume of sand contained from the foredune to a reference depth determined by FEMA.

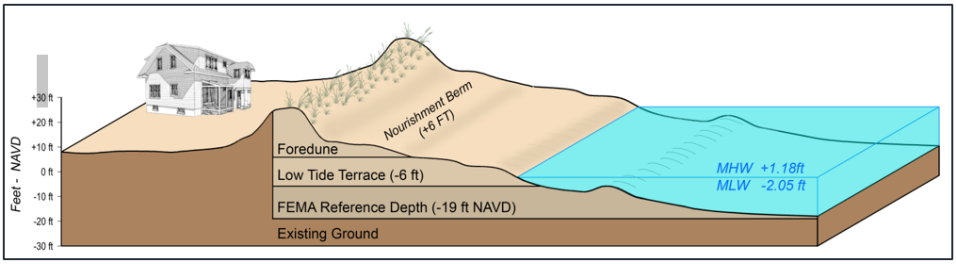

Figure 3.4: Illustration of the three lenses used in the profile volume analysis for Nags Head. Lens 1 includes the dune and the upper portion of the beach above the 2011 project construction berm. Lens 2 represents the active beach to low-tide wading depth; and Lens 3 represents the outer surf zone extending to the FEMA depth limit CSE (2011a).

Lens 1) "Foredune" — From the face of dune to +2 m (+6 ft) NAVD. The volume above the +2 m (+6 ft) elevation is a measure of the sand quantities shifted toward the dunes and upper beach. Therefore, this is a measure of storm and flood protection levels associated with the project or gains in dune volume due to post-project buildup above this contour.

Lens 2) "Beach" — Between +2 m (+6 ft) and -2 m (-6 ft) NAVD. It includes the dry-sand beach ("berm") and the wet-sand beach, and extends to low-tide wading depth. This is not only the primary recreational portion of beach, but also is the inner surf zone where a significant proportion of wave-breaking and energy dissipation occurs.

Lens 3) "Underwater" — Between -2 m (-6 ft) and -6 m (-19 ft) NAVD. It represents the outer surf zone extending seaward from low-tide wading depth to the depth set forth for the FEMA post-storm restoration criteria (-6 m NAVD).

Unit volumes for Nags Head profiles were calculated to determine the quantity of sand in one linear foot of beach at each lens at each survey line. These unit volumes were then used to calculate the line-to-line net volumes, the reach net volumes, and finally the net volume for the entire project. The line-to-line net volumes are proportional to the distance between lines and represent the longshore distribution of sand volume in the project area. The net volumes by reach were subsequently divided by the applicable reach lengths to yield weighted average unit volumes, taking into account the variations in applicable shoreline distances from line to line. Conveniently, the

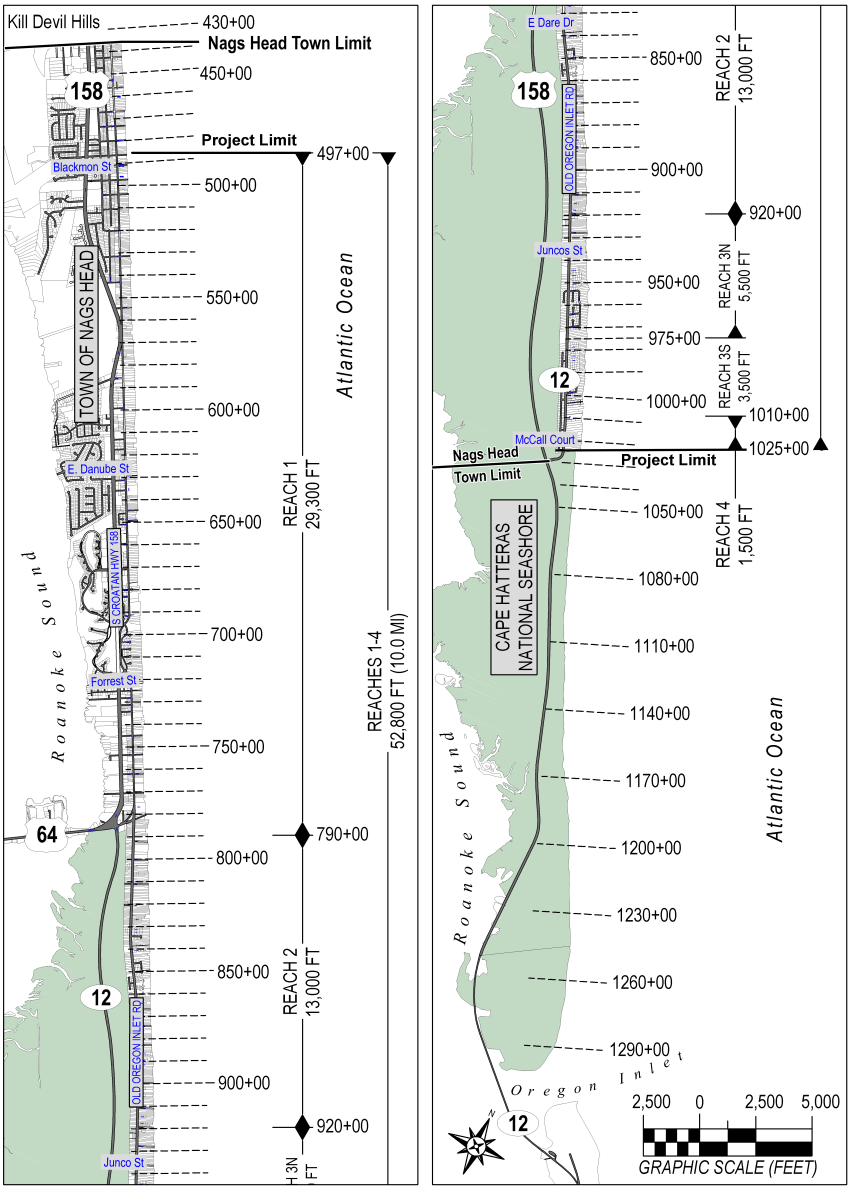

Figure 3.3: General location map of beach profile lines (1,000-ft spacing) established in 1994 USACE (2000). The same alignment of the USACE profile lines and resurveyed the project area at 500-ft spacing were later on surveyed. Lines south of Nags Head were established by CSE (2006) by extending the USACE baseline south to Oregon Inlet.)

stations for Nags Head are evenly spaced at 500 ft. If they are not evenly spaced, the station-to-station net volumes should be proportional to the distance between stations in order to represent the actual longshore distribution of sand volume.

3.4 Erosion and Longshore Variabilities

The erosion losses along the Nags Head project site show a strong gradient, with higher erosion rates in the south compared to the north. The main driver for this increase in erosion is thought to be Oregon Inlet, which is approximately 8 kilometers to the south of the southern border of Nags Head. This longshore variable erosion rate is a characteristic for barrier islands, especially at the East US coast (Kana, 1995).

To calculate the erosion rates, the volume in each station's beach profile is integrated and compared to the previous survey to see the net differences in volume. The profile is integrated to the FEMA Reference Depth at – 6 m (-19 ft), which is known to be extended further offshore than the depth of closure. This way, all the erosion losses have to be caused by changes in longshore transport.

For a large-scale nourishment project at Nags Head in 2011, the background erosion rates were estimated from survey data between August 1994 and April 2005. Results show that a total of 2.927.000 cy (2.237.850 m^3) of sediment was lost in that period, resulting in an average loss of 272.200 cy/yr (208.100 m^3/yr), see Figure 3.5. The computed erosion losses are divided in four [1] reaches and two lenses.

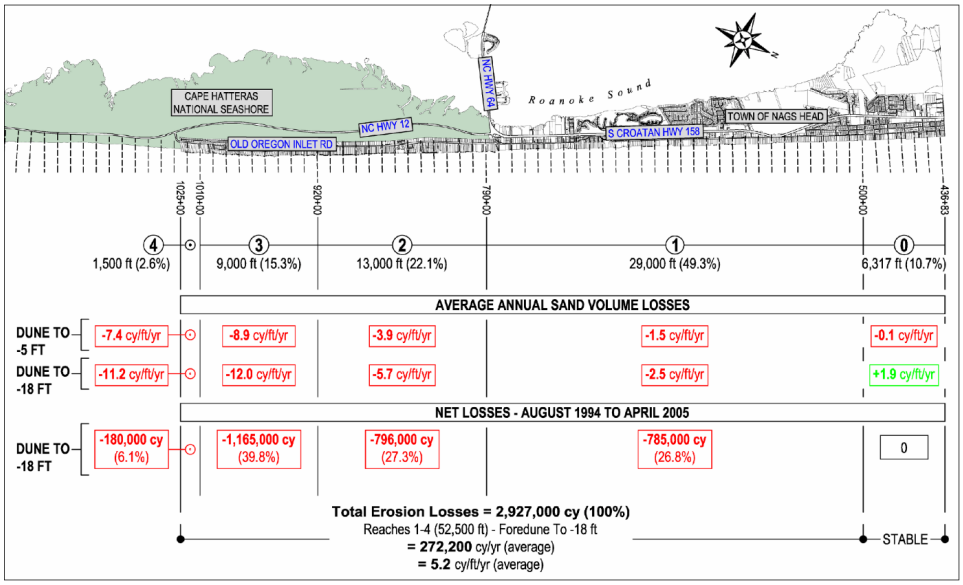

Figure 3.5: Average annual and net sand volume losses per reach between August 1994 and April 2005. With an average yearly loss of 272,200 cy/ft. Oregon Inlet is in the south, located at the left-hand site of the figure.

[1] *in previous projects, reach 3N and 3S were combined into reach 3, and the lenses were divined to -5 ft and – 18 ft respectively*

3.5 Hydrodynamics

3.5.1 Wave Climate

Offshore wave information is typically obtained from a wave gauge or a global- or regional scale wave hindcast or forecast. Nearshore wave information is required for littoral processes analysis and for the design of almost all coastal engineering projects. Three types of wave stations are available offshore of the study area. One is a real-time wave buoy ~24 km offshore with nine years of wave records, and the other is a hindcast wave station located ~17 km offshore with 35 years of data. The third type is by creating a virtual hindcast station using a NOAA WAVEWATCH III dataset (Tolman et al., 2009). The remainder of this report is focused on the The Wave Information Studies (WIS) dataset. In Section Appendix C.1 - Delft3D, the use of the WAVEWATCH III dataset is explained and compared with the WIS dataset. See also Wu et al. (2017) for WAVEWATCH III applications in South Carolina. The WIS dataset is chosen here because of the more accurate computed longshore transport rates as well as its long-standing use in many USACE coastal engineering projects.

3.5.2 Real-Time Wave Buoy — Station 44100

Station 44100 at the USACE pier and Field Research Facility (FRF) (Duck, NC), owned and maintained by the National Data Buoy Center (NDBC), appears to be the closest real-time wave buoy to the Nags Head project site. Located at 36.259°N 75.592°W, 24 km northeast of the Nags Head northern offshore boundary, the water depth at the station is 26 m. Because of its proximity to Nags Head, the wave data collected at FRF were used to approximate wave conditions at Nags Head. A previous study by Vandever and Miller (2003) suggested that the wave climate summaries collected at FRF are representative of the wave climate as far away as Oregon Inlet, nearly 25 miles to the south. The wave height, period, and direction analyses based on available data are listed in Table 3.1. It shows that June, July, and August have the lowest wave heights compared to other months.

Table 3.1: Monthly average wave climates from 1986 through 2006. [Source: USACE–FRF, unpublished data]

	Wave Height (m)	**Wave Period (s)**	**Wave Direction (°)**
January	1.09	8.58	75.3
February	1.17	8.55	71.2
March	1.17	8.74	79.0
April	1.04	8.60	79.4
May	0.92	8.45	84.2
June	0.75	8.13	96.4
July	0.64	8.15	95.2
August	0.84	8.66	92.6
September	1.09	9.16	84.9
October	1.18	8.67	76.7
November	1.07	8.53	72.0
December	1.12	8.49	70.5

3.5.3 Wave Information Studies — Station 63220

Wave Information Studies (WIS) (e.g. – Hubertz (1992)) is a project sponsored by USACE that generates consistent, hourly, long-term (20+ years) wave climatology along all US coastlines, including the Great Lakes and US island territories. Unlike a forecast, a wave hindcast predicts wave conditions using a computer model and observed wind fields. By using value-added wind fields, which combine ground and satellite wind observations, hindcasted wave information is generally of higher accuracy than forecast wave conditions and is often representative of observed wave conditions. Hindcast data available from each WIS site include hourly wind speed, wind direction, and bulk wave parameters (significant wave height, period, and direction) as well as discrete

directional wave spectra at 1-hour to 3-hour intervals. WIS wave direction uses meteorological convention, ie-a direction of 0° corresponds to a wave arriving from true north; similarly, a direction of 90° corresponds to a wave from due east.

There are three WIS stations (63220, 63221 and 63222) close to the Nags Head project site. Previous studies by CSE have shown that station 63220 produces the most realistic results and is therefore used in this study as well (CSE, 2011a). It is located 17 km due east of Nags Head at 36.08°N and -75.50°W in water depths of 20 m . This station has hindcast data for 35 years between 1980 and 2014. Figure 3.6 is a polar histogram of the frequency of occurrence of wave directions based on the 35-year record, and Table 3.2 lists percent occurrence of wave height and period by directions. The majority of waves (88.6 percent) are from northeast to south (45°–180°), but the northerly waves are generally larger than those from other directions. Waves coming from the 45° band from east, east-southeast to southeast (ie – 90° to 135° band) occur 55.1 percent of the time, and waves coming from southeast have the highest occurrence of 19.9 percent compared to the other directions.

The series of graphics in Figure 3.7 and 3.8 show the monthly polar histograms of wave directions and wave heights. In late spring and summer months between May and August, waves are mainly from the southeast with most wave heights smaller than 1 m, and the rest of the year waves are mainly from northeast to east with most wave heights between 1 and 2 m. The extreme wave conditions were analyzed at WIS station 63220, linearly fit for the top 21 events, and used to extrapolate 50-year and 100-year return-period events of 7.8 m and 8.2 m (respectively) (Fig 3.9).

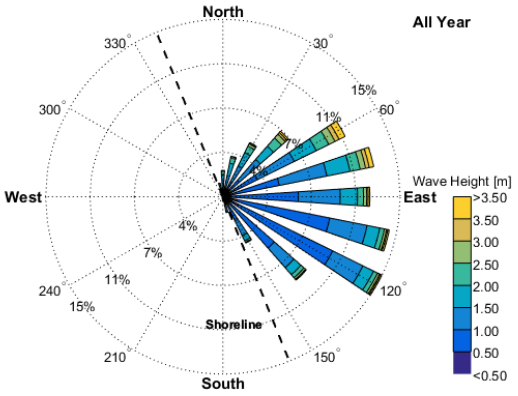

Figure 3.6: Wave rose of WIS station 63220 showing the occurrence frequency of wave direction and wave height based on the 35-year record between 1980 and 2014. [Source: USACE WIS]

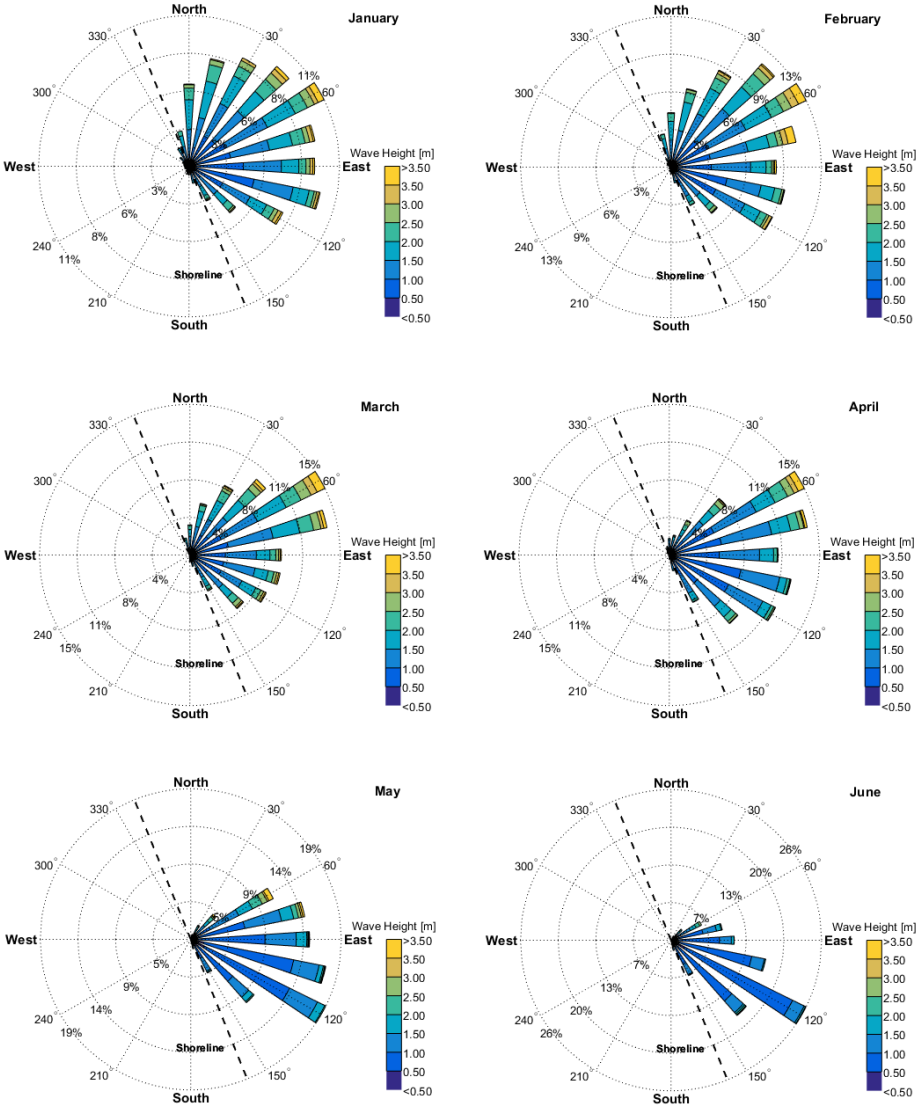

Figure 3.7: Wave roses of WIS station 63220 in the months January – June, showing the occurrence frequency of wave direction and wave height based on the 35-year record between 1980 and 2014.

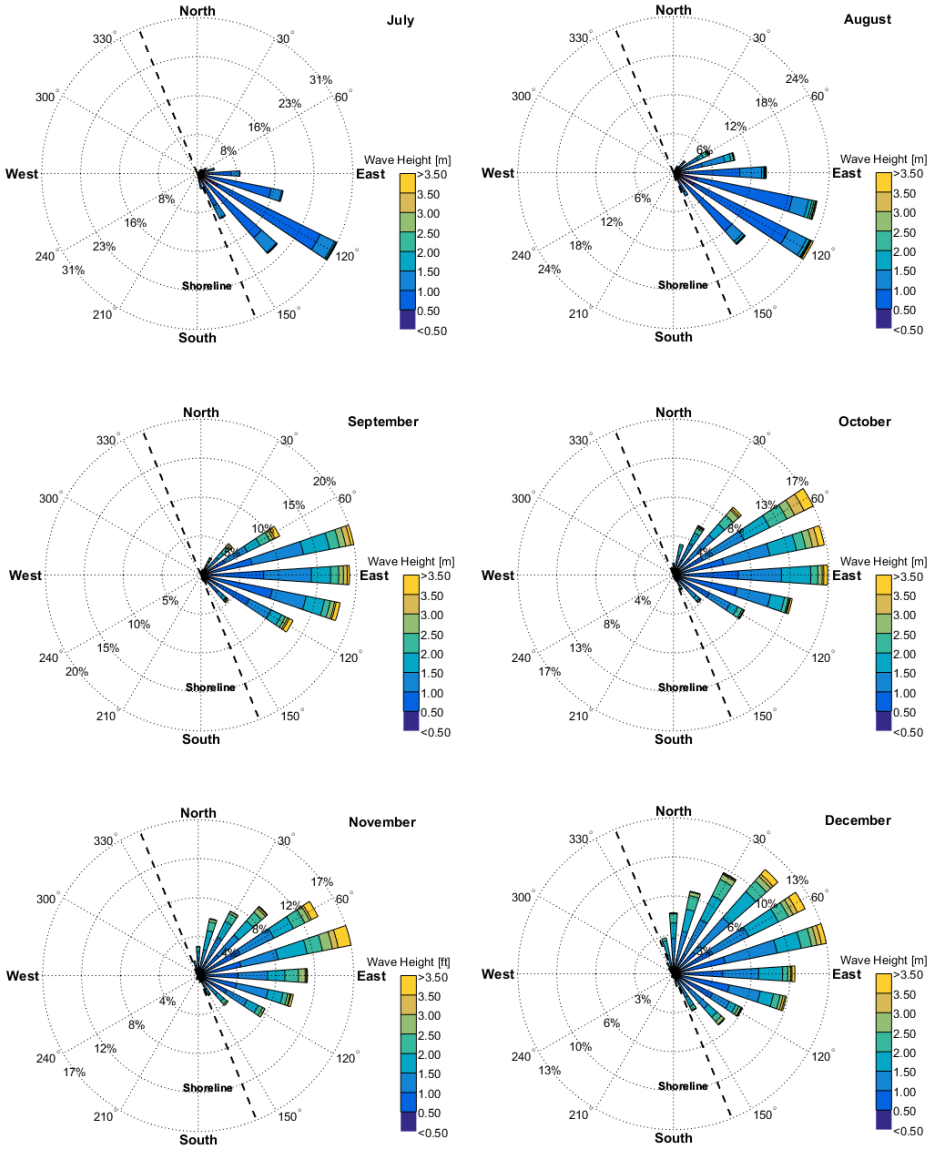

Figure 3.8: Wave roses of WIS station 63220 in the months July – December, showing the occurrence frequency of wave direction and wave height based on the 35-year record between 1980 and 2014.

Table 3.2: Percentage of occurrence of the 35-Year Record (1980-2014) at WIS 63220 of wave directions in 16 bands with 22.5° increments, associated wave heights (in ft), and wave periods (seconds). Note: Nags Head shore-normal is ≈68° from true north. [Source: USACE-WIS] [After CSE (2011a)]

Direction from °North	Percentage of Occurrence (%)	Mean Wave Height (ft)	Mean Wave Period (s)
0 ± 11.25	3.2	4.92	6.7
22.5 ± 11.25	5.8	4.92	7.6
45 ± 11.25	9.7	5.25	8.7
67.5 ± 11.25	16.5	5.25	9.8
90 ± 11.25	18.3	4.26	9.8
112.5 ± 11.25	19.9	3.28	9.4
135 ± 11.25	16.9	3.61	8.5
157 ± 11.25	6.1	3.61	7.5
180 ± 11.25	1.2	3.28	7.4
202.5 ± 11.25	0.3	3.28	6.5
225 ± 11.25	0.2	3.28	6.3
247.5 ± 11.25	0.1	3.61	6.7
270 ± 11.25	0.1	3.61	6.3
292.5 ± 11.25	0.2	3.61	6.6
315 ± 11.25	0.4	3.94	6.1
337.5 ± 11.25	1.0	4.59	6.0

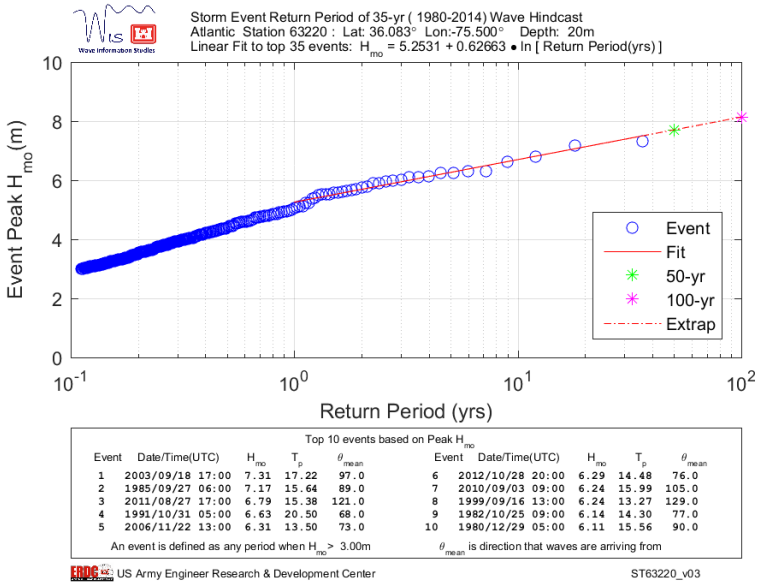

Figure 3.9: Peak wave heights of storm events over 35 years (1980–2014) based on wave hindcasts at station 63220. The linear trend of the highest 21 wave events was used to extrapolate 50-year and 100-year return-period storm-wave heights for the Nags Head offshore area

3.5.4 Wave Climate Analysis

Obtaining satisfactory wave data is a necessary and crucial task in the preparation and execution of wave and numerical models. As discussed in the previous sections, there are no site-specific, long-term wave records for the Nags Head project area, a wave data source was selected in the vicinity of the site (i.e. – WIS station 63220). The WIS station 63220 is located 17 km to the east of Nags Head and has 35 years of hindcast data between 1980 and 2014. This station was chosen because of the long-term wave records, and the net transport generated under the wave climate of this station agreed with historical observations (CSE, 2011a).

The wave data was then characterized by grouping the significant wave heights, peak spectral wave periods, and vector mean wave directions at the peak spectral frequencies. The histogram of percent occurrence of these three wave parameters are graphed in Figure 3.10. Wave direction in these figures uses meteorological convention (i.e. – a wave direction of 0° corresponds to a wave that is coming from due north, and 90° is from due east). There are 6 wave-direction bins, 8 wave-period bins, and 8 wave-height bins categorized in this study and shown in the histogram of Figure 3.10 as well.

The largest significant wave height identified in the 35-year WIS wave hindcast was 7.31 m. The mean significant wave height was 1.23 m, and the mean wave period for this dataset was 7.2 seconds. Based on the statistical wave summary, the majority of deep-water waves approached the Nags Head shoreline from southeasterly directions. The most predominant wave height fell within the 0-1 m and 1-2 m bands, and only 11.9 percent of waves exceed 2m. The 6–8 second wave-period band was the most dominant, containing 49.2 percent of all occurrences.

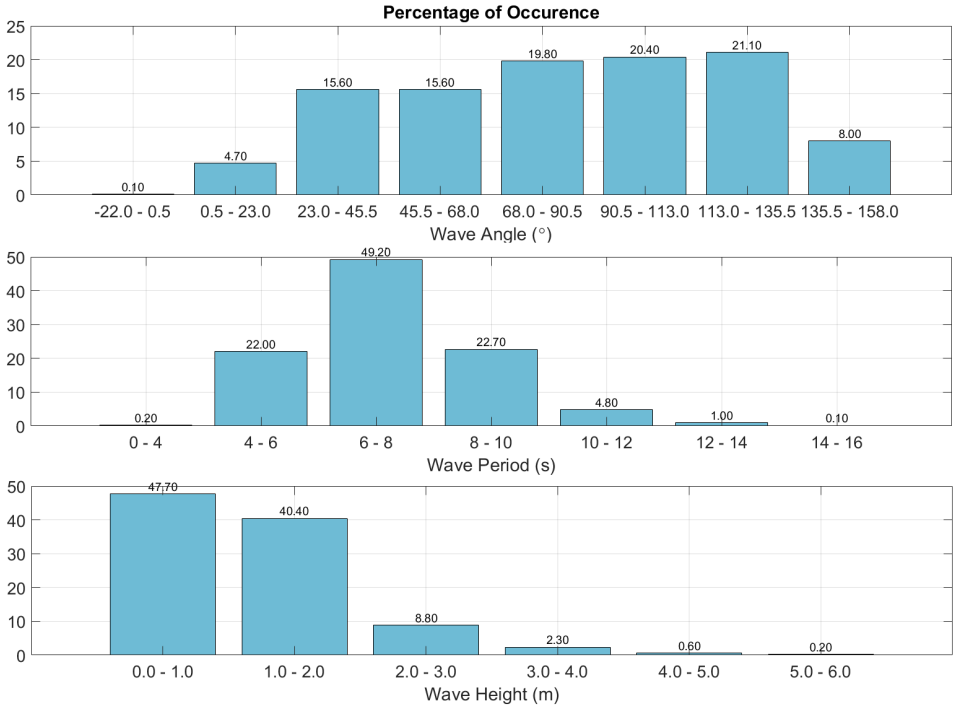

Figure 3.10: Histogram of percent occurrence of wave height, period, and direction for WIS station 63220.

4

Equilibrium Beach Profiles

How is the EBP shape determined and how can its concept be used for shoreface nourishment design?

The concept of an equilibrium beach profile (EBP) has found applications in coastal engineering such as studies in nearshore morphological evolutions and designs of beach nourishments. The EBP hypothesis holds that the beach profile shapes into a constant or equilibrium profile corresponding to given sediment characteristics and constant incident wave type.

The first experimental studies of equilibrium beach profiles using a potential function were performed by Waters (1939) and Saville Jr (1958) showing a concave shape where a steeper slope is observed in the wet beach area. Concurrently, Rector (1954), under controlled laboratory conditions (uniform sets of waves), established an invariant profile, from which Bruun (1954) and later Dean (1977) presented the potential function, the most commonly used in coastal engineering:

$$h = Ax^{2/3} \tag{4.1}$$

Where h is depth below mean water level at a distance x offshore and A is a scale factor, correlated to the environmental parameter H_b^2/gDT^2, where H_b is breaker height, D is sediment grain size, T is wave period and g is gravitational acceleration. The main disadvantage of this simple profile formula is that the potential function is purely based on dissipation of wave energy. In order to better describe the beach profile, wave reflection also has to be taken into account. This work was done by Bernabeu et al. (2003) which was based on earlier works of Inman et al. (1993) and came with a two-sectioned (bi-polynomal) profile as shown in Figure 4.1. Tidal forcings are included in the proposed equilibrium beach profile by adding the tidal wave elevation as expressed in the average spring tidal range in the calibration process.

The beach profile is now divided in a shoaling and surf profile with the outer bars as the hinge point. The main idea behind this is that in the shoaling profile the wave dissipation due to bottom friction is constant, where this varies in the surf profile. The following section will explain the theoretical background in more detail in order to better understand the applicability of a bi-polynomal EBP.

4.1 Theoretical Background

The main principle of the EBP is based on the energy balance equation, in which the total available flux is expressed as the energy flux in a cross-shore profile. Previous EBP theories were based on balancing the incoming wave energy flux with the wave energy dissipation (Dean, 1977). In this case the energy loss associated with wave reflection has to be accounted for in the energy balance as well (Medina et al., 2001):

$$\frac{dF_t}{dx} = \frac{dF_I}{dx} - \frac{dF_R}{dx} = \epsilon \tag{4.2}$$

In which variations of the total energy flux (F_t) are expressed as the sum of variations in onshore directed incident wave flux (F_I) and the offshore directed wave reflection flux (F_R) over a distance increment to the coast (dx).

To preserve energy, this total flux should be balanced by the wave energy dissipation per unit area. See Figure 4.2 for a schematization of the total energy balance equation. From section 2.1 - Coastal Terminology, it is known that wave energy dissipation by breaking waves is dominant at the breaker zone and bottom friction dissipation in the area offshore. It is therefore convenient to divide the beach profile in two sections, based upon the work of Inman et al. (1993). The onshore zone, referred to as the surf profile, starts at the coastline at mean sea level continuing up to the breakpoint. The offshore zone, named the shoaling profile, starts at the breakpoint continuing up to the depth h_a. These two profiles will intersect at the breakpoint which will be referred to as the discontinuity point. The bi-polynomal EBP consists of the two profiles and is characterized by several morphological parameters, as expressed in Figure 4.1.

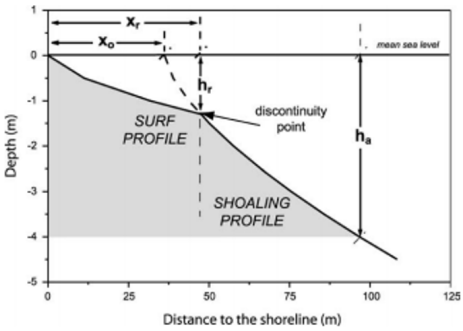

Figure 4.1: Proposed two-section EBP (modified from Inman et al. (1993)) and representative morphological parameters: x_r is the horizontal distance between the beginning of the surf profile and the discontinuity point; h_r is the discontinuity point depth; x_o is the horizontal distance between the beginning of the surf profile and the virtual origin of the shoaling profile over the mean sea level; and h_a determines the offshore limit of the model validity.

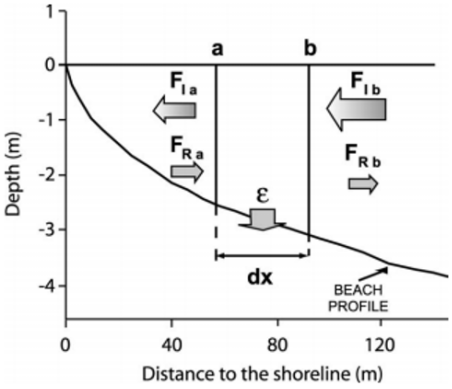

Figure 4.2: The energy flux excess between two consecutive sections, a and b, is due to dissipation and reflection processes: F_{Ib} and F_{Ia} are the incident energy flux through the sections a and b, respectively; F_{Ra} and F_{Rb} are the reflected energy flux through the sections a and b, respectively; ϵ is the energy dissipation between the sections a and b (after Bernabeu et al. (2003)).

Surf Profile The applicability of Eq. 4.2 in the surf zone is based on two assumptions:

1. Constant wave energy dissipation per unit volume (Dean, 1977)
2. Constant wave height over depth parameter $y = H/h$ along the surf profile (Thornton and Guza, 1983)

Consequently, the energy balance equation for the surf profile can be rewritten as:

$$\frac{1}{h}\left[\frac{dF_I}{dx} - \frac{dF_R}{dx}\right] = \frac{\epsilon_b}{h} = D_b^* \tag{4.3}$$

In which ϵ_b is the wave breaking induced turbulence dissipation (Thornton and Guza, 1983) and D_b is the incident energy per unit volume turbulence dissipation. The incident wave flux (F_I) is defined as $F_I = 1/8\rho g H^2\sqrt{gh}$ by the shallow water linear theory. The reflected wave flux will be defined as a function $V(x)$ as proposed by (Baquerizo and Losada, 1998), in which (F_R) can be reformulated per unit volume for a given profile and wave period under the surf profile initial dissipation hypothesis as:

$$V(x) = -\frac{1}{h}\frac{1}{F_I}\frac{dF_R}{dx} = k\frac{1}{\sqrt{h}}\frac{dh}{dx} \tag{4.4}$$

In which k is a coefficient that is primarily wave period dependent. This function describes local variation in the reflected flux per unit of the incident flux and per volume of the beach profile. By integrating the surf profile energy balance (Eq. 4.4) and substitute Eq. 4.4 in Eq. 4.3, the following equation holds:

$$x = \left(\frac{h}{A}\right)^{\frac{3}{2}} + \frac{B}{A^{\frac{3}{2}}}h^3 \; for \; 0 \leq x \leq x_r \tag{4.5}$$

Where $A = \left[\frac{24D_b^*}{5\rho g^{\frac{3}{2}}\gamma^2}\right]^{\frac{2}{3}}$, $B = \frac{k}{5}$, using the relation $D^* = \frac{5}{24}\gamma^2\rho g^{\frac{3}{2}}$ and x_r is the distance between the mean sea level and the discontinuity point.

In the case of a bi-polynomal EBP, the surf zone is expressed by two terms; the first describes the wave dissipation, the second reflection. Note that the first term would be obtained in a case while only considering dissipation, as was done in the Dean (1977) profile and is characterized by the A ($m^{\frac{1}{3}}$) coefficient. By accounting the reflection phenomenon in the model, the second term appears and is characterized by B ($m^{\frac{-3}{2}}$).

Shoaling Profile Previous work by Bruun (1954) concluded that the bottom friction dissipation beyond the surf zone can be assumed constant. Applying this in the shoaling profile energy balance yields:

$$\left[\frac{dF_I}{dx} - \frac{dF_R}{dx}\right] = D_f^* = cte \tag{4.6}$$

In which D_f is the dissipation by bottom friction per unit area.
To reformulate Eq. 4.6, the function $V(x)$ will be similarly defined for the reflected flux as happened for the surf profile. By assuming a shallow water depth in the shoaling profile with constant bottom shear stress per unit area, the relationship between depth and wave height is given by[1]: $H = \left[\frac{H_{sa}}{h_a}\right]\sqrt{h}$

h_a	=	maximum profile depth in which the shallow-water assumptions can be satisfied, in the case where the horizontal length scale of the incoming waves is much greater than the vertical length scale	$[m]$
H_{sa}	=	corresponding wave height reaching the depth h_a	$[m]$

Using this relationship and integrating the energy balance for the shoaling region (Eq. 4.6), yields in the following expression:

[1]The offshore limit of the shoaling profile can be roughly estimated by, $h_a \sim 3.5H_s$, based on the highest incoming significant wave height in the applied wave heights in the month prior to EBP model calibration (Bernabeu et al., 2003)

$$X = x - x_0 = \left(\frac{h}{C}\right)^{\frac{3}{2}} + \frac{D}{C^{\frac{3}{2}}}h^3 \quad for \quad x_r \leq x \leq x_a \tag{4.7}$$

In which $C = \left[\frac{24D_f^*}{\rho g\sqrt{g}H_{sa}}\right]^{\frac{2}{3}} = \left[8c_f H_{sa}\sqrt{h_a}\right]^{\frac{2}{3}}$, $D = \frac{k'}{3}$ and x_o is the distance between the virtual origin of the shoaling profile and the beginning of the surf profile. Here, c_f is a friction coefficient and k' is defined as shoaling profile reflection coefficient. Comparison of the surf and shoaling profiles show similar expressions for both profiles, with a horizontal displacement of x_0 for the shoaling profile. Another improvement of the bi-polynomal EBP compared to previous works is that the morphological coefficient C ($m^{\frac{1}{3}}$) now also depends on the wave height, not just the energy dissipation, thereby more accurately reproducing the beach shape.

Offshore Limit The validity of the proposed EBP is based on the dissipation and reflection of incoming wave energy. Therefore, the offshore limit for this EBP is the extent of where the waves first start dissipating wave energy. In other words, the depth of closure (DoC) is used as the offshore limit. The location of the DoC is defined as the most seaward location of which there are no significant changes in bottom elevation over time (Coelho et al., 2006). Nourishment design is also based on the offshore limit of the EBP. In case of intersecting lines between the initial and the equilibrium profile, the initial profile holds more volume of sediment compared to the EBP. Therefore, no need for a surplus of material to extend the profile to the DoC is needed.

However, nonintersecting profiles, which occur in most beach nourishment projects, always extend out to the DoC. In this case the nourished equilibrium profile is extended to the DoC and then, from this point, the beach profile continues with a constant slope shape to intersect the native profile normally associated with the underwater angle or slope of repose of the material. The best option to determine the DoC is to carry out an empirical analysis with the existing profile data of the study area. This work of estimating the DoC in the case of Nags Head is previously done by comparing changes in cross-shore profiles over time, and is approximately at 7.5m of depth, based on a maximum annual profile variation of 0.1m (CSE, 2017). In the current application, the DoC is located within the boundaries of the depth in which the shallow-water assumptions are satisfied for the EBP ($h_a \approx 3.5H_a \approx 9m$).

4.2 EBP Functionality

It is not the first time that simpler variants of the bi-polynomal profiles based upon summing two Dean profiles have found successful applications, e.g. Inman et al. (1993); Larson et al. (1999); Medina et al. (2001). By taking wave reflection into consideration, significant improvements have been made for developing an EBP profile.

This section will check if the equilibrium profile can accurately adapt to varying scenarios. Here, the model coefficients will be compared with the grain size and wave climate to determine if it can accurately reproduce profile morphology.

In order to improve the EBP applicability, an approximation for the shape parameters A, B, C and D is attempted to be established by using different dimensionless variables (Bernabeu et al., 2003). This work concluded that the best fit was found by using the dimensionless fall velocity to approximate the shape parameters: $\Omega = \frac{H}{wt}$.

In which, H is the significant wave height, w is the fall velocity and t is the period. Among others, the main advantage of using the dimensionless fall velocity for the approximation is that it automatically includes sediment characteristics in the fall velocity w. By including the sediment characteristics in the EBP equations, the model can be validated to determine whether the profile is capable in shifting between reflective and dissipative beach states (Dean, 1977).

Over 50 profiles were correlated to best fit using Eqs. 4.5 and 4.7 in order to determine the relationship between the shape parameters (A, B, C, and D), the discontinuity point location (x_r, h_r), and the wave or the sediment characteristics of the beach.

Results of this best-fit technique using the dimensionless fall velocity obtained the following expressions to compute the EBP:

$$A = c_1 - c_2\Omega,\ B = c_3 \exp(-c_4\Omega),\ C = c_5 + c_6\Omega,\ D = c_7 \exp(-c_8\Omega) \tag{4.8}$$

$$x_r = \left(\frac{h_r + M}{A^R}\right)^{\frac{3}{2}} + \frac{B}{A_R^{\frac{3}{2}}}(h_r + M)^3$$

$$\mathrm{h}_r = c_9 H_{sa}$$

In which c_{1-9} stands for site-specific calibration parameters and M the average spring tidal range. The dimensionless fall velocity will be changed from dissipative to reflective beach states to see if the EBP is able to reproduce such results. Table 4.1 shows the generic outcomes of changing this parameter, and Figures 4.3 and 4.4 show the EBPs in both respective beach states. Results show that each morphological coefficient describes either the dissipation or reflection phenomenon in both profiles.
Coefficients A and C show to be directly proportional to the slope of the surf or shoaling profile respectively. Higher values for the dimensionless fall velocity causes widening of the beach profile, coinciding with a dissipative beach state. A reflective beach state is found for lower values.
Coefficients B and D show a relation with the concavity of the profiles. In highly dissipative beaches, the beach reflection is assumed to be insignificant, which the results clearly show. Changing the EBP to a dissipative state shows that the values for B and D approach zero, thereby canceling the wave reflection effects. Including this ability of changing beach state improves the model applicability significantly as it's able to adapt to seasonal variabilities.

Table 4.1: Relationship between dimensionless fall velocity (Ω) and the proposed EBP.

Ω ↑	*Surf Profile*	A ↓	Flattened upper part	Dissipative profile
		B ↓↓	Steep lower part	
	Shoaling Profile	C ↑	Steep upper part	
		D ↓↓	Steep lower part	
Ω ↓	*Surf Profile*	A ↑	Steep upper part	Reflective profile
		B ↑	Flattened lower part	
	Shoaling Profile	C ↓	Flattened upper part	
		D ↑	Flattened lower part	

In dissipative beaches with high Ω values, the proposed EBP defines a surf profile characterized by a smooth initial slope and a very steep shoaling profile (Figure 4.3). In contrast, the proposed EBP of reflective beaches with low values of Ω, show very steep surf profiles and flat shoaling profiles, such as the discontinuity point, are difficult to identify (Figure 4.4). Functionality checking of the proposed EBP therefore shows that the model is capable of switching morphological beach states and this information is compiled in the EBP shape parameters.

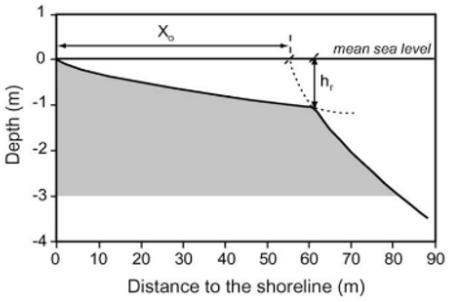

Figure 4.3: Dissipative profile morphology

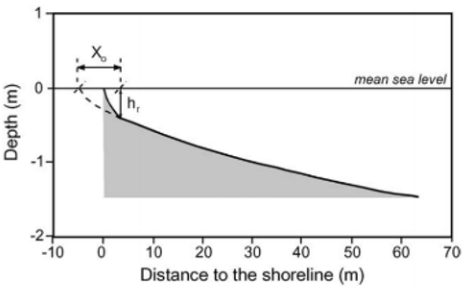

Figure 4.4: Reflective, after (Bernabeu et al., 2003)

4.3 Equilibrium Beach Profile Calibration

Section 4.2 - EBP Functionality already has proposed that the best fit for the EBP shape parameters (A, B, C and D) is found by using the dimensionless fall velocity. By doing so, the expressions from Eq. 4.8 were obtained.

Previous works regarding EBP calibration (González et al., 2010) used 50 different beach profiles along 13 different beaches located on the Spanish coast to find a calibration set applicable to the entire coast of Spain. The calibration process was done by randomly sampling the unknown constants (c_{1-9}) within user-specified ranges and express the difference in the predicted and observed bed profiles by a cumulative mean-squared error and qualitatively (by eye). After calibration, the relationship between; the sediment- and wave-data (D_{50} and H_s) of a beach profile, the intercepting profile points (X_r and H_r) and its corresponding shape parameters (A, B, C and D) was found in which the EBP could accurately predict the beach profile.

A similar calibration technique is applied for the Nags Head case. The major difference, however, is found in selecting the beach profiles for calibration. Where previous studies tried to find a best fitting EBP for countries or regions, this study will only use local beach profiles in the Nags Head vicinity. The advantage of using only local profiles outweighs the benefit of a more universe applicability of the calibrated EBP by introducing a higher beach profile fitting accuracy.

Furthermore, beach profiles along the Outer Banks and the rest of the US East coast show stronger uniformities compared to Spanish coasts, reducing the generic applicability even further. By using only site specific beach profiles, possibly interestingly applications are introduced regarding site specific nourishment design efficiency rates, which will be explored in detail in Chapter 7 - Practical Application. Beach profiles of all 107 stations at Nags Head were used to calibrate the local EBP, the results are summarized in Table 4.2 and are as follows:

$$A = 0.15 - 0.01\Omega, \quad B = 0.005 + 0.26\exp(-0.75\Omega) \tag{4.9}$$

$$C = 0.611 + 0.025\Omega, \quad D = 0.506 + 0.1\exp(-0.03\Omega)$$

$$x_r = \left(\frac{h_r + M}{A}\right)^{\frac{3}{2}} + \frac{B}{A^{\frac{3}{2}}}(h_r + M)^3, \quad h_r = 1.1H_{sa}$$

4.3.1 Results

Figures 4.5a,b show an example of the EBP plotted over the beach profile of station 545+00 and 930+00 in 2016. Accuracy of the EBP model calibration is expressed by a cumulative mean-squared error and resulted in respectively $R^2 = 0.9521$ and $R^2 = 0.9378$ for the north and south representative profiles. Results therefore show that profiles in north Nags Head are better calibrated and fitted to the EBP compared to profiles in the south. Two representative profiles for each reach including the EBP are found in the series of figures in Appendix B - Equilibrium Beach Profiles.

Compared to the initial profile, the EBP in both cases only shows a mild discontinuity between the shoaling and the surf zone, resulting in a rather smooth profile around the hinge point. As the concavity per section is dominated by the wave reflection parameters, the current applied incoming waves and tidal data are of a less reflective character. The explanation of the surf profile in section 4.1 - Theoretical Background has shown that whenever the reflection coefficient is neglected, the EBP would follow the Dean (1977) profile. The relative effect wave reflection influences the EBP shape can therefore be determined as: $B/A \sim 1 : 4.5$. Wave dissipation effects are thus ~4.5 times as high compared to wave reflection effect, confirming that the initial profile is in a dissipative state. Which means that the overestimation of the wrong directed reflection induced orbital velocity is insignificant as compared to the dissipation induced velocities

The averaged monthly wave statistics in Figure 3.7 show that between January and April, a relatively rough wave climate prevails. High waves caused by so-called Nor'easters result in increasing wave energy approaching the Nags Head shoreline. As a result the beach profile shapes into a dissipative beach state, thereby extending the cross-shore profile and allowing more wave energy dissipation and loosing its reflective characteristic. The bathymetry survey was performed early June in 2016, only days after the last significant storm impact. A dissipative shape for both the EBP and the beach profile are therefore to be expected which are both clearly visible from Figures 4.5a,b and the series of figures in Appendix B - Equilibrium Beach Profiles.

Moreover, comparison of beach profiles between the north and south of Nags Head shows that the EBP follows the initial profile more accurately in the north as opposed to the south, as is to be expected. Erosion and longshore transport rate analysis in section 3.4 - Erosion and Longshore Variabilities already showed a strong increase in longshore transport rates from north to south, with rates ~2.5 times as high in the south. Higher erosion rates indicate that the beach profiles are further from an equilibrium state and as the EBP shape has no longshore variability, the vertical deviations between the initial profile and the EBP should increase towards the south as well which is clearly visible. This confirms the applicability of concept of EBP to approximate the beach profiles at Nags Head and allows for shoreface nourishment design using such concept.

Table 4.2: Input and calibrated applied parameters for the EBP model.

Ω	H_{sa}	M	A	B	C	D	x_r	h_r
3.345	1.54	1.5	0.117	0.026	0.695	0.597	164.88	1.694

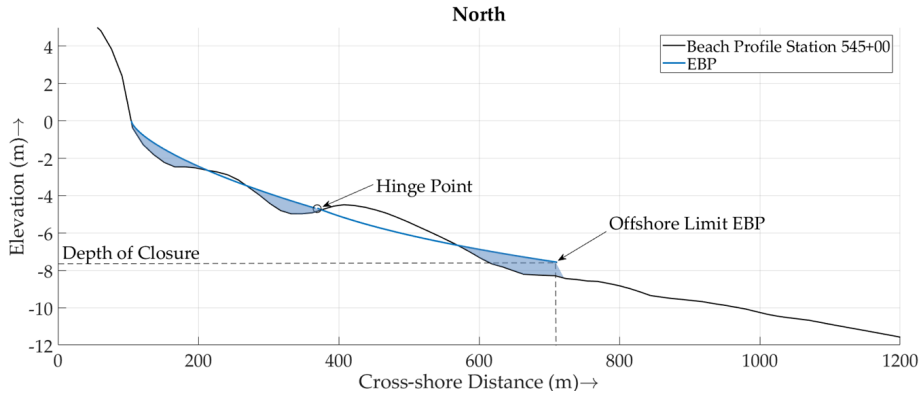

(a)

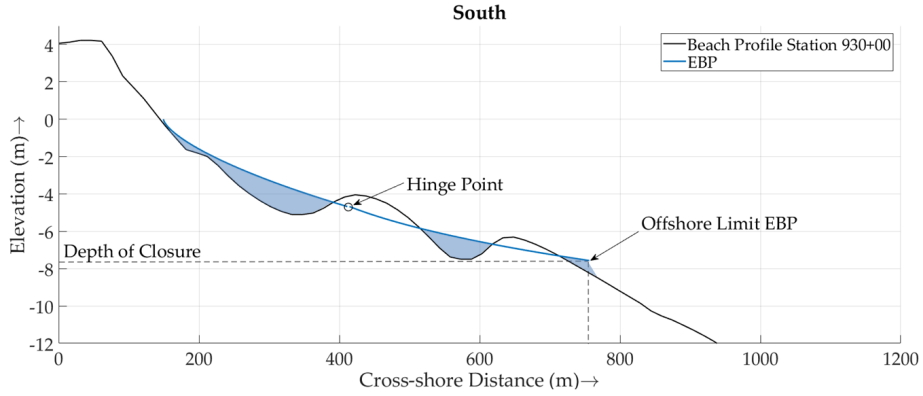

(b)

Figure 4.5: Example of an Equilibrium Beach Profile plotted over the initial cross-shore beach profile at a representative station at the north of Nags Head (a: 545+00, $R^2 = 0.9521$) and in the south (b: 930+00, $R^2 = 0.9378$). Highlighted areas show the EBP-design nourishment fill template.

4.4 Discussion

Recent studies regarding the fitting of bi-polynomal equilibrium beach profiles (with the hinge point between the surf and shoaling zone to fit the initial beach profile), verified the fitting accuracy compared to unique curve models (Larson et al., 1999). Adding the beach reflection parameters in the fitting process resulting in a variable concavity per beach section certainly enhances the shape-fitting ability to approximate the natural profile. This static approach for beach profile approximations is preferred over the use of dynamic profiles, mainly because of its restrictions for an universal application. The current application of a bi-polynomal allows for a quick assessment using only one beach profile dataset and historical wave data, compared to an more intensive and costly periodical beach profile dataset highlighting the profile development over the years resulting in a dynamic EBP. Not only is the static approach for an EBP-based nourishment design cheaper and higher in applicability, the model can also be calibrated site-specifically, showing interesting morphological features while looking at the discrepancies between the initial beach profile and the EBP. These morphological features are studied in detail in the final Research Question in Chapter 7 - Practical Application.

Functionality checking of the proposed EBP shows that the model is capable of switching morphological beach states and this information is compiled in the EBP shape parameters. The effect of the introduced reflection parameters are clear from changes in B and D for the surf and shoaling profiles respectively, where lower values indicate a higher dimensionless fall velocity corresponding to a more dissipative and reflective profile and vice versa. The A and C parameters contain the dissipation processes and are therefore responsible for mean slope of the surf and shoaling zone respectively.

This ability to reproduce profile morphology and seasonal variations are meaningful to address, due to the underlying economic assets these profiles might have for coastal engineering applications, particularly for sand volume estimations. The few studies trying to reflect second-order morphological features of profile discrepancies such as sand bars result in complicated mathematical expressions with little to no practical use. In the current application after calibration, all profiles show a strong correlation between the natural initial profile and the proposed EBP, with found R^2 values of 0.9521 and 0.9378. These values are only marginally lower as compared to the values found in the Bernabeu et al. (2003) study, where these values ranged between 0.944 and 0.999, making the current calibrated is a good fit as compared to previous literature. This new proposed EBP model is thus capable of estimating the beach morphodynamic states knowing the sediment characteristics and the forcing agents' variability and will be further explored in Chapter 7 - Practical Application.

4.5 Summary

The proposed EBP is based on a bi-polynomal figuration where the division between the surf and shoaling profile acts as a hinge point. The main emphasis is to improve the fitting accuracy including second-order morphodynamics such as an offshore sand bar by adding the beach reflection phenomena in the model fitting derivations. By modeling the surf and shoaling profile indifferently, the beach concavity as expressed in the reflection parameters are optimized. The results is an accurate representation of the beach profile and the ability to reproduce the beach morphodynanamics by changing in either dissipative or reflective states, depending on the forcing agents, making it a possible practical tool in coastal engineering.

The remainder of this study uses the EBP for shoreface nourishment design. The shape parameters are therefore calibrated accordingly to the Nags Head project by randomly sampling the unknown constants (c_{1-9}) within user-specified ranges and express the difference in the predicted and observed bed profiles by a cumulative mean-squared error. After calibration, the relationship between; the sediment- tidal and wave-data (D_{50}, average spring tidal range and H_s) of a beach profile, the intercepting profile points (X_r and H_r) and its corresponding shape parameters (A, B, C and D) was found. Increasing incoming wave energy widens the EBP and transforms it into a dissipative state by decreasing A and increasing C. The beach reflectivity is included in the surf and shoaling profile concavity, where a stronger effect of wave reflection happens by increasing the concavity parameters B and D. The effect of the tide is included by adding the average spring tide elevation in the calibration process.

5

Cross-shore Nourishment Effects

How do cross-shore transport rates lower while reshaping the cross-shore profile towards an EBP using nourishments compared with conventional nourishment designs?

5.1 Introduction

The previous chapter showed the concept of equilibrium beach profiles and how the shape depends on the wave climate and sediment characteristics. With constant waves and water level, the beach profile evolves to a stable form in which the net cross-shore sediment transport approaches zero (Wang and Kraus, 2005). In this chapter the relation between cross-shore sediment transport and the incoming wave climate is analyzed to determine if the shape of a nourishment design can lower the wave-induced cross-shore transport and thereby reduce the coastline erosion.

The concept of assuming constant wave energy dissipation while deriving an equilibrium beach profile bring cause to several practical beach profile evolution and cross-shore sediment-transport models (e.g. Kriebel and Dean (1985)) and will furthermore be extrapolated in this study.
While developing the equilibrium beach profile theories, dissipation of wave energy is associated to represent the average condition of the wave climate. In reality, however, the beach profile is subject to varying forcing agents, thus generating variable wave energy dissipation rates. Higher dissipation rates are observed during storms as are strong morphological changes in the beach profile.

Knowing this, a relation between the cross-shore sediment transport rates and the deviation between the equilibrium beach profile and its corresponding evolution due to such forcing agents can be developed:

$$q = K(D - D^*)^n \tag{5.1}$$

Stating that beach profile evolution and resulting cross-shore sediment transport depend on how far the new profile deviates from the EBP. Where K and n are empirical coefficients and D^* is the wave energy dissipation rate corresponding to a stable cross-shore profile with a net cross-shore transport rate of zero.

A large-scale laboratory experiment was performed to visualize wave energy dissipation patterns over a Dean (1977) equilibrium beach profile (Wang and Kraus, 2005). Different regular and irregular wave conditions were applied in the SUPERTANK laboratory over a non barred profile to analyze cross-shore sediment transport and wave dissipation over the profile. All tests show strong agreement in the cross-shore morphological behavior, with bar development at the main breaker line. Results concluded that strongest changes in net cross-shore transport rates occur at locations where dissipation of wave energy differs most considerably from the equilibrium rate. This increase in cross-shore transport might result in coastline retreat, which might harm vulnerable structures or dunes.

Furthermore, with any kind of nourishment design, the beach profile has to re-adjust to the incoming wave climate by redistribution of the sediment over the profile. Just like conventional beach nourishment high in the profile, the sediment is transported elsewhere in cross-shore direction for a (temporal) new equilibrium profile. During this redistribution process, sediment is either transported via bed-load or suspended load. The moment sediment gets in motion, the possibility arises that it either gets transported out the domain of interest by either the offshore depth contour (DoC) or in longshore direction out of the study area. Reasoning behind this possibility is that whenever the beach profile has to increase the total volume of sediment redistribution after nourishment, then more sediment is lost thereby lowering the nourishment efficiency. This feature is also the main tenet of using a static EBP for such design. By reshaping the beach profile using nourishments based on the concept of (optimal) wave energy dissipation and wave reflection, the distribution of wave energy dissipation follows the equilibrium wave energy dissipation distribution more closely, thus lowering the total volume of cross-shore sediment transport (Eq. 5.1). In addition, the possibility of losing sediment in the redistribution process lowers as well, increasing the nourishment efficiency along these lines.

5.2 Methodology

Since the concept of a bi-polynomal EBP is largely based on equilibrium of wave energy dissipation, it is hypothesized that cross-shore transport rates also reduce in a varying real-time wave climate if the beach profile follows the EBP, as is reflected in the research question. To answer the research question, a modeling study is set-up in UNIBEST-TC, see Bosboom et al. (2000). Using this model, the cross-shore behavior of different shoreface nourishment profiles are checked, to examine the effects of how the shape of the cross-shore profile will influence wave energy dissipation and wave height are examined.

First, the selection of UNIBEST-TC is substantiated with the modeling approach and model schematization, after which the hydro- and morphodynamic characteristic of the applied beach profiles are described. A model is set up and calibrated on the morphological behavior of the study area and the EBP is calibrated to the cross-shore profiles measured in this study area.

Different shoreface nourishment designs will be tested with this model to compute which design adapts the wave energy dissipation in such a way that the cross-shore transport rates are lowered most effectively (see Eq. 5.1). Also the changes in wave height throughout the profile are checked. The calibrated EBP will be used to shape the 'EBP-design' and is compared with conventional nourishment designs. These conventional shapes will be explained and resized so that all different nourishment designs will have the same fill density, in order to compare each other's results. This approach is applied for two different cross-shore profiles surveyed at two different years, resulting in a total of four individual studies. By looking at several profiles variable over time the sensitivity of varying wave climate and bathymetry is incorporated. Validation of the morphological response is carried out based on the analysis of sediment transport volumes.

5.3 Modeling Approach

The UNIBEST-TC cross-shore profile model is used to study sediment transport and morphologic profile development in the cross-shore direction. The model assumes a sandy uniform coast and computes cross-shore sediment transport and the resulting profile changes under the combined action of waves and longshore tidal currents. Longshore tidal currents were generated in the model with tidal constituents, and the nearshore wave transformation of the wave conditions at the open boundaries are calculated using SWAN, see Booij et al. (1999). The UNIBEST-TC model is chosen as the model is capable of producing results on seasonal to multi-annual time scales (Pape et al., 2010; Ruessink and Kuriyama, 2008).

One of the main advantages of using a cross-shore profile model over the use of a coastal area model is the rather low amount of computational cost per run. This way, efforts to reduce the computational time such as wave reduction techniques proposed in Walstra et al. (2013) are unnecessary and the original chronology of the wave climate is preserved, which will highly increase the model's accuracy in computing the wave energy dissipation.

Furthermore, a study on shoreface nourishments using a coastal area model checked the influence of rearranging the wave climate chronology (Hartog et al., 2008). The authors found a large variation in morphodynamic response in the model due to changes in the wave schematization and emphasizes the importance of the selection of the wave conditions in predicting the beach nourishment behavior of wave event-driven area.

5.3.1 Schematization UNIBEST-TC model

UNIBEST-TC stands for UNIform Beach Sediment Transport Time dependent Cross-shore and is a model which computes sediment transport and bed-level evolution by taking into account coupled wave-averaged equations of mean currents, waves and wind. Simulations are run under the assumptions of a longshore uniform coast with parallel and straight depth contours. By using offshore boundary conditions and an initial bed profile the hydrodynamics and sediment transport rates in the cross-shore profile are computed.

Computations are performed by using 6 different coupled sub-modules as follows: first, by use of the boundary conditions, the wave propagation module is updated over the initial profile, which in turn drive the wave orbital velocity and the mean current profile modules. Gradients in these modules drive the bed-load and suspended load transport models to compute the final bed level change module. Via a feedback loop the bed level module is coupled at the subsequent time step to the wave propagation module, forming a coupled model, see Figure 5.1. A detailed description of the model is shown in (Ruessink et al., 2007). Summary of the model formulations is found in the UNIBEST-TC technical reference (Bosboom et al., 1997).

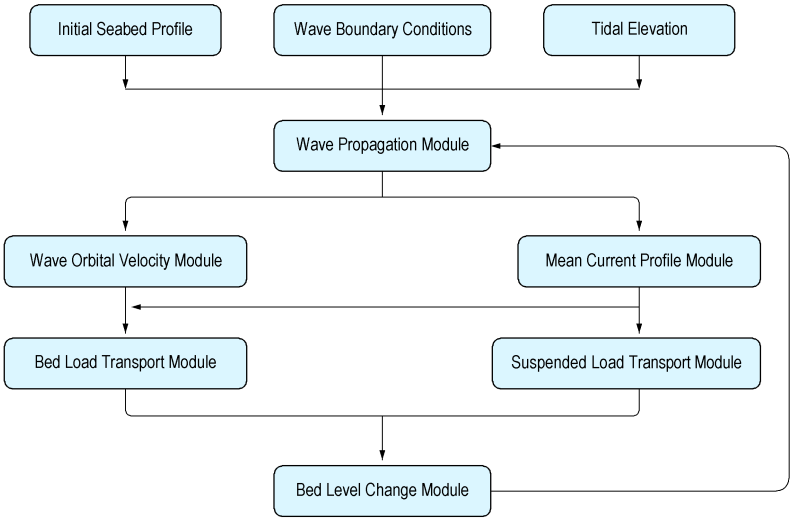

Figure 5.1: UNIBEST-TC model schematization.

5.3.2 Main Sediment Transport Formulations

It has been previously stated in Chapter 4.1 - Theoretical Background and 5.1 - Introduction that the amount of cross-shore sediment transport is dependent on the distribution of wave energy dissipation, which in turn has a strong dependency on the incoming wave climate and the beach profile. The previous research question already hypothesized that the transport rates are lowered by shifting the beach profile into a more equilibrate state.

This chapter therefore analyzes how incoming waves influence the sediment transport formulae applied in the UNIBEST-TC model and how changes in the beach profile will lower the transport rates while relating them to the wave climate. To do so, a summary of the main sediment transport formulations is listed:

Bed-load Transport Formulations: A generalized equation for bed load transport is obtained by correlation of non-dimensional parameters obtained from different sediment transport datasets containing oscillatory flow over horizontal beds (Ribberink, 1998). Complemented with a correction factor for the slope, the following formulation is used in the model:

$$\Phi_{bd}(t) = \frac{q_b(t)}{\sqrt{\Delta g d_{50}^3}} = 9.1 \frac{\beta_s}{1-p} \{|\Theta'(t)| - \Theta_{cr}\}^{1.8} \frac{\Theta'(t)}{|\Theta'(t)|} \tag{5.2}$$

$\Phi_{bd}(t)$	=	Non-dimensional bed-load transport vector	[-]
q_b	=	Bed-load transport rate in volume per unit width and time including pores	$[m^3/ms]$
g	=	Gravity acceleration	$[m/s^2]$
d_{50}	=	Median grain size diameter	$[m]$
Δ	=	$(\rho_s - \rho_w)/\rho_w$ = Relative density	[-]
β_s	=	Slope correction factor	[-]
p	=	Porosity	[-]
Θ'	=	Dimensionless effective shear stress	[-]
Θ_{cr}	=	Dimensionless critical shear stress	[-]

The dimensionless effective shear stress is computed using:

$$\Theta'(t) = \frac{0.5 \rho_w f'_{cw} |u_b(t)| u_b(t)}{(\rho_s - \rho_w) g d_{50}} \tag{5.3}$$

f'_{cw}	=	Weighted friction factor, accounting both current and wave friction	[-]
u_b	=	Time dependent, intra wave, near bottom horizontal velocity vector of the combined wave-current motion	$[m/s]$

Suspended Transport Formulations: The suspended sediment transport is computed from the vertical distributions of sediment concentrations and velocities and is as follows:

$$\tilde{q}_s = \int_a^h vc dz + \int_a^h \tilde{v}\tilde{c} dz \tag{5.4}$$

$\bar{q}_s$	=	Suspended transport rate averaged over space and time	$[kg/m^3]$
a	=	Thickness of the bed-load layer	$[m]$
h	=	Water depth	$[m]$
v	=	Fluid velocity averaged over space and time at height z above the seabed	$[m/s]$
c	=	Sediment concentration averaged over space and time at height z above the seabed	$[kg/m^3]$
$\tilde{v}$	=	Oscillating velocity component, including turbulence	$[m/s]$
$\tilde{c}$	=	Oscillating concentration component, including turbulence	$[kg/m^3]$

It is assumed that the current related suspended sediment transport is dominant over the wave related suspended sediment transport. The total suspended sediment transport per unit width and time, including pores, is therefore computed as:

$$q_{s,c} = \frac{\int_a^h vcdz}{(1-p)\rho_s} \tag{5.5}$$

Where $q_{s,c}$ is the suspended sediment transport per unit width and time, including pores $[m^3/ms]$. The sediment concentration (averaged in time and space) is computed by solving the following equation:

$$w_{s,m}.c + \phi_d.\epsilon_{s,cw}\frac{dc}{dz} = 0 \tag{5.6}$$

$w_{s,m}$	=	Fall velocity of the suspended sediment in a fluid sediment mixture	$[m/s]$
ϕ_d	=	Damping factor dependent on the concentration	[-]
$\epsilon_{s,cw}$	=	Sediment mixing coefficient for combined action of waves and current	$[m^2/s]$

To solve the averaged sediment concentration, numerical integration using a concentration type boundary condition has to be applied. This boundary conditions is given by:

$$c_a = 0.015\rho_s\frac{d_{50}}{a}\frac{T^{1.5}}{D_*^{0.3}} \tag{5.7}$$

a	=	The maximum value of the current and wave related roughness heights	$[m]$
T	=	The dimensionless bed shear stress parameter	[-]
D_*	=	The non-dimensional sediment grain size	[-]

The dimensionless bed shear stress parameter T is computed as:

$$T = \frac{\tau_{b,cw} - \tau_{b,cr}}{\tau_{b,cr}} \tag{5.8}$$

$\tau_{b,cw}$	=	Time averaged effective bed shear stress	$[N/m^2]$
$\tau_{b,cr}$	=	Time averaged critical bed shear stress, according to Shields	$[N/m^2]$

Overview Equation 5.2 shows that the relation between the wave climate and the non-dimensional bed load transport vector is largely influenced in the differences between the effective and critical dimensionless shear stress ($\Theta'(t)$–Θ_{cr}). The same type of relationship is found in the suspended sediment transport (Eq. 5.4). Here, the sediment transport is determined by the factor of the velocity and sediment concentration. The reference concentration (c_a) at a computed reference level (a) depends on the dimensionless bed shear stress parameter T, which in turn depends on the difference in the time-averaged effective bed shear stress and time averaged critical bed shear stress according to Shields ($\tau_{b,cw} - \tau_{b,cr}$).

The incoming waves drive the near bottom velocity vector, which will be higher with increasing wave energy. Therefore, in order to decrease the sediment transport and the stirring of sediment, the effective shear stress should be reduced to approach the critical shear stress. This is possible by making vertical adjustments in the beach profile, since the near bottom velocities will decrease with increasing water depth.

A beach profile with zero time-averaged sediment transport is therefore distributing the wave energy in such a way that the effective shear stress is approaching the critical shear stress throughout the profile. The profile is then allowing the maximum amount of wave energy dissipation per cross-shore location, without inducing time-averaged sediment transport. Such a profile could therefore be hypothesized as the corresponding profile for D^*, the wave energy dissipation rate corresponding to a stable cross-shore profile with a net cross-shore transport rate of zero. Furthermore, the EBP as proposed in Chapter 4 - Equilibrium Beach Profiles is also based on distributing the wave energy in a way to minimize the time-averaged sediment transport. This means that the main benefit of using an EBP to re-shape the cross-shore beach profile is that the effective shear stress automatically approaches the critical shear stress and thereby reduces the transport rates more effectively compared to the original beach profile.

5.3.3 Model Set-up

The UNIBEST-TC model is first set to compute the morphological behavior of a cross-shore profile in Nags Head for calibration purposes. After calibration, the model is used to compute differences in wave energy dissipation using different shoreface nourishment designs, including nourishment designed using an EBP. As the model only computes the hydrodynamic and morphodynamic processes of one cross-shore profile, a representative profile is chosen. Due to the presence of an offshore ridge at the south of Nags Head, which might influence offshore wave translation, a station in north Nags Head is applied in the model. After visual inspection, station 930+00 is chosen to best represent the full cross-shore characteristics without significantly affecting nearshore wave translation (CSE, 2017). After calibration, the shoreface nourishment effects comparison study is performed over two cross-shore profiles (station 520+00 and station 930+00) using two different survey data sets (2009 and 2016).

The main modeler agents for the model (H_{rms}, T_p, $^\circ$ and η) are used as offshore wave boundary conditions for the model and are obtained from the WIS 63220 station, see section 3.5 - Hydrodynamics. The offshore distance of this station is ~17 km, whereas the maximum allowed offshore model distance is 5 km. Previous studies (CSE, 2017) have shown that offshore wave translation is unnecessary at Nags Head as the water is deep enough to not influence this translation. Therefore, the wave time series from WIS 63220 is directly applied in the UNIBEST-TC model. Water level elevation data is obtained from the Duck FRF tidal gauge ~25 km north of Nags Head. Average D_{50} and D_{90} for station 930+00 were taken as 0.350 mm and 0.420 mm respectively (CSE, 2011a).

5.4 Model Calibration

The model is calibrated on the morphological dynamics of station 930+00 in the period March 2009 to October 2010, resulting in a 20 month model run. This period was chosen as the town of Nags Head was in a pre-nourishment construction phase (which started construction in 2011), so accurate survey data was available. Also, no significant storm impacts due to hurricanes occurred at Nags Head during that period of time. The calibration period for the 2016 dataset is between the June 2016 and the June 2017 survey, encompassing a total duration of 12 months. Calibration procedure is based on Ruessink et al. (2007), which indicates that the calibration parameters can be limited to the maximum stable angle slope ($\tan(\phi)$), scale factor for vertical viscosity distribution for undertow (α_w) and the current-related roughness (k_c). This same study regarding UNIBEST-TC calibrations show strong agreements upon this calibration method and have shown realistic results. Model settings after calibration for the Nags Head case are compared with earlier mentioned UNIBEST-TC researches in Table 5.1. Results show that the found parameter setting for the Nags Head model lie well within the boundaries of acceptable application.

The variation in grain size distribution differs largely along the cross-shore profile. Smaller particles are easier transported offshore while coarse sediment accretes around the shoreline. The focus on this part of the study is to analyze the sediment redistribution before and after nourishment. It is therefore decided to place a fixed layer from the top of the dune to ~ -1m below MSL and is denoted with x_{fix}. By doing so, all morphological features are focused on offshore phenomena like bar migration and decay, and sediment redistribution. Since the median grain size is lower as compared to the average d_{50} of the entire cross-shire profile, the applied d_{50} is reduced from 0.420mm to 0.350mm to better approximate the offshore sediment characteristics. Moreover, a sensitivity analysis on the grain size distribution is performed and is shown in Appendix C.2 - UNIBEST-TC. Here, the grain size is lowered to match the measured d_{50} of the outer bar resulting in higher concentrations of suspended sediment and thereby an over-prediction in offshore directed transport. The remainder of the report therefore uses d_{50} = 0.350mm, d_{90}=0.420mm and d_{ss} = 0.340mm.

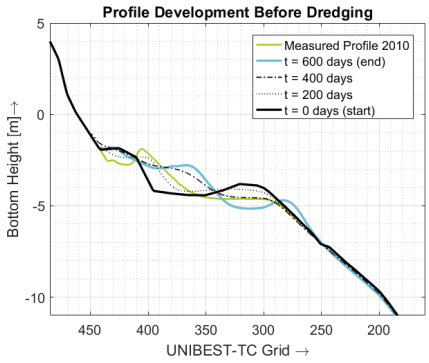

Figure 5.2: Beach profile development of the BD scenario at station 930+00 between March 2009 and October 2010.

Table 5.1: Model settings after calibration for the Nags Head model, compared to model settings as found in the study of Ruessink et al. (2007).

Location	α_w	$tan(\phi)$	c_r	k_c
Nags Head	**0.100**	**0.170**	**0.001**	**0.055**
Duck94	0.077	0.466	0.001	0.027
Hasaki	0.056	0.141	0.093	0.037
Duck 1982	0.120	0.253	0.011	0.059
Egmond	0.106	0.102	0.001	0.061

5.4.1 Shoreface Nourishment Evaluation

Effects of shoreface nourishments have been studied all over the world for the past couple of decades, with results showing that such nourishments can have fruitful applications in reducing the significant wave height and longshore transport rates, e.g. Dean et al. (1997).

Recent work by Van Duin et al. (2004) examines effects of shoreface nourishment effects by setting up a modeling study and comparing its results with the 1999 Egmond aan Zee (NL) shoreface nourishment. With high-resolution bathymetry surveys, changes in the cross-shore volume was measured to see the morphological changes of the nourishment in time. Later, hindcast models were set up to reproduce this nourishment behavior in order to compute the nourishment effects. The study concluded that the main purpose of constructing shoreface nourishments were their function as of a submerged breakwater or a reef, creating a shelter zone shoreward of it that influences longshore and cross-shore sediment transport. The main driving processes for the efficiency of shoreface nourishments were furthermore defined as; processes that can be described by an increase of net onshore transport (feeder effect) and a reduction of longshore transport behind the nourishment (lee effect).

To check these effects, changes in significant wave height throughout the profile and differences in longshore transport rates are measured. Also, the main emphasis of this research question is to lower cross-shore transport rates by shifting the cross-shore profile to a more equilibrated state so that wave energy will be dissipated more efficiently, see Eq. 5.9. This is done by computing the total volume of the absolute averaged transport rates. Nourishment efficiency is therefore computed by integrating the absolute yearly averaged transport rates over the cross-shore profile from the end of the fixed layer x_{fix} around -1m MSL to the location furthest offshore x_{off}, see Eq. 5.10. Changes in significant wave height and cross-shore sediment transport rates will be computed in this research question, changes in longshore transport rates and gradients in these rates are measured in Research Question 3 with a model better fit for such calculations.

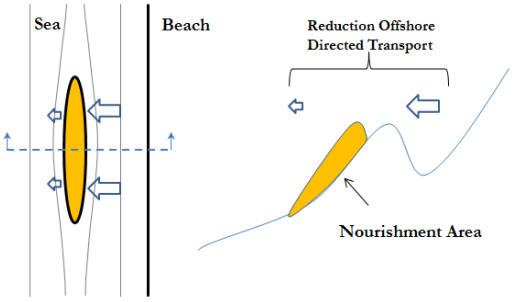

Figure 5.3: Expected cross-shore effects to occur after nourishing the shoreface, i.e. a net reduction in offshore directed transport.

$$q = K(D - D^*)^n \tag{5.9}$$

$$q = \int_{x_{fix}}^{x_{off}} |\bar{q}| dx \tag{5.10}$$

Shoreface Nourishment Effects Comparison Study: As section 5.4 - Model Calibration already introduced, the evaluation of the three conventional shoreface nourishment designs are compared to a fourth alternative, the 'EBP-design', over two different cross-shore profiles measured in two different survey data sets. This is done to implement the sensitivity study of the results with regards to the varying wave climate and bathymetry. All other parameters will remain constant. First the model results of the dataset used to calibrate the model (station 930+00 in 2009) are explained in detail and the differences in effects between each shoreface nourishment alternative are treated. When finished, the results of the same cross-shore profile using a later survey dataset are checked (station 930+00 in 2016) and will finally be compared to the results of another cross-shore profile (station 520+00 in 2009 and 2016).

5.5 Results

First, the model results including shoreface nourishments of Station 930+00 in 2009 are investigated whether the model is capable of accurately incorporating the nourishment design with respect to realistic sediment redistribution (Figure 5.5). Furthermore, significant wave height and cross-shore transport rate distributions are checked during certain storm events to see whether the model is able to accurately produce realistic hydro- and morphodynamics during such events.

Second, the four alternative designs are compared to check the significant wave height and cross-shore sediment transport relative to each other and to the initial situation, the "Before Dredging" scenario. The distribution of the significant wave height over the cross-shore profile for each of the conventional nourishment designs (Alternative 1, 2 and 3) is plotted against the results of the 'EBP-design' (Alternative 4). Results of this comparison are found in Figures 5.7 - 5.10. The significant wave heights shown are time-averaged over the one year model duration.

Third, the total volume of the net cross-shore sediment transport rates are compared between nourishment alternatives. Cross-shore transport rates, averaged over the 20 months modeling period for the different profiles vary substantially. Results of each comparison study are treated separately in the following chapters. A summary of all results is shown in Figure 5.11.

5.5.1 Station 930+00

Storm Impact:

The models ability to reproduce hydro- and morphodynamics are checked by analyzing the significant wave height and resulting cross-shore transport rates of incoming waves with H_{rms} = 2.60m. As the waves propagate to the outer bar, wave steepening and increasing wave height occurs until the largest break over the bar. This wave breaking result in a lower wave height after the breaker bar and a strong net offshore directed sediment transport. Similar results occur when the waves propagate over the swash bar until the waves reach the shoreline. Onshore directed transport is shown before wave breaking due to wave asymmetry, which is directed offshore after breaking. Note that no sediment transport is allowed in the fixed layer.

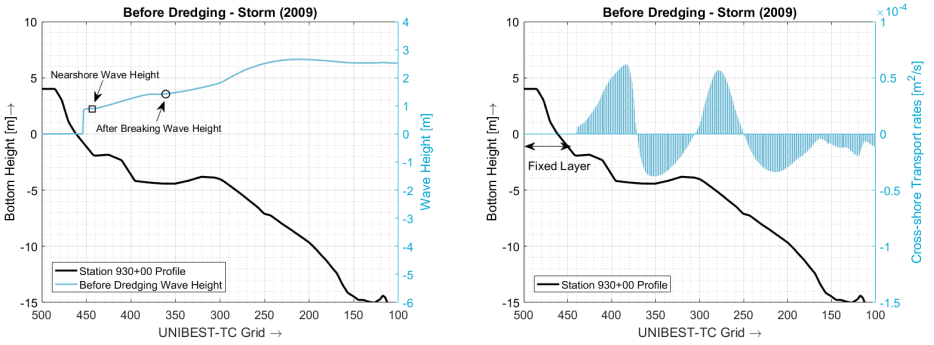

(a) Significant wave height distribution

(b) Cross-shore transport distribution

Figure 5.4: a: Distribution of the significant wave height with an incoming wave height of 2.60m, indicating the after breaking wave height location (*circle*) and the nearshore wave height location (*square*). b: Resulting distribution of the net cross-shore sediment transport rates over the beach profile. The total cross-shore transport rates for the applied waves and time steps are obtained by integrating the surface area of the transport rates. In the current application, positive transport rates are *offshore* directed.

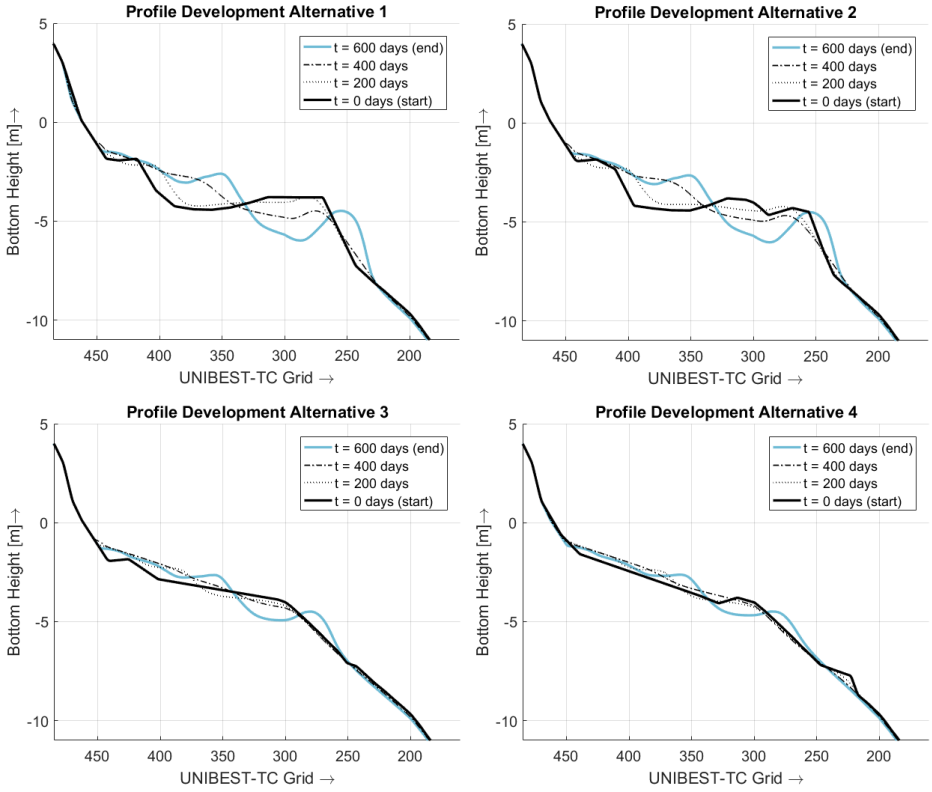

Figure 5.5: Beach profile development of the four nourishment alternatives at station 930+00 between March 2009 and October 2010.

Profile Development:
After shoreface nourishment implementation in the model, the profile development during the 20 month run of each nourishment design is show in Figure 5.5. All nourishment designs show similar responses in the first 200 days. Gradual reappearance of the pre-nourishment bar-trough morphology is occurring as the incoming wave climate is forcing the cross-shore distribution of sediment transport rates to pre-nourishment rates, i.e. the beach is reshaping its cross-shore profile back into its previous two barred state. Stronger differences between nourishment designs are found after 400 days, in which a clear division between seaward nourishment of the outer bar (Alternatives 1 and 2) and shoreward nourishment (Alternatives 3 and 4) is shown. Seaward nourishment will distribute more sediment into the outer bar and will merge with the initial offshore migrating outer bar. Shoreward nourishments show less enhancement of the outer bar volume and distribute more sediment in shoreward direction, resulting in shallower waters and a wider beach as compared to seaward nourishments.

A better visualization of these processes is shown in Figure 5.6, in which the profile after the 600 days model run is subtracted from the Before Nourishment scenario after the model run. Again, both Alternatives 1 and 2 show a larger difference in bottom height seaward of the outer bar where Alternatives 3 and 4 result in higher nearshore differences in bottom height at compared to the Before Dredging scenario.

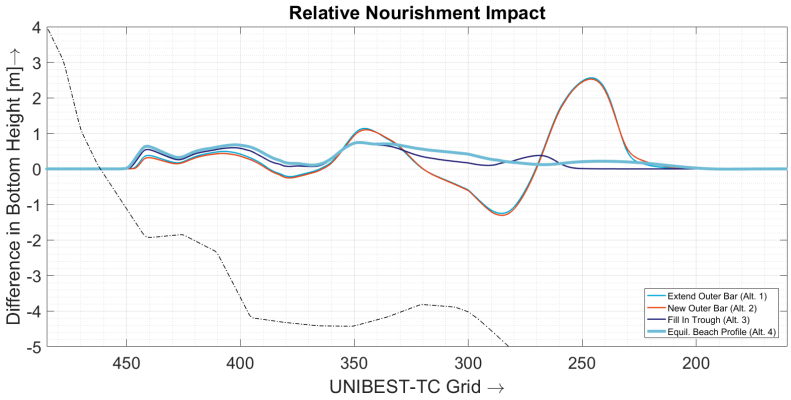

Figure 5.6: UNIBEST-TC model results expressing the differences in changes in bottom height as compared to the Before Dredging scenario. By subtracting the final profile after the model run of each nourishment design from the Before Dredging scenario, the relative nourishment impact is shown.

Nourishment Results:
As derived in section 5.1 - Introduction and formulated in Eq. 4.1; the cross-shore transport rates are directly coupled to the difference in the wave energy dissipation in the case of an equilibrium beach state and the current wave energy dissipation. The incoming wave energy in each scenario is equal, so the total wave energy dissipation over the cross-shore profile has to be equal in each scenario as well. Therefore, instead of looking at the wave energy dissipation over the cross-shore profile, the effects that different shoreface nourishments have on the incoming wave climate are checked by plotting the transformation of the significant wave height over the cross-shore profile. Comparison of the wave height between nourishment designs is highlighted at the location just after breaking over the outer bar and the nearshore wave height, marked with respectively the *circle* and *square* markers as seen in Figure 5.4a. The net averaged cross-shore sediment transport rates are computed by integrating the transport distribution over the beach profile, as illustrated in Figure 5.4b.

The results are shown in Figure 5.7. Each plot in this figure shows the difference between either one of the three conventional nourishment designs compared with a design based on the concept of an equilibrium beach profile. The values for the wave height and cross-shore transport rates in Figure 5.7 are not to scale, but resized for better visualization on the right y-axis. The results are summarized in Tables 5.2 and 5.3. Note that some of the plots show peaks in the cross-shore transport values in the grid cells around the shoreline, indicating that the model is sensitive in transport computations in this region. Possible reason is that the model keeps equilibrating in these grid cells due to the variable wave climate, combined with the low order of morphodynamic timescale. Constant redistribution in between these grid cells results of this profile equilibration, thereby not affecting the total volume of sediment transport over the profile. This, combined with possible discretization errors in these shallow waters might result in over-sensitivity of sediment computations. In some cases nourishment design overlaps the fixed layer allowing sediment transport. These transport rates are excluded for the nourishment efficiency analysis as well. For the remainder of the report, all nearshore transport peaks are excluded for the total volume of cross-shore sediment transport computations, by integrating the absolute transport values from the end of the fixed layer x_{fix}.

EBP – Alternative 1
Wave Height: The first nourishment alternative is constructed by nourishing the seaward slope of the outer bar at the peak of the bar height. This way the larger incoming waves are broken further offshore and less wave energy will reach the shoreline. Figure 5.7 also shows such a reduction of offshore wave height with an average reduction of 10%. The wave height shoreward of the outer bar, however, is ~20% higher compared to the EBP-design.

Cross-shore Transport: By integrating the surface of both cross-shore transport plots, the total cross-shore transport volume is estimated. In the case of Alternative 1 the total volume of transport is ~19% higher compared to the EBP-design. Especially near the shoreline the EBP-design shows far better results compared to this conventional nourishment design, indicating lower coastal erosion.

EBP – Alternative 2
Wave Height: The second nourishment alternative is constructed by creating a new bar located further offshore than the original one. On average, the wave height shoreward of the original outer bar shows no difference between the two scenarios. This is probably caused by the fact that in the one year run of the model, no significant impact due to storms occurred, which temporarily shifted the Depth of Closure (DoC) into shallower water closer onshore. Closer to the shoreline, results show that the maximum increase in average wave height of Alternative 2 is ~25% higher compared to the EBP-design.

Cross-shore Transport: The total volume of cross-shore transport of Alternative 2 is ~19% higher compared to the EBP-design and shows even more transport near the coastline compared to Alternative 1.

EBP – Alternative 3
Wave Height: The third nourishment alternative is constructed by filling in the trough between the inner and outer bar. Wave height distribution over the cross-shore profile show strong agreement between the two nourishment design scenario's. Locally there are changes on the order of centimeters, which are assumed to be negligible in this comparison.

Cross-shore Transport: Distribution of the cross-shore transport rates between Alternative 3 and the EBP-design have strong agreement up to the shoreline, where the EBP-design locally lowers the cross-shore transport rates. The total volume of transport is ~5% higher in case of the conventional nourishment design.

The values for the wave height and cross-shore transport rates in Figure 5.8 are not to scale, but resized for better visualization. The results are summarized in Tables 5.4 and 5.5.

EBP – Alternative 1
Wave Height: Larger incoming waves break further offshore and less wave energy will reach the shoreline. Figure 5.8 also shows such a reduction of offshore wave height with an average reduction of 10%. The wave height shoreward of the outer bar, however, is ~10% higher compared to the EBP-design.

Cross-shore Transport: In the case of Alternative 1 the total volume of transport is ~29% higher compared to the EBP-design. The EBP-design shows far better results compared to this conventional nourishment design, indicating lower coastal erosion especially near the shoreline.

EBP – Alternative 2
Wave Height: On average, the wave height shoreward of the original outer bar shows no difference between the two scenarios. Closer to the shoreline, results show that the maximum increase in average wave height of Alternative 2 is ~10% higher compared to the EBP-design.

Cross-shore Transport: The total volume of cross-shore transport of Alternative 2 is ~40% higher compared to the EBP-design and shows more transport near the coastline compared to Alternative 1.

EBP – Alternative 3
Wave Height: Wave height distribution over the cross-shore profile show strong agreement between the two nourishment design scenarios.

Cross-shore Transport: Distribution of the cross-shore transport rates between Alternative 3 and the EBP-design have strong agreement up to the shoreline, where the Alternative 3 locally lowers the cross-shore transport rates. The total volume of transport is ~13% lower in case of the conventional nourishment design.

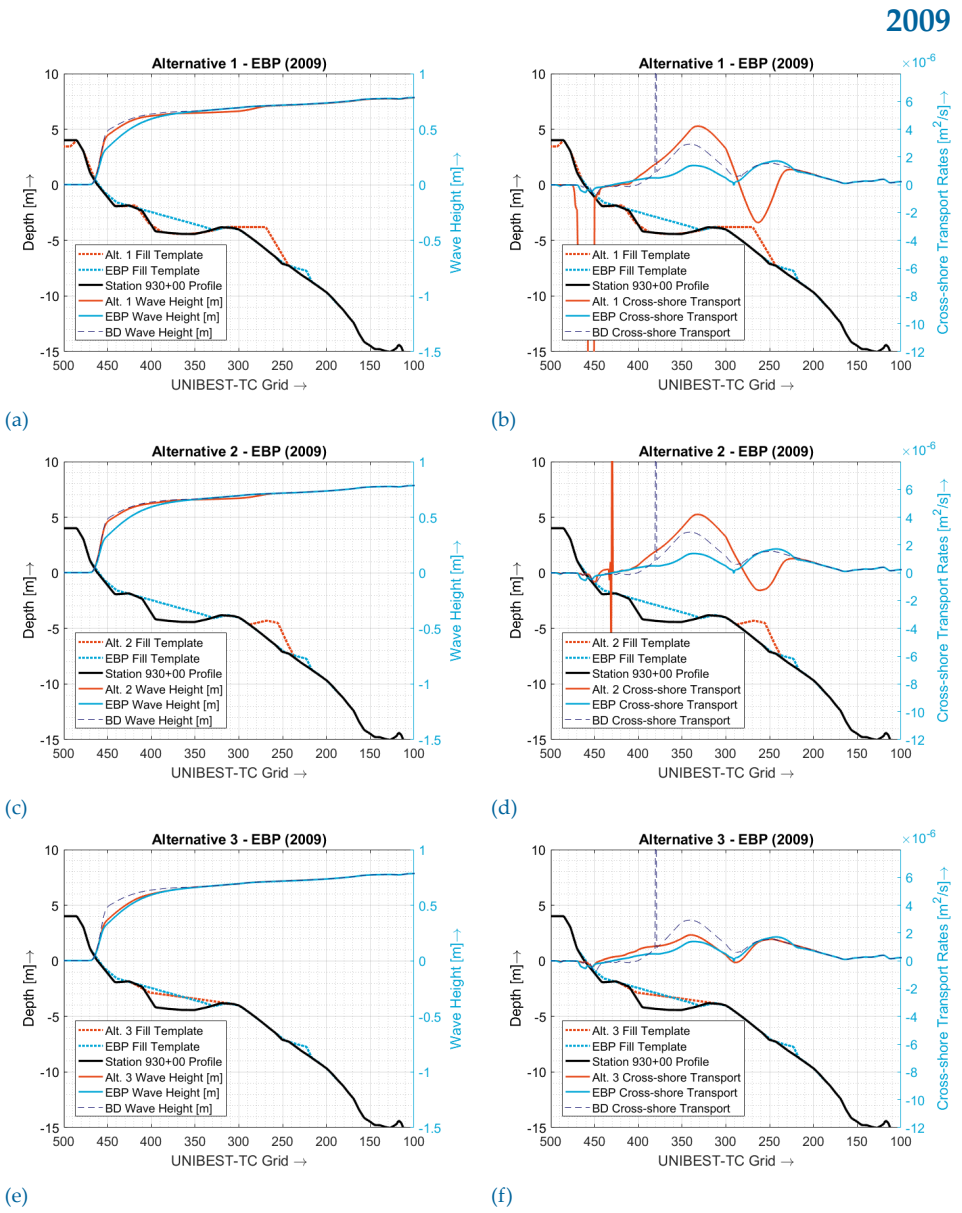

Figure 5.7: *left:* the distribution of the significant wave height over the cross-shore profile for each of the conventional nourishment designs (Alternative 1, 2 and 3) plotted against the results of the 'EBP-design' (Alternative 4). *right:* the net averaged cross-shore transport rates distributions plotted over the profile. Total absolute average cross-shore transport rates per scenario are: Before Dredging = 0.0024, Alt. 1 = 0.0026, Alt. 2 = 0.0026, Alt. 3 = 0.0023, Alt. 4 = 0.0022.

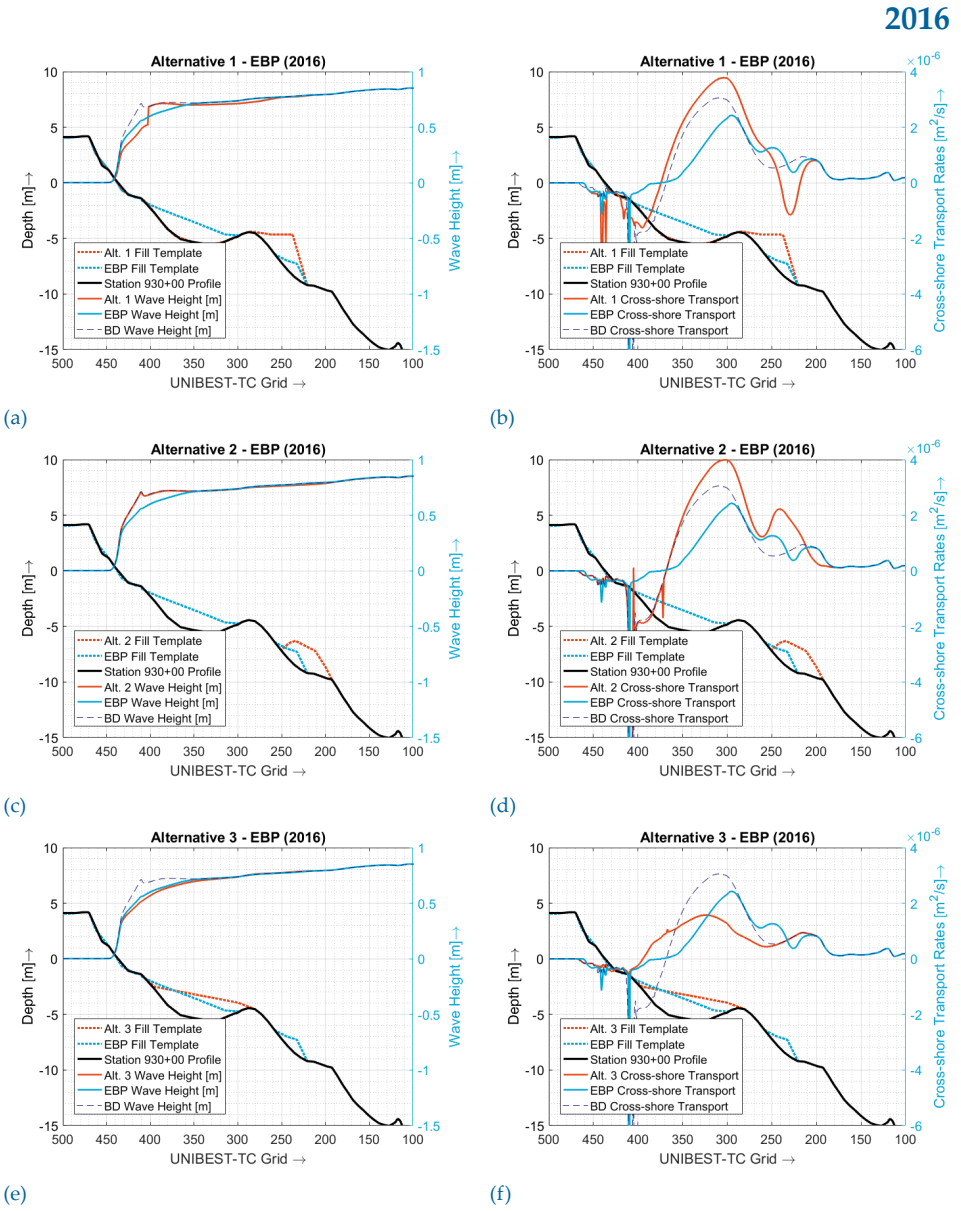

Figure 5.8: *left:* the distribution of the significant wave height over the cross-shore profile for each of the conventional nourishment designs (Alternative 1, 2 and 3) plotted against the results of the 'EBP-design' (Alternative 4). *right:* the net averaged cross-shore transport rates distributions plotted over the profile. Total absolute average cross-shore transport rates per scenario are: Before Dredging = 0.0010, Alt. 1 = 0.0011, Alt. 2 = 0.0013, Alt. 3 = 0.0008, Alt. 4 = 0.0009.

2009

Table 5.2: Comparison of the significant wave height and cross-shore transport rates between Alternatives 1, 2 and 3 to the EBP-design (Alternative 4) of Station 930+00 (2009)

(Compared to EBP-Design)	**Alternative 1**	**Alternative 2**	**Alternative 3**
Wave Height Reduction Seaward Outer Bar (%)	10%	0%	0%
Wave Height Reduction Shoreward Outer Bar (%)	-20%	-25%	0%
Total Cross-shore Volume Reduction (%)	33%	29%	14%

Table 5.3: Comparison of the total volume in cross-shore transport rates of each nourishment design to the before dredging scenario of Station 930+00 (2009). Results are obtained by subtracting the integrated area of the transport distribution of the before dredging scenario of the nourishment design scenario

	Cross-shore Transport Reduction
Alternative 1 'Extension Outer Bar'	+8%
Alternative 2 'New Outer Bar'	+8%
Alternative 3 'Fill In Trough'	-4%
Alternative 4 'EBP-design'	-8%

2016

Table 5.4: Comparison of the significant wave height and cross-shore transport rates between Alternatives 1, 2 and 3 to the EBP-design (Alternative 4) of Station 930+00 (2016)

(Compared to EBP-Design)	**Alternative 1**	**Alternative 2**	**Alternative 3**
Wave Height Reduction Seaward Outer Bar (%)	10%	0%	0%
Wave Height Reduction Shoreward Outer Bar (%)	-10%	-10%	0%
Total Cross-shore Volume Reduction (%)	56%	55%	25%

Table 5.5: Comparison of the total volume in cross-shore transport rates of each nourishment design to the before dredging scenario of Station 930+00 (2016). Results are obtained by subtracting the integrated area of the transport distribution of the before dredging scenario of the nourishment design scenario

	Cross-shore Transport Reduction
Alternative 1 'Extension Outer Bar'	+12%
Alternative 2 'New Outer Bar'	+33%
Alternative 3 'Fill In Trough'	-31%
Alternative 4 'EBP-design'	-21%

5.5.2 Station 520+00

2009

The values for wave height and cross-shore transport rates in Figure 5.9 are not to scale, but resized for better visualization. The results are summarized in Tables 5.6 and 5.7.

EBP – Alternative 1
Wave Height: Larger incoming waves break further offshore and less wave energy will reach the shoreline. Figure 5.9 also shows such a reduction of offshore wave height with an average reduction of 10%. The wave height shoreward of the outer bar, however, is ~10% higher compared to the EBP-design.

Cross-shore Transport: In the case of Alternative 1 the total volume of transport is ~15% higher compared to the EBP-design. Especially near the shoreline the EBP-design shows far better results compared to this conventional nourishment design, indicating lower coastal erosion.

EBP – Alternative 2
Wave Height: On average, the wave height shoreward of the original outer bar shows no difference between the two scenarios. Closer to the shoreline, results show that the maximum increase in average wave height of Alternative 2 is ~10% higher compared to the EBP-design.

Cross-shore Transport: The total volume of cross-shore transport of Alternative 2 is ~15% higher compared to the EBP-design and shows even more transport near the coastline compared to Alternative 1.

EBP – Alternative 3
Wave Height: Wave height distribution over the cross-shore profile show strong agreement between the two nourishment design scenarios.

Cross-shore Transport: Distribution of the cross-shore transport rates between Alternative 3 and the EBP-design have strong agreement up to the shoreline, where the EBP-design locally lowers the cross-shore transport rates. The total volume of transport is ~5% higher in case of the conventional nourishment design.

The values for wave height and cross-shore transport rates in Figure 5.10 are not to scale, but resized for better visualization. The results are summarized in Tables 5.8 and 5.9.

EBP – Alternative 1
Wave Height: Larger incoming waves break further offshore and less wave energy will reach the shoreline. Figure 5.10 also shows such a reduction of offshore wave height with no average reduction. The wave height shoreward of the outer bar is comparable to the EBP-design.

Cross-shore Transport: In the case of Alternative 1 the total volume of transport is ~9% higher compared to the EBP-design. Especially near the shoreline the EBP-design shows far better results compared to this conventional nourishment design, indicating lower coastal erosion.

EBP – Alternative 2
Wave Height: On average, the wave height shoreward of the original outer bar shows no difference between the two scenarios. Closer to the shoreline, results show that the wave height is approximately the same compared to the EBP-design.

Cross-shore Transport: The total volume of cross-shore transport of Alternative 2 is ~9% higher compared to the EBP-design and shows even more transport near the coastline compared to Alternative 1.

EBP – Alternative 3
Wave Height: Wave height distribution over the cross-shore profile show strong agreement between the two nourishment design scenarios.

Cross-shore Transport: Distribution of the cross-shore transport rates between Alternative 3 and the EBP-design have strong agreement up to the shoreline. The total volume of transport is equal in case of the conventional nourishment design.

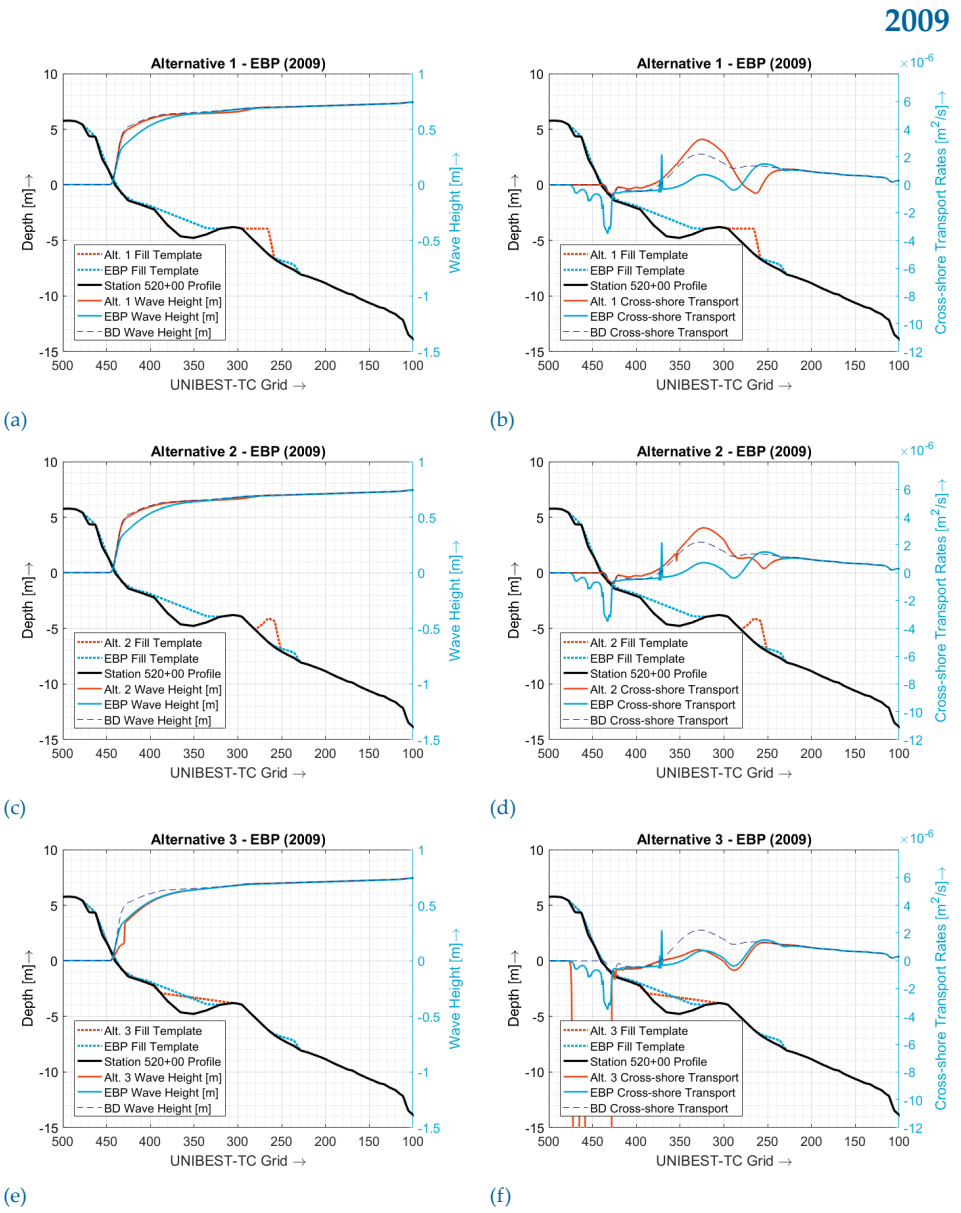

Figure 5.9: *left:* the distribution of the significant wave height over the cross-shore profile for each of the conventional nourishment designs (Alternative 1, 2 and 3) plotted against the results of the 'EBP-design' (Alternative 4). *right:* the net averaged cross-shore transport rates distributions plotted over the profile. Total absolute average cross-shore transport rates per scenario are: Before Dredging = 0.0020, Alt. 1 = 0.0023, Alt. 2 = 0.0023, Alt. 3 = 0.0021, Alt. 4 = 0.0020.

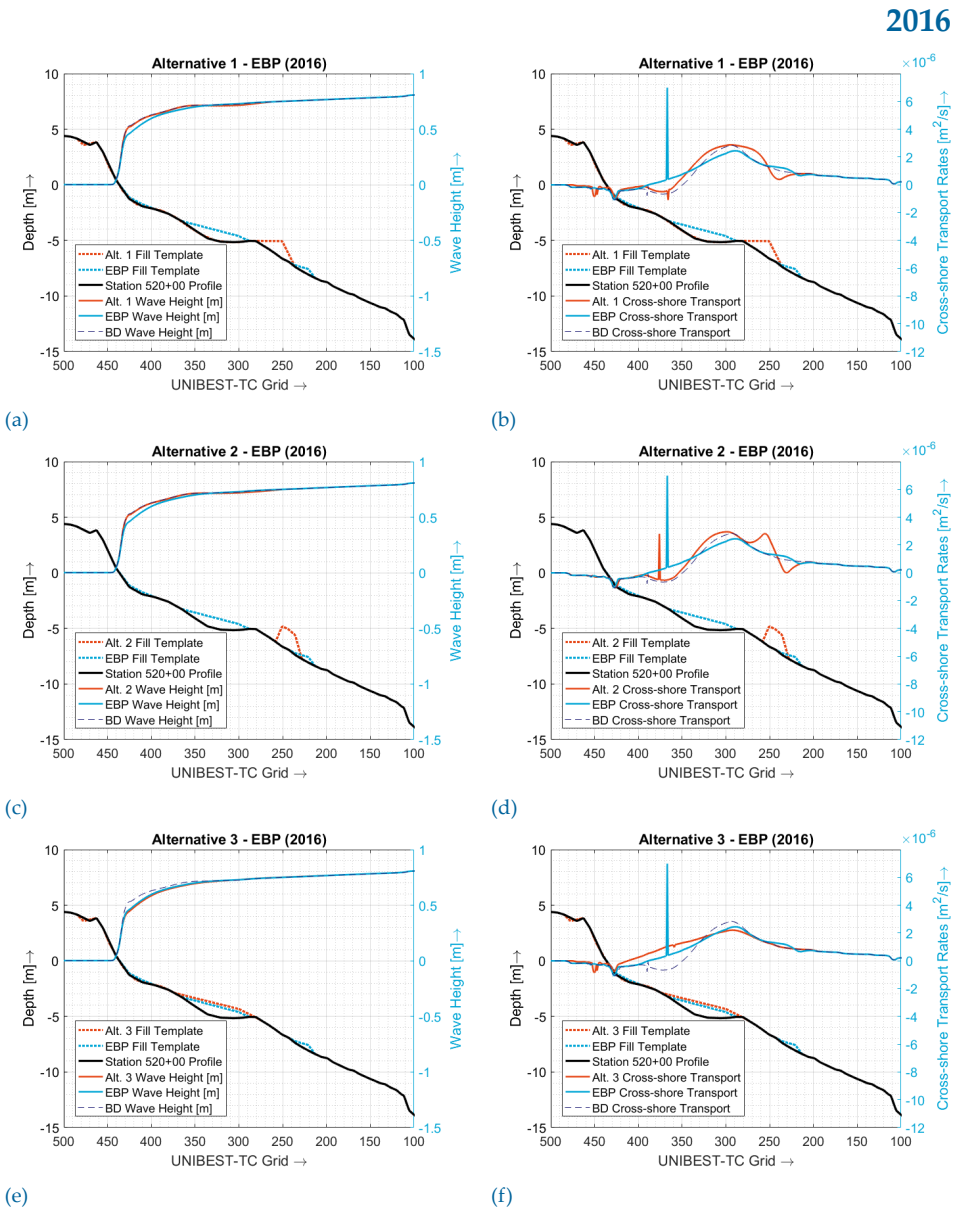

Figure 5.10: *left:* the distribution of the significant wave height over the cross-shore profile for each of the conventional nourishment designs (Alternative 1, 2 and 3) plotted against the results of the 'EBP-design' (Alternative 4). *right:* the net averaged cross-shore transport rates distributions plotted over the profile. Total absolute average cross-shore transport rates per scenario are: Before Dredging = 0.0011, Alt. 1 = 0.0012, Alt. 2 = 0.0012, Alt. 3 = 0.0011, Alt. 4 = 0.0011.

2009

Table 5.6: Comparison of the significant wave height and cross-shore transport rates between Alternatives 1, 2 and 3 to the EBP-design (Alternative 4) of Station 520+00 (2009)

(Compared to EBP-Design)	**Alternative 1**	**Alternative 2**	**Alternative 3**
Wave Height Reduction Seaward Outer Bar (%)	10%	0%	0%
Wave Height Reduction Shoreward Outer Bar (%)	0%	0%	0%
Total Cross-shore Volume Reduction (%)	20%	22%	10%

Table 5.7: Comparison of the total volume in cross-shore transport rates of each nourishment design to the before dredging scenario of Station 520+00 (2009). Results are obtained by subtracting the integrated area of the transport distribution of the before dredging scenario of the nourishment design scenario

	Cross-shore Transport Reduction
Alternative 1 'Extension Outer Bar'	+15%
Alternative 2 'New Outer Bar'	+15%
Alternative 3 'Fill In Trough'	+15%
Alternative 4 'EBP-design'	0%

2016

Table 5.8: Comparison of the significant wave height and cross-shore transport rates between Alternatives 1, 2 and 3 to the EBP-design (Alternative 4) of Station 520+00 (2016)

(Compared to EBP-Design)	**Alternative 1**	**Alternative 2**	**Alternative 3**
Wave Height Reduction Seaward Outer Bar (%)	0%	0%	0%
Wave Height Reduction Shoreward Outer Bar (%)	0%	0%	0%
Total Cross-shore Volume Reduction (%)	35%	30%	15%

Table 5.9: Comparison of the total volume in cross-shore transport rates of each nourishment design to the before dredging scenario of Station 520+00 (2016). Results are obtained by subtracting the integrated area of the transport distribution of the before dredging scenario of the nourishment design scenario

	Cross-shore Transport Reduction
Alternative 1 'Extension Outer Bar'	+9%
Alternative 2 'New Outer Bar'	+9%
Alternative 3 'Fill In Trough'	0%
Alternative 4 'EBP-design'	0%

5.6 Relative Impact of Shoreface Nourishment Designs

In the previous sections, the results for all the simulated shoreface nourishment designs per cross-shore profile were discussed separately. Results showed that the variation in wave height distribution between all nourishment designs and the Before Dredging scenario is only minorly significant. Specifically the comparison between Alternative 3 (Fill In Trough) and Alternative 4 (EBP-design) shows minor differences.

As the relative low average wave height over the modeling period is plotted over the profile, the differences in wave height deviations are small as well. Storm events show stronger differences, but the study emphasis involves the sediment volume budget before and after the model run. Therefore, the focus of the remainder of this chapter is to determine the impact the investigated alternative designs have on the total volume of onshore directed sediment transport, which will in term be an indicator how each nourishment design will counteract the coastal erosion. This is worked out by integrating the absoute yearly averaged cross-shore sediment transport curves to compute the gross total volume transport, see Figure 5.11.

In Figure 5.11, the effect of each nourishment scenario per beach profile is plotted against the initial Before Dredging situation to compare the nourishment impact between the four alternatives. Each beach profile analysis shows different results, but a general trend is clearly noticeable:

Nourishment seaward of the outer bar, by either extending the existing bar or creating a new bar (Alt. 1 and 2) has hardly any influence to lower the cross-shore transport rates compared to the Before Dredging scenario and will only enhance them. Not entirely coincidently both seaward nourishments are further offshore and approach the depth of closure, as compared to the shoreward scenarios (Alt. 3 and 4). When approaching the depth of closure, only the less frequent larger waves will influence the sediment transport. In the Nags Head case, the outer bar is located relatively far offshore, making a nourishment seaward of the outer bar less effective as compared to shoreward nourishment.

Shoreward nourishment of the outer bar shows stronger and more promising effects to reduce the cross-shore transport rates. Especially a nourishment that is designed along the concept of EBP shows a strong reduction while adding a surplus of sediment in the beach profile, making it a useful nourishment design when applied at the Nags Head project site. Compared to the averaged wave height, both alternatives 1 and 2 also show the largest reduction in lowering the nearshore wave height, which will increase the nourishment lee effects.

The relative impact per shoreface nourishment is also analyzed by averaging the results per beach profile and computing the percentage reduction of total volume of sediment transport compared to the Before Dredging scenario (Table 5.10). Again, the EBP-design results in the lowest cross-shore transport, concluding that coastal erosion can indeed be counteracted most effectively while designing a nourishment using the concept of EBP. The effect the longshore variability has on the EBP based nourishment design and how it can be implemented in a project-wide nourishment is further checked in Chapter 6 - Longshore Nourishment Effects.

Table 5.10: The averaged total volume of cross-shore transport per nourishment design compared to the Before Dredging scenario. The left column shows the average value of the four beach profiles applied in this study. The right column shows the percentage reduction due to each nourishment.

	Average Cross-shore Trans	Difference	Reduction (%)
Before Dredging	0.00160		
Extension Outer Bar (Alt. 1)	0.00185	+0.00025	+15.6
New Outer Bar (Alt. 2)	0.00181	+0.00021	+13.1
Fill In Trough (Alt. 3)	0.00153	-0.00007	-4.4
EBP-design (Alt. 4)	0.00151	-0.00009	**-5.6**

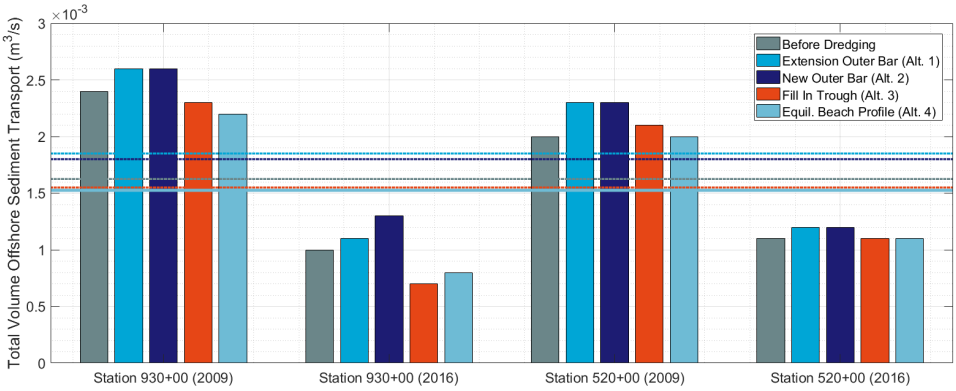

Figure 5.11: Total volume of net averaged cross-shore transport rates of all scenarios with all shoreface nourishment alternatives. The average values of each nourishment scenario computed over four different profiles are indicated with the dashed lines. Higher negative values indicate higher offshore directed sediment transport.

5.7 Discussion

While the models presented in the previous chapters area able to predict the main features of long-term cross-shore sediment transport behavior, it remains difficult to accurately predict the morphodynamical trends between survey datasets. In the current applications, model calibration is purely based on beach profile predictability between datasets and the corresponding total volumes of sediment transport. A lack of accurate daily bathymetry sets prevents hindcasting of the actual beach morphology such as sandbar migration. Accurate predictions of the after dredging cross-shore sediment distribution and its resulting nourishment impact are therefore infeasible, arising for impact approximations in the form of reduction of total sediment transport, see Table 5.10.

This lack of data could also explain the overall trend found in all nourishment results. Analysis of the model output revealed a considerable variation in reduction of cross-shore transport rates between different beach profiles for different nourishment alternatives. However, not a single nourishment alternative was able to significantly reverse the net sediment transport rates, necessary for accretive coastal features to counteract coastal erosion. Another overlooked feature are the error accumulation that arise from introducing errors in the model building process, wave forcings based on hourly sampled hindcast data, inaccurate representations of the beach profile and the relative short duration of the modeling study. Especially the latter influences the results, since literature shows that most sandbar cycle-periods extend well beyond the 1-year model duration, net sediment transport reversal might occur after a certain amount of time after nourishment placement (Walstra et al., 2017).

A inconsistent feature in the model results is the nourishment impact on the total volume of transport reduction compared to the Before Dredging scenario. Alternative 1 and 2 show an increase in total transport rates, which means that only Alternatives 3 and 4 are able to reshape the beach profile in such a way that the wave-energy dissipation distribution after dredging is following the equilibrium rate of distribution more precisely, resulting in a lower total cross-shore transport as previously mentioned in Eq 5.1. This feature was the main emphasis of this Research Question and shows that a shoreface nourishment designed in the right effectively reduces coastal erosion. But, nourishment alternatives to extend or create a new outer bar (Alt. 1 and 2) show little to no effect on the total volume of transport, whereas literature shows dissimilar results (Bruins, 2016). Study site location together with the relative short modeling duration could mainly be responsible for these effects. Considerable differences in model results were unanticipated in the first place, as the applied wave climate is roughly constant in each simulation. Different study sites possibly influences the model outcomes, which will be treated in more detail in Chapter 9 - Recommendations. Another important aspect on coastal erosion omitted from the results analysis is the bulk of extra sediment placed by nourishment. The surplus of sediment acts as an erosional buffer, thereby possibly reducing coastal erosion as well.

In the present work and as previously explained in the project scope, longshore variabilities, such as rip channels and crescentic shapes, were averaged out and considered as a noise term. However, as the cross-shore and longshore sediment transport rates have a strong dependency on each other, it would be interesting to know how longshore variations affect the distribution of cross-shore sediment transport before and after nourishment and how they relate to long-term nourishment efficiency predictions. Nourishment impact on the longshore transport rates is the main emphasis of Research Question 3, but it still doesn't highlight the importance of the longshore noise terms.

5.8 Summary

This research question emphasizes decreasing coastal erosion by lowering the cross-shore transport rates. It therefore further supports the hypothesis that significant net cross-shore sediment transport and beach profile change occurred at locations where the rate of wave energy dissipation deviated substantially from the equilibrium rate. Therefore, beach profile evolution and resulting cross-shore sediment transport depend on how far the new profile deviates from the EBP.

Three different conventional shoreface nourishment designs are compared with a design based on the concept of an EBP (the so called 'EBP-design', Alternative 4) to ascertain which design lowers the cross-shore transport rates most efficiently. Furthermore, the wave height distribution over the cross-shore profile was checked to see which design had the lowest nearshore wave height. The bi-polynomal EBP, as described in Chapter 4 - Equilibrium Beach Profiles first had to be calibrated before a nourishment design can be derived from it. Calibration was performed by expressing the difference in the predicted and observed bed profiles of all cross-shore profiles in Nags Head by a cumulative mean-squared error. The three conventional designs were executed as: Alternative 1, shoreward nourishment of the outer bar at the top height. Alternative 2, create a new outer bar shoreward of the existing one. Alternative 3, fill in the trough in between the outer and swash bar. Shoreface nourishments on four beach profiles (Station 520+00 in 2009/2016 and Station 930+00 in 2009/2016) were modeled to check the nourishment design impact under varying wave climates and initial profiles.

The four alternative designs were compared to check the lee and feeder effects relative to each other and to the initial "Before Dredging" scenario. The lee effect is a result of offshore breaking of waves, which result in a calmer wave climate shoreward of the nourishment. The significant wave height over the beach profile of each scenario was therefore analyzed. A general trend was

found in this analysis; nourishments placed seaward of the outer bar hardly influenced the wave height as opposed to shoreward placed nourishments. The increased offshore location tends to be the main cause. As the nourishment is placed in deeper water closer to the depth of closure, the number of waves that will influence sediment transport decrease, thereby reducing the nourishment efficiency on lowering the wave height. Nourishments placed in the trough of the beach profile are located in shallower depths, resulting in a larger decrease of the average significant wave height.

The total absolute yearly averaged cross-shore sediment transport rates per scenario were computed to estimate nourishment efficiency of reducing coastal erosion by lowering the offshore directed sediment transport (feeder effect). The reduction of these transports per scenario are averaged over each beach profile and are compared to the "Before Dredging" scenario. Per nourishment design the respective reduction of total volume of cross-shore sediment transport for Alternative 1 - 4 was; +15.6%, +13.1%, -4.4% and -5.6%. Again, results show that the EBP-design shows a strong reduction of cross-shore transport rates compared to conventional shoreface nourishments, especially compared to nourishments placed shoreward of the outer bar (Alternatives 1 and 2). It can therefore be concluded that the cross-shore transport rates lower using an EBP based nourishment design as compared to nourishments based on guidelines.

6

Longshore Nourishment Effects

How do longshore transports and local gradients in sediment transport decrease by using the concept of EBP during nourishment design?

Shoreface nourishments are used to maintain or increase the sand volume in the nearshore zone by natural processes. Those processes can be described by an increase of net onshore transport (feeder effect) and a reduction of longshore transport behind the nourishment (lee effect). Ideally a shoreface nourishment would not only lower the longshore transport rates but also lower the local variability. Therefore, this part of this study focuses on the reduction of longshore transport rates and local gradients.

This chapter gives a brief introduction in coastal modeling and the substantiation of the applied numerical model used in this study. The model set-up, calibration, and verification are explained in detail. Main inputs of the models including wave climate, bathymetry and sediment characteristics used in the models are discussed. The model results are interpreted and nourishment impact is concluded at the end of this chapter.

The proposed nourishment scenarios as described in Section 1.5 - Tested Nourishment Design Scenarios are modeled using software fit for the current application. The modeling domain encompassing in total of ~15 miles of shoreline extends north and south of the Nags Head project limits with ~2.5 miles and extending ~6 miles seaward. Two different modeling scenarios are created in the Delft3D numerical suite. The first one is modeled without nourishment (a so called 'Before Dredging' scenario) and was calibrated by historic erosion rates. The second scenario represents the condition after nourishment is placed (a so called 'After Dredging' scenario). By subtracting the results of the two scenarios, the nourishment impact is computed.

Moreover, a reduction in longshore transport rates after nourishment construction should increase the nourishment longevity as well. When less nourished sediment were to leave the littoral zone due to longshore transport, the counteracting effects a nourishment has on coastal erosion are prolonged. Nourishment efficiency is therefore in a likewise manner expressed in the nourishment longevity. Finally, the local gradients in the longshore transport rates per nourishment design are analyzed to see which design lowers these gradients the most efficient. A reduction in these gradients indicate a less obstructive flow (i.e. - a divergence of non-linear local sediment transport rates over the coastal zone) thereby increasing nourishment efficiency as well. This phenomena and its substantiation will be treated in detail in the following sections.

6.1 Delft3D Substantiation and Description

Process-based modeling of the beach zone can be divided into three main categories: coastline (1D), coastal profile (2D), and coastal area (2DH/3D) modeling, each having a different applicability regarding its spatial and temporal scale (Figure 6.1). Coastline models (sometimes referred to as one-line models) are used mainly to calculate the total longshore transport without taking into account the effects of cross-shore gradients and bathymetry. Because nourishment evolution is highly dependent on the cross-shore profile; these types of models necessarily provide little detail and involve many simplifying assumptions.

Coastal profile models evaluate the shoreline in two dimensions (2D), but assume a longshore uniform bathymetry in order to isolate and compute the processes in cross-shore direction. These models take into account principal transport components such as cross-shore currents and wave asymmetry. The bed-level changes are computed via mass conservation balance. These models provide good estimates of the variation in longshore transport over which the cross-shore direction is calculated.

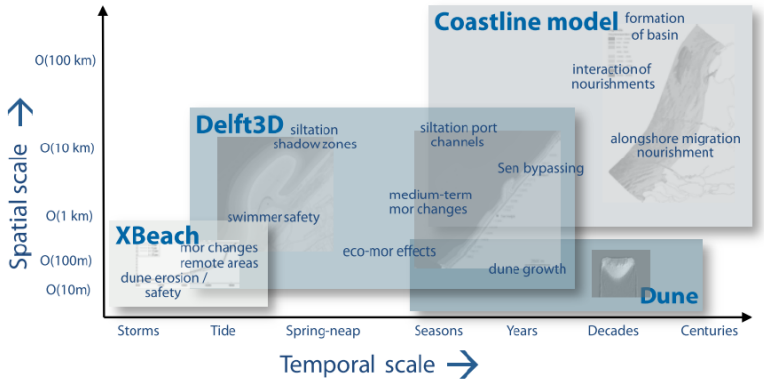

Figure 6.1: The schematization of which computational model is applicable in different time and spatial scales for hydrodynamic processes (Baart et al., 2012).

Coastal area models seek to simulate three-dimensional (3D) beach changes by fully integrating currents, waves, and sediment transport to provide continually updated model bathymetry after each time step (Lesser et al., 2004). These models are the strongest tools for studying the impacts of morphological changes to the coastal system. Although coastal area models require high computational power, they are useful for describing all the currents in a 2DH or 3D grid, offering the advantage of including the vertical structure of the flows and sediment concentration by either dividing the vertical computational axis in several layers or by depth-averaged transport distributions. This potentially yields the most accurate predictions of how beaches will behave under the influence of the currents and waves acting at a particular site. Within coastal area models, the 2DH approach is used most commonly due to the strong reduction of computational cells and wide range of applicability. Only in cases with accurate data for the calibration of the vertical distribution of flow and transport, the 3D set-up possibly results in more accurate computations. While 3D or 2DH models are preferred for the evaluation of coastal erosion, they are dependent on more complex input data such as the site-specific tide and wave climate. Figure 6.1 illustrates the time and spatial scales applicable for various models.

In the simulation of the hydrodynamic and morphodynamic processes of Nags Head, the process-based numerical model Delft3D is used. Delft3D is a modeling system developed by Deltares (the same developer as the previous UNIBEST-TC model). It allows for hydrodynamic computations in coastal, river, and estuarine areas. The Delft3D software package consists of several modules. Each module focuses on specific processes such as hydrodynamic flow, sediment transport, morphodynamics, water quality, ecology, and waves. The modules can be coupled for process interaction.

To compute the effects of the nourishment, two different Delft3D modules are were used—the "FLOW" and "WAVE" modules. Delft3D-FLOW was applied to simulate non-steady flow, sediment transport, and morphology. Delft3D-WAVE was applied to simulate the evolution of short waves using the third generation SWAN-model (Booij et al., 1999). The general modeling approach in Delft3D is that hydrodynamic flow is calculated on a boundary-fitted grid to which bathymetry, initial conditions, and boundary conditions are applied. Sediment transport quantities are calculated following the flow and wave field according to the applied sediment transport formula. Variations in sediment transport, in turn, determine the morphological development of the model. The processes of flow, waves, sediment transport, and morphological updating are all executed at each model time step according to the "online" approach; meaning that information of each module is transferred between each other at every computational time step (Roelvink, 2006). A schematic overview and the interaction between the modules is shown in Figure 6.2.

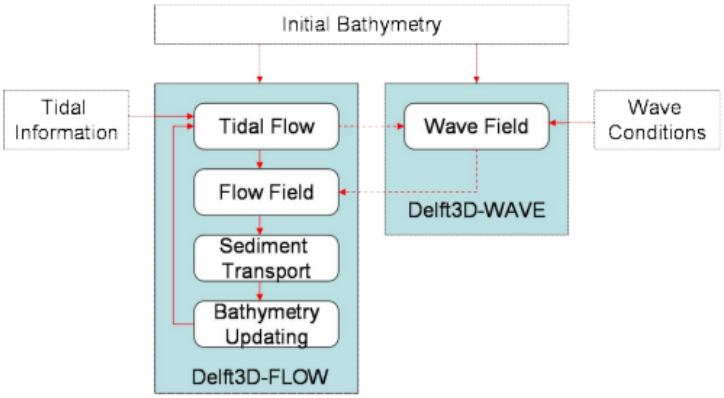

Figure 6.2: Modeling approach Delft3D, after (Sun, 2004).

6.2 Delft3D Grid and Computational Time Steps

Delft3D requires specification of existing physical characteristics in each grid cell used for simulations. Generally, a grid of calculation nodes is established for the study area with some areas represented by a coarse grid (WAVE-module) of more widely spaced points and other areas represented by a fine grid of closer spaced points (FLOW-module). The selection of grid sizes depends on site characteristics and the desired degree of detail. Each grid point requires physical characteristics such as water depth and sediment size.

The coarse grid spanned the nearshore and offshore regions up to the wave data recording stations for accurate nearshore wave translations. The wave data were then directly coupled to the fine grid which encompassed the nearshore bathymetry and the primary area of interest. Along the boundaries of the finer grid, the site-specific input conditions (tides, wind, waves etc.) were specified to force the physical processes acting within the grid. Using these boundary conditions, the model computed water levels, currents, waves, and sediment transport in each grid cell per time step. For the Nags Head simulations, the morphological changes due to beach nourishment were computed over a one-year and a five-year period, respectively. The model's resolution is expressed in the distance between grid cells. A higher resolution indicates smaller spacing and thereby an increase of the accuracy to resolve small-scale processes and features like nourishment impacts and beach profile changes.

In the current application, the coarse grid spans 10142 m in cross-shore and 24411 m in longshore direction with a grid cell size of 610 m in longshore and 457 m in cross-shore direction, creating 3081 active grid cells. The fine grid spans 4816 m cross-shore and 17830 m in longshore direction with a varying grid size through the domain. Offshore, the grid size is 145 m in both cross-shore and longshore direction, 67 m in longshore and 30 m cross-shore around the dredge pits, and 67 m in longshore and 15 m in cross-shore direction nearshore, resulting in total of 40006 active grid cells, see Figures 6.3 and 6.4 for a schematic overview of both grids.

The wave translation data computed in the coarse grid were "online-coupled" with the finer grid over a 60-minute interval using the WAVE module (i.e. – the fine grid uses the same wave conditions for an hour, after which it is coupled and updated again with the FLOW module). The fine grid then computed the water levels, currents, wave-current interactions, and sediment transport using the FLOW module. All modeling scenario's are executed in ''2DH'', meaning only one vertical layer is used in the vertical grid and the velocity is depth averaged. Cross-shore hydrodynamic and morphodynamic processes are taken into account, by approximating the depth averaged calculations. The time step to run the FLOW module was based on the Courant criterion (a mathematical technique necessary to achieve convergence in a solution for differential equations) for numerical stability and was set to 15 seconds. This way, the results of each module were transferred back and forth between each other, and the results of each were used to compute sediment transport and seabed changes in every grid cell in the fine grid. The remainder of this section gives a detailed description of the setup of the modules.

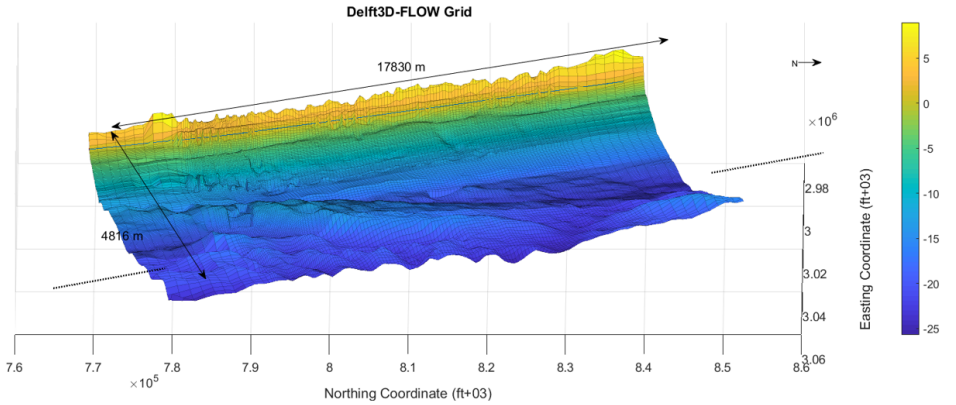

Figure 6.3: Overview Delft3D-FLOW model grid and bathymetry. Colors represent the bed level elevation in m NAVD.

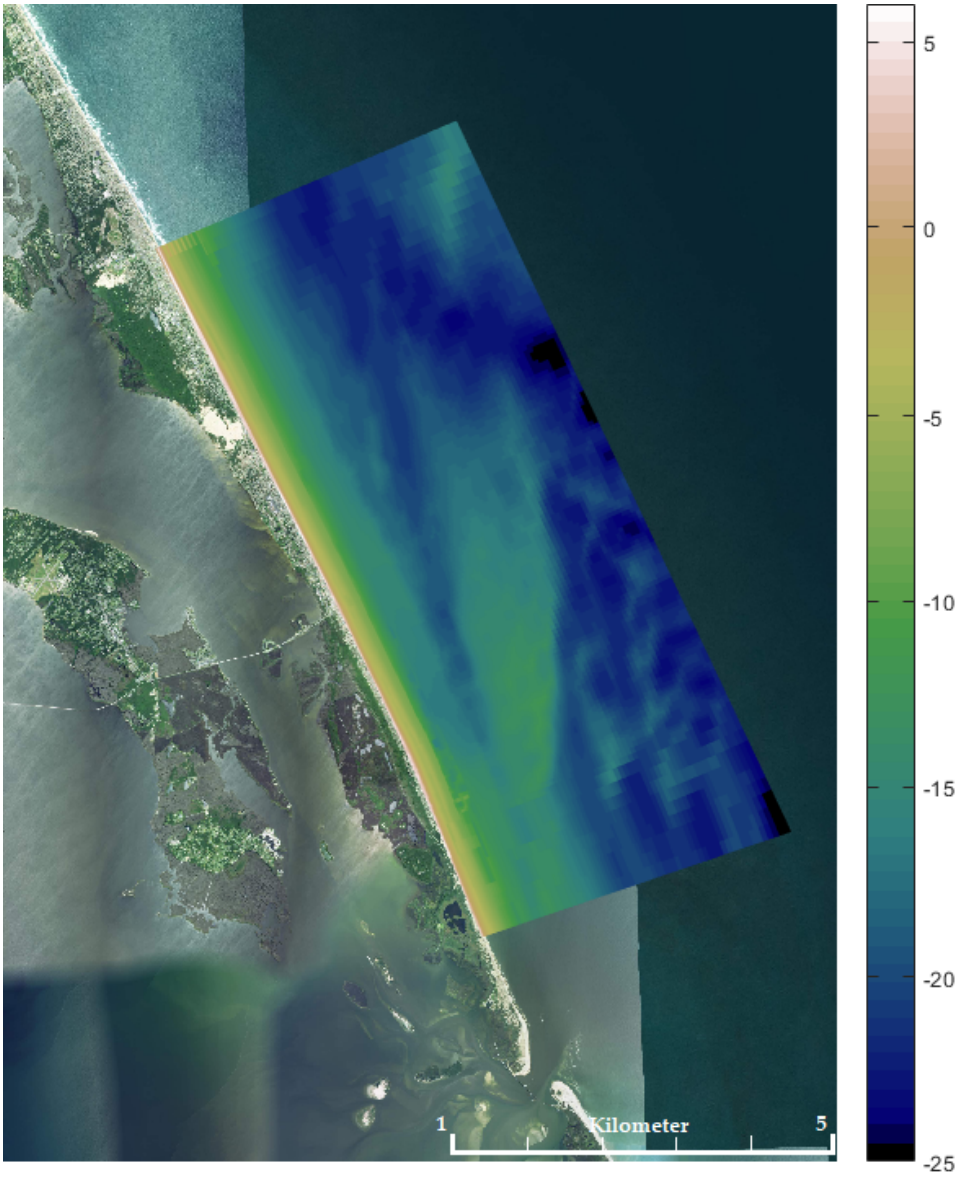

Figure 6.4: Visualization of the Delft3D-FLOW domain over the Nags Head shoreline. Colors represent the bed level elevation in m NAVD.

6.2.1 Delft3D Sediment Transport Calibration Parameters

In the Chapter 5.3.2, the relation between the incoming waves and their influence on the sediment transport formulations for the UNIBEST-TC model was analyzed. This chapter will do a likewise analysis, with the emphasis on the main Delft3D sediment transport formulations. Here, the sediment transport is summarized, and shows the origin of the user-defined sediment transport calibration parameters f_{BED}, f_{SUS}, f_{BEDW} and f_{SUSW} as based on (Grunnet et al., 2004).

When using the 3D approach, no vertical momentum equation is solved since the assumption is made that the vertical accelerations are small compared to the gravitation acceleration. The vertical velocity is computed from the continuity equation. In the 2DH approach the terms containing the vertical coordinate (z), the vertical flow velocity (ω) and the vertical eddy viscosity (ν_v) are not taken into account. These terms only influences the vertical distribution of momentum. Therefore, in fact, the same set of equations is solved in the 2DH approach as in the 3D approach only the vertical distribution of momentum is not computed using the 2DH approach.

Bed-load Sediment Transport: For Delft3D morphological simulations including waves and using the Van Rijn et al. (2001) model for sediment transport approximation, the bed-load transport is computed as[1]:

$$q_b = 0.006 \rho_s w_s D_{50} M^{0.5} M_e^{0.7} \tag{6.1}$$

ρ_s	=	Sediment density	$[kg/m^3]$
w_s	=	Fall velocity	$[m/s]$
M	=	$\frac{v_{eff}^2}{(s-1)gD_{50}}$ = Sediment mobility number driven by currents and waves	[-]
M_e	=	$\frac{(v_{eff}-v_{cr})^2}{(s-1)gD_{50}}$ = Excess sediment mobility number	[-]
v_{eff}	=	Effective velocity due to currents and waves	$[m/s]$
v_{cr}	=	Critical velocity	$[m/s]$
s	=	$\frac{\rho_s}{\rho_w}$ = Relative density	[-]

The direction of the bed-load transport vector is composed of the contribution in the direction of the near-bed current and the contribution in the direction of wave propagation, each of which with a magnitude determined by:

$$|q_{b,c}| = \frac{|q_b|}{\sqrt{1 + r^2 + 2|r|\cos(\phi)}} \quad and \quad r = \frac{(|u_{on}| - v_{cr})^3}{(|\bar{u}| - v_{cr})^3} \tag{6.2}$$

$$|q_{b,w}| = r|q_{b,c}|$$

u_{on}	=	Near-bed peak orbital velocity, onshore directed (Kraus et al., 1982)	$[m/s]$
$\bar{u}$	=	Depth-averaged velocity	$[m/s]$
ϕ	=	Angle between wave and current direction	$[\circ]$

In the present model, $q_{s,w}$ is included in the bed-load transport vector based on the concept that the bulk of the suspended sediment transport within about 0.5 m of the bed reacts instantaneously to wave oscillations, similar to $q_{b,w}$. The wave-related suspended sediment transport, as introduced by Houwman and Ruessink (1997), is approximated as:

[1]For more detail on v_{eff} and v_{cr}, see (Van Rijn et al., 2001).

$$q_{s,w} = k_{as} \frac{u_{on}^4 - u_{off}^4}{u_{on}^3 + u_{off}^3} L_T \tag{6.3}$$

k_{as}	=	0.2 = A phase lag coefficient, resulting from a delay of sediment response to orbital velocities	$[m/s]$
u_{off}	=	Near-bed peak orbital velocity, offshore directed	$[m/s]$
L_T	=	$0.007 \rho_s D_{50} M_e$ = Suspended sediment load	$[kg/m^3]$

The three transport contributions are combined and yield for each of the directions of a computational grid cell:

$$q_{b,u} = f_{BED} \frac{u_b}{|\overrightarrow{u_b}|} |q_{b,c}| + (q_{b,w} + f_{SUSW} q_{s,w}) \cos(\phi) \tag{6.4}$$

$$q_{b,v} = f_{BED} \frac{v_b}{|\overrightarrow{u_b}|} |q_{b,c}| + (q_{b,w} + f_{SUSW} q_{s,w}) \sin(\phi)$$

f_{BED}, f_{SUSW}	=	User-defined calibration factors	[-]
u_b, v_b, $\overrightarrow{u_b}$	=	Velocity components and vector in the bottom computational layer	$[m/s]$
ϕ	=	Local angle between the direction of wave propagation and the computational grid	[∘]

The magnitude and direction of the bed-load transport vector is adjusted for bed-slope effects based on a modification of Bagnold (1966).

Suspended Sediment Transport: The current-related, suspended load transport is defined as the transport of sediment particles by the time-averaged current velocities given by:

$$q_{s,c} = \rho_s \int_{z_a}^{h} cudz \tag{6.5}$$

c	=	Time-averaged concentration	$[kg/m^3]$
u	=	Time-averaged current velocity	$[m/s]$
z	=	Height above the bed	$[m]$
z_a	=	Reference height	$[m]$
h	=	Water depth	$[m]$

The near-bed reference concentration c_a at height z_a is computed as:

$$c_a = f_{SUS} 0.015 \frac{D_{50}}{z_a} \frac{T^{1.5}}{D_*^{0.3}} \tag{6.6}$$

f_{SUS}	=	User-defined calibration factor	[-]
T	=	Dimensionless bed-shear stress parameter	[-]
D_*	=	The non-dimensional sediment grain size	[-]

The dimensionless bed shear stress parameter T is computed as:

$$T = \frac{\tau_{b,cw} - \tau_{b,cr}}{\tau_{b,cr}} \tag{6.7}$$

$\tau_{b,cw}$	=	Time-averaged effective bed shear stress	$[N/m^2]$
$\tau_{b,cr}$	=	Time-averaged critical bed shear stress, according to Shields	$[N/m^2]$

The transport of suspended sediment is calculated by solving the 2DH advection-diffusion equation:

$$\frac{\delta c}{\delta t} + u\frac{\delta c}{\delta x} + v\frac{\delta c}{\delta y} + \frac{\delta w_{s,c} c}{\delta z} - \frac{\delta}{\delta x}\left(D_H \frac{\delta c}{\delta x}\right) - \frac{\delta}{\delta y}\left(D_H \frac{\delta c}{\delta y}\right) = 0 \tag{6.8}$$

$u,\ v$	=	Current velocities in respectively a grid cell's x and y directions	$[m/s]$
$w_{s,c}$	=	Fall velocity of suspended sediment in a fluid-sediment mixture	$[m/s]$
$D_H,\ D_V$	=	Eddy diffusivities, derived from the $k-\epsilon$ turbulence model[2]	$[m^2/s]$

In order to update the bed level, the exchange of sediment in suspension from the bottom computational layer to the bed (and vice-versa) is modeled by means of sediment deposition and erosion fluxes, D and E (respectively) applied to the bed of each computational cell as:

$$D = c_a\left(\frac{D_V}{\Delta z}\right) \quad and \quad E = c_k\left(\frac{D_V}{\Delta z} + w_s\right) \tag{6.9}$$

D_V	=	Vertical diffusion coefficient at the bottom cell	$[m^2/s]$
Δz	=	Vertical distance from the reference level z_a	$[m]$
k	=	Concentration for the reference cell	$[kg/m^3]$

Overview: A lot of similarities with the UNIBEST-TC transport formulations are observed while following the chain of events occurring in the Delft3D sediment transport formulations. In both models, the difference in time-averaged effective and critical bed shear stress is the factor that is influenced the strongest by incoming waves, hence driving the sediment transport.
In Delft3D, the wave influence on the bed-load transport is primarily caused by affecting the sediment mobility number (M) and the excess sediment number (M_e), see Eq. 6.1. Wave influence on suspended sediment transport is caused by increasing the effective bed shear stress.

6.3 Delft3D - FLOW Module Set-up

6.3.1 Model Capabilities

Tidal currents and wave-current interactions are a main driving force for sediment transport along the coast. The FLOW module simulates these important forces. However, using real-time series of the astronomical tide as a boundary condition to force the tidal flow is impractical, because it results in longer run times. To solve this problem, the real-time astronomical time series was schematized into a "morphological tide." To compute such a tide flow, a method based on tidal stations was applied which interpolates data from nearby tidal stations to force a tidal wave through the fine grid.

6.3.2 Tidal Wave Schematization

One option for simulating tides would be to extend the coarse grid to nearby tidal stations and translate the tidal wave from the tidal station to the finer grid. The major downside of this method is that all the finer grid boundaries have to be specified as a water level. Slight mismatches between these boundaries induce strong unrealistic currents at the borders of the domain which then propagate throughout the grid. An alternate method used for the Nags Head analysis is the "tidal

station method". It prevents these boundary errors by applying a "Neumann boundary" at the lateral boundaries as proposed by the study of Roelvink and Walstra (2004). This technique uses the gradient of the water level to force a tidal flow.

To create the longshore boundary conditions for Nags Head, the tidal and harmonic constituents from Duck FRF and Cape Hatteras tidal stations are interpolated. The derivative of these longshore water-level variations is needed to calculate the gradient for the cross-shore boundaries. By using this approach, the cross-shore boundaries will always follow the longshore water-level variations and thereby prevent any mismatches. An example of such a model is as follows:

The offshore boundary (blue line in Figure 6.5) is a water elevation boundary type driven by tidal constituents and is specified as follows[3]:

$$\eta = \hat{\eta}\cos(\omega t - kx) \tag{6.10}$$

η	=	Free surface elevation above the reference plane (at $z = 0$)	$[m]$
$\hat{\eta}$	=	Amplitude of the surface elevation	$[m]$
ω	=	$\frac{360^\circ}{T(hour)}$ = Angular velocity or frequency	$[\circ/hr]$
k	=	Wave number, in which $\frac{2\pi}{L} = \frac{360^\circ}{L}$, where L is the tidal length	$[\circ/m]$
x	=	Length of offshore boundary (distance from A to B in Figure 6.5)	$[m]$
ϕ	=	$k \cdot x$ = Phase and is zero at point A and ϕ at point B	$[\circ]$
		provided that the tide runs from A to B	$[\circ]$

The cross-shore boundaries (red lines in Figure 6.5) have to be of Neumann type and have to be specified as follows:

$$\frac{\delta\eta}{\delta x} = k\hat{\eta}\sin(\omega t - kx) = \frac{2\pi}{L}\hat{\eta}\sin(\omega t - \phi) = \frac{2\pi}{L}\hat{\eta}\cos(\omega t - (\phi + 90^\circ)) \tag{6.11}$$

$\frac{\delta\eta}{\delta x}$	=	Water level gradient	[-]
ϕ	=	$360 \cdot \frac{x}{L}$ = Phase	$[\circ]$

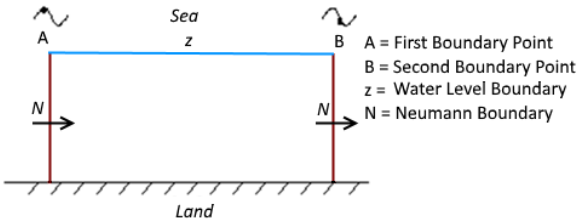

Figure 6.5: Example model using Neumann boundaries to force a tidal flow (after Roelvink and Walstra (2004)). Water-level curves at the two boundaries indicate different tide heights and, therefore, a net flow direction derived from the differences.

[3]For additional information on the computational strategy, refer to (Roelvink and Walstra, 2004).

6.4 Delft3D-WAVE Module Set-up

6.4.1 Model Capabilities

The purpose of applying nearshore wave transformation models is to quantitatively describe the change in wave parameters (wave height, period, direction, and spectral shape) between the offshore and the nearshore (typically depths of 40 meters or less). In relatively deep water, the wave field is fairly homogeneous on the scale of kilometers; but in the nearshore, where waves are strongly influenced by variations in bathymetry, water level, and currents, wave parameters may vary significantly on a scale of meters.

Since the coastal currents are highly dependent on the way of transformation of waves throughout the domain, the DELFT3D-WAVE model is used. It stimulates the evolution of wind-generated waves by coupling it to a third generation numerical wave propagating model like SWAN (Booij et al., 1999). By using these modules, Delft3D calculates how the offshore generated waves propagate through the domain driving longshore and cross-shore currents.

Wave height computations are performed using the Roller model, included in the FLOW-module (Reniers et al., 2004). First the propagation of short wave energy is calculated using the short wave energy balance equation (Eq. 6.12). The wave energy dissipation is then computed in Eq. 6.13 which in term is the source term for the roller energy propagation (Eq. 6.14), which will be dissipated using Eq. 6.15. This lag in wave energy dissipation is related to a spatial shift between gradients in sediment transport gradients and beach profile morphology that result in bar migration and development (Grunnet et al., 2004). The use of the roller model counteracts a rapid decay in bar height and therefore seems to be of upmost importance to simulate long-term morphological processes in the shoreface. Calibration of the roller model is according to Briere et al. (2011) based on the lack of accurate offshore hydrodynamics data.

$$\frac{\delta E_w}{\delta t} + \frac{\delta E_w c_g \cos(\Theta)}{\delta x} + \frac{\delta E_w c_g \sin(\Theta)}{\delta y} = -D_w \tag{6.12}$$

$$D_w = 2\alpha f_p E_w \left[1 - exp\left[-\left(\frac{E_w}{\gamma^2 E_{ref}}\right)^{\frac{n_d}{2}}\right]\right] \tag{6.13}$$

$$\frac{\delta E_r}{\delta t} + \frac{\delta 2 E_r c \cos(\Theta)}{\delta x} + \frac{\delta 2 E_r c \sin(\Theta)}{\delta y} = -D_r + D_w \tag{6.14}$$

$$D_r = \frac{\delta 2 g \sin(\beta)}{c} \tag{6.15}$$

α	=	Wave dissipation calibration coefficient	[−]
γ	=	Wave breaker calibration parameter	[−]
β	=	Wave breaker slope calibration parameter in roller model	[−]

Conclusively, as stated before in Chapter 5.3.2 - Main Sediment Transport Formulations, while doing a comparative analysis of the sediment transport formulations, it is shown that wave energy is dissipated via the Roller model. As long as this distribution of wave energy dissipation will not exceed the critical value, the optimal amount of wave energy dissipation takes place at that location. This should indicate that the EBP as proposed in Chapter 4 should be able to lower the sediment transport rates effectively as well, since the main forcing agents to shape the EBP are based on wave dissipation and reflection. This main hypothesis will be further elaborated in the next sections by using the EBP to shape a shoreface nourishment design and compare it with conventional designs.

6.4.2 Wave Climate Schematization

For purposes of reducing computational time during normal model simulations under Delft3D, the full wave climate was schematized in a set of representative wave conditions. The choice of these representative conditions uses sediment transport calculations as a target in such a way that the net and gross longshore sediment transport rates of the reduced set of representative wave conditions are comparable to the entire wave record (Walstra et al., 2013). The full wave climate, which was based on hourly sampled hindcast data for a one-year simulation, was binned in classes of wave heights and directions, and described by "p_i" (the probability of occurrence) (see Figure 3.10). The corresponding wave period was calculated analytically after the schematization.

To calculate the sediment transport rates for the wave-reduction technique, the two-dimensional (2DH) profile model UNIBEST-TC[4] (Bosboom et al., 1997; Van Rijn et al., 2003) was used. The advantage of using a profile model is its ability to accurately calculate the gross and net longshore sediment transport rates using a time series for the wave data. UNIBEST-TC was chosen to calculate the transport rates because it uses the same transport formulation by Van Rijn et al. (2001) as Delft3D. The schematized wave climate is referred to as a "morphological wave climate" and is applied with tidal boundary conditions prescribed as a morphological tide, based on the harmonic components as described in Section 6.3.2 - Tidal Wave Schematization. This representation of wave and tide enables the use of a morphological factor, MorFac, which is an acceleration trick used to speed up computer processing with the difference in time-scales between short-period hydrodynamics and longer-period morphological changes. It works by first dividing the total duration of each representative wave class by the duration of the morphological tidal wave (12 hours, 25 minutes) to obtain a constant morphological factor per representative class (i.e. – the MorFac).

Secondly, the transport rate "q_i" for each wave class is calculated during one tidal wave using Delft3D and is multiplied with its corresponding MorFac to obtain the total amount of bed-level changes due to the representative wave class (Ranasinghe et al., 2011). The use of MorFac effectively reduced the one-year wave climate to an ~14-day simulation run. The results of the wave schematization are given in Table 6.1. Figure 6.6 shows the degree to which the applied MorFac schematization yielded nearly the same sediment transport as the full wave record. The total yearly volume of longshore sediment transport is equal between the two wave climate, which was used as the schematization target. The schematized climate shows strong resemblance around the outer and inner breaker bar (first two peaks) in both peak volume and location. The schematized climate peaks, however, shows a wider spread which is the result of a relative invariable incoming wave field combined with the wave spreading due to the tide. In the swash zone (900-1000ft) that are caused by either errors in the computed sediment transport rates in very shallow water and the lack of variability in low wave characteristic to better incorporate the high morphodynamic variability in this region.

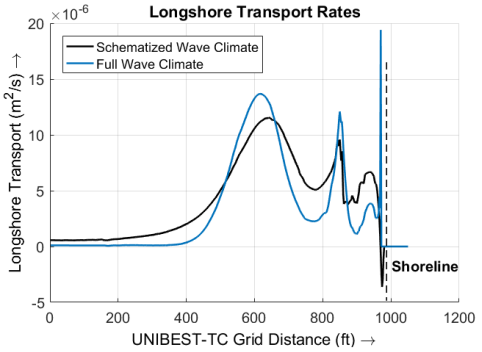

Figure 6.6: Computed longshore transport rates in UNIBEST-TC before wave climate schematization (blue line) and after schematization (black line).

[4]developed by the same developers as Delft3D (Deltares)

6.5 Delft3D Model Calibration

6.5.1 FLOW Module Calibration

Proper application of Delft3D requires the model to be calibrated by adjusting model setup and various model parameters until it can reasonably reproduce hydrodynamics and morphological changes. In the Flow module, the tidal wave velocities and amplitudes are first calibrated by adjusting the bottom roughness coefficients in such a way that the computed velocities and amplitudes match with the measured data from FRF Duck (Duck) and still reflect the real bottom conditions at Nags Head. The results after calibration are presented in Figure 6.7. These results show similar results between the computed and measured data, especially during high tides. During low tides the model slightly underestimates the water level elevation. In deeper water, the inertia terms in the shallow water equations are becoming more dominant, thereby reducing the computed tidal amplitude, especially affecting the lower tide amplitudes. To prevent the discrepancies of the first two computed tidal waves affecting the morphological behavior of the model, a 'spin up time' is introduced. All sediment transports are canceled during this time in order to accurately reproduce water level elevation. Overall, the computed results show strong agreement with the measured data with a maximum difference of 0.05%.

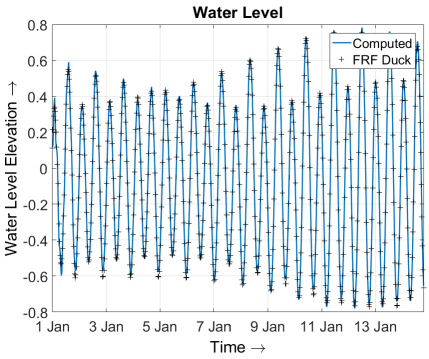

Figure 6.7: Computed water level elevation (blue) plotted against the measured water level elevation at the Field Research Facility at Duck (black).

Table 6.1: Applied wave conditions in the Nags Head model.

Wave Condition	Hs (m)	Tp (s)	Dir (°)	MorFac (-)	Perc. of Occur.
1	1.2	6.9	12.8	65.1	3.0
2	2.2	8.8	123.4	5.6	0.9
3	3.0	10.8	12.8	1.4	0.8
4	3.4	12.7	78.3	1.4	0.6
5	2.2	8.8	78.3	18.2	1.8
6	0.2	5.4	101.1	25.2	24.6
7	2.2	8.8	34.1	63.1	1.4
8	3.2	10.8	57.4	3.5	0.9
9	1.9	6.9	101.1	45.0	6.6
10	2.2	8.8	12.8	6.3	3.0
11	3.4	12.7	57.4	1.4	0.2
12	0.4	5.4	12.8	25.0	25.1
13	2.2	8.8	101.1	9.8	0.9
14	2.2	8.8	57.4	11.9	2.5
15	2.8	10.8	34.1	1.4	0.2
16	1.9	6.9	78.3	75.0	9.0
17	3.0	10.8	78.3	5.6	0.2
18	1.2	6.9	24.1	70.1	4.8
19	1.5	6.9	123.4	30.1	5.7
20	1.2	6.9	57.4	90.0	7.6
21	2.8	10.8	101.1	1.4	0.2

6.5.2 WAVE Module Calibration

In the Wave module, the wave propagation and transformation is calibrated by adjusting the depth-induced breaking and bottom friction parameters. To simulate the evolution of random, short-crested wind-generated waves in estuaries, tidal inlets, lakes etc., Delft3D-WAVE uses the third-generation SWAN model (Booij et al., 1999). All calibration parameters are pre-defined and originate from extensive studies for application procedures. Bottom friction is included by the Hasselmann formulations (Hasselmann, 1973) and the bore-based model for wave induced breaking (Battjes and Janssen, 1978) is applied. The SWAN model has successfully been validated and verified in several laboratory and (complex) field cases, see (Hydraulics, 2000a,b). The 35-year hindcast wave climatology for WIS station 63220 can directly be used since the border of the Wave grid extends to the WIS station location.
The computed wave data is compared with the measured wave data at Duck, the closest real-time wave buoy to Nags Head. As mentioned earlier, a previous study by Vandever and Miller (2003) suggested that the wave climate data collected at FRF are representative of the wave climate as far away as Oregon Inlet, nearly 25 miles to the south. The translated wave data is recorded in a virtual output station in the Delft3D model, which is located at the same offshore distance and depth as compared to the Duck FRF data. The measured wave data is compared with the computed wave data while changing the Wave module calibration parameters.

6.5.3 Sediment Transport Calibration

Delft3D incorporates a sediment-transport model based on the approximation of Van Rijn et al. (2001). The use of this model is motivated by its applicability to reduce computational time, thereby allowing 3D morphodynamic simulations over large spatial (10–100 km) and temporal scales (months to decades) (Grunnet et al., 2004). Based on the engineering approach of the van Rijn (2000) model, the Delft3D model can be used to calculate sediment transport for combined steady and oscillatory flow. Therefore, the model is able to more accurately compute current-wave interactions, which are known to be the main driver of nearshore sediment transport. Calibration is critical and this is accomplished by performing sensitivity studies on the current-related bed-load and suspended sediment transport.

The main objective of the Delft3D model is to compute how each nourishment design affects the existing longshore transport rates and how the design possibly affects the real-life occurring morphodynamics. For accurate calibration purposes, however, it is decided to cancel the wave-related bed-load bed_w and suspended sediment transport sus_w parameters. These parameters (among others) mainly influence the cross-shore morphodynamics. Since the sediment transport rates are computed in Generalized Lagrangian Mean (GLM) velocities, rather than Eulerian velocities, the onshore directed Stokes drift is counterbalanced by the offshore directed return flow, resulting in a net zero cross-shore transport rate (Ton, 2017). As a result, the model is only capable of assessing the yearly averaged longshore transport rates with a variable wave climate per nourishment design. All cross-shore morphodynamics like bar migration and the interaction in how cross-shore variations induce variations in local longshore transport gradients are canceled out.

The transport parameters are adjusted to match the real-life longshore transport rates, the results of which are shown in Figure 6.8. After calibration, a yearly average of ~270,000 cy southerly directed longshore transport rate is computed as to the ~272,200 cy caused by erosion losses. The modeled average annual sand losses are computed and compared to the measured rates. Results in north Nags Head show close agreements for between the modeled and measured results. The results in south Nags Head show a little offset, with over-estimation of the modeled erosion rates in Reach 4 and under-estimation in Reach 3. Nonetheless, when linearly approximating the computed results, the same average increase in transport rates with rates ~2.5 times as high in the south are found, corresponding to survey data from the past years as explained in Chapter 3.4.

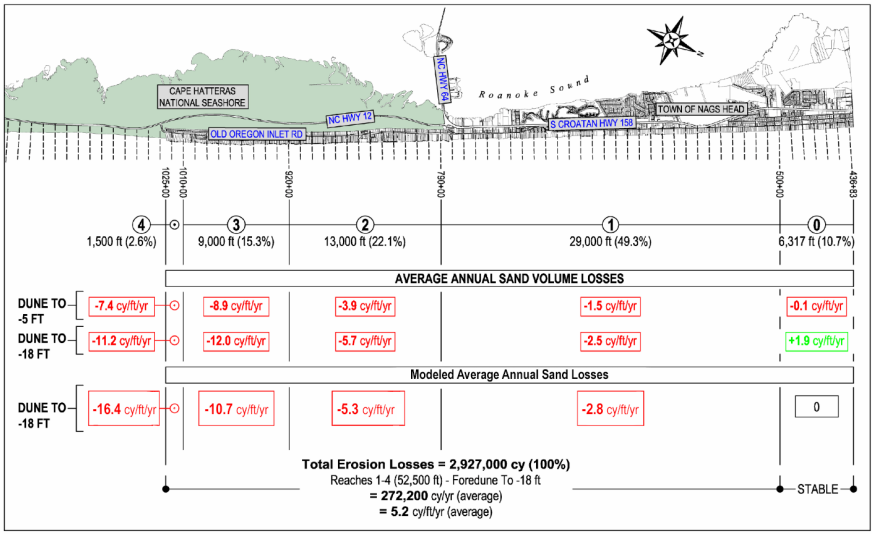

Figure 6.8: Average annual and net sand volume losses per reach between August 1994 and April 2005, average yearly loss of 272,200 cy/yr. Top row show the measured sand loss in cy/ft/yr, bottom row shows the modeled sand losses per reach after calibration. (source: CSE (2006))

6.6 Model Validation

An objective evaluation method is needed to check the whether the models are calibrated correctly and to evaluate results of the hydro- and morphodynamic models. The model performance is assessed by calculating a skill score, which is expressed with the Brier Skill Score (BSS) (Sutherland et al., 2004), and is formulated as follows:

$$BSS = 1 - \frac{\langle (z_{b,c} - z_{b,m})^2 \rangle}{\langle (z_{b,o} - z_{b,m})^2 \rangle} \tag{6.16}$$

Equation 6.16 expresses the skill as the fraction between the predicted anomaly and the measured anomaly, which in term is used to qualify the accuracy of the model. To classify the model performance, the Van Rijn et al. (2003) classification system is used, with negative scores indicate bad model performance, 0 - 0.3 poor performance, 0.3 - 0.6 reasonable, 0.6 - 0.8 good and 0.8 - 1.0 excellent. The model skill is therefore determined computing the difference in the computed (c) bed level after one year of morphological modeling and the measured bed level (m) and compare it with the 2017 survey dataset (o). An average model skill score is determined by taking the mean of the BSS score of each grid cell in between the dune foot and the depth of closure, as no morphological changes are expected outside these reaches. In the current application, the model BSS is 0.10, and is considered to poorly reproduce the observed morphodynamics.

The validation values are obtained by lowering the model dependency on cross-shore transport rates, making the model better suited for analyzing nourishment impact on longshore transport rates. Cross-shore transport processes are almost canceled by reduction of the horizontal uniform eddy viscosity and diffusivity have been strongly reduced, and the wave-related bed-load and suspended load sediment transport factors turned off, thereby not allowing wave asymmetry. As a result the model is able to accurately compute the yearly averaged longshore transport rate per nourishment scenario. Exact computations of the nearshore morphodynamics like bar migration and nourishment efficiency over a variable and bathymetry-interacting wave climate are neglected.

Model results show that the measured profile follows the modeled profile accurately and even while lowering the cross-shore transport dependency, the model still correctly models the total transport in both cross-shore and longshore direction, see Figure 6.9. Here, the distribution of transport rates during wave condition 11 (H_s=3.4m, T_p=12.7, dir=57.4°) is plotted over the beach profile. This shows that the model is capable of accurately reproducing wave-induced transport rates after wave breaking over the bars in both volume and location, necessary for computations of yearly averaged longshore transport rates and local gradients.

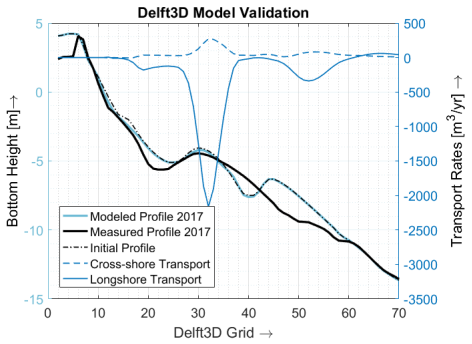

Figure 6.9: Computed and measured beach profiles in 2017 plotted against the initial profile in 2016 used for model validation (BSS=0.801), compared to the cross-shore transport rates (~50.000m^3/yr) and longshore transport rates (~235.000m^3/yr).

Several sensitivity studies are also performed for model validation to check whether changes in the input parameters show expected changes in the results. For the Nags Head model, the wave dataset, the angle of wave incidence and the median grain size are altered in accordance to historical or geological observation, or different data sources. Results are summarized in Appendix C.1 - Delft3D. All aforementioned studies show either an increase or decrease of net averaged longshore transport rates. However, the variability in these transports stay unaltered, meaning that only the magnitude of sediment transport is affected which also means that the overall differences in erosion rates are unaffected as well. During the calibration process, the current related sediment transport magnitudes are adapted to match the measured historical longshore transport and erosion rates, and show little to no effect on the longshore variability and distribution of the sediment transport rates (eg. see Eqs. 6.4 and 6.6). The sensitivity analysis therefore validates the current model setup is capable of transforming the offshore wave data and properly computing longshore transport rates in response to changes in nearshore bathymetry.

6.7 Model Results

To simulate the different nourishment impacts and to see how the nourishments affect the longshore transport rates, a one-year modeling study was set up. Primary goal while optimizing the shoreface nourishment design is to use as little amount of sediment to lower construction costs while reshaping the cross-shore profile, or to maximize nourishment longevity using the same amount of sediment. In this study, four different nourishment designs with the same total nourishment volume of ~500 m^3/m (200 cy/ft) are applied. Nourishment longevity and thus the nourishment efficiency of each nourishment is computed by calculating the net absolute longshore transport rates of each design after a one-year time period. The net longshore transport rate of each nourishment design along the Nags Head project site are plotted in Figure 6.10. The dashed lines represent the linear regression trend of the four different designs. All four lines again show the earlier observed increase in transport rates from north to south.

Extension Outer Bar (Alt. 1): When extending the top of the outer bar the longshore transport rates almost double compared with the EBP-design (459.000 cy/yr), showing strong sediment losses and thereby indicating a low nourishment longevity.

New Outer Bar (Alt. 2): Creating a new outer bar shows to be rather efficient, with a longshore transport of 281.000 cy/yr.

Fill In Trough (Alt. 3): The option of filling in the trough between the inner and outer bar shows comparable results to the EBP-design, with a longshore transport of 260.000 cy/yr (an approximate 5% increase compared to Alt. 4).

EBP-Design (Alt. 4): A nourishment designed using the concept of Equilibrium Beach Profiles shows the best results, with a total net longshore transport of 251.000 cy/yr. Other shoreface nourishment designs based on conventional designs show higher transport rates.

Compared to the Before Dredging scenario with a longshore transport rate of 270.000 cy/yr, only the nourishment alternatives shoreward of the outer bar seem to lower the initial transport rates. The nourishment lee effects, where increased offshore wave breaking should reduce the nearshore transport rates does not seem to be as effective. These results coincide with the earlier findings in chapter 5.6 - Relative Impact of Shoreface Nourishment Designs, which only show a minor decrease in significant wave height of each nourishment design compared to the Before Dredging scenario. For both designs seaward of the outer bar (Alt. 1 and 2) the initial profile seems to have trouble redistributing the surplus of sediment of the after dredging profile. As a result, inefficient wave energy dissipation along the beach profile occurs, stirring up more sediment and transporting it out of the littoral zone. Alternatives 3 and 4 do not seem to have this problem and are only affecting the wave energy dissipation distribution in an effective way.

Previous studies on coastal erosion (Ruggiero et al., 2009) concluded that the local gradients (variability) in longshore transport dominate coastal erosion at the scale of nourishments. Therefore, the local gradient in the net longshore transport per design is computed, and plotted in Figure 6.12. Comparison of the four different designs show comparable results with the net longshore transport results, with only one exception. The design based on Equilibrium Beach Profiles (Alt. 4) show a strong reduction of the longshore transport variability compared to the design by filling in the trough (Alt. 3). A reduction of ~40% in the local gradient is found between Alt. 3 and Alt. 4, compared to the ~5% reduction in net longshore transport. Results shows that the EBP-design is highly effective for smoothing out the cross-shore irregularities along the shoreline, creating a more uniform longshore profile. This way the longshore flow can flow more easily without being obstructed by such irregularities (i.e. - less sediment transport and local gradients because of a divergence of non-linear local sediment transport rates over the coastal zone).

To make a better visualization of how the different shoreface nourishment designs perform over the project site, the shoreline is divided into four equally spaced sections. The total longshore nourishment length in each scenario was 10.14 miles, therefore each section represents ~2.5 miles of shoreline. The bar plot in Figure 6.11 shows the net absolute longshore transport per section of each nourishment design. The dashed lines represent the average values, as found in Figure 6.11 and the blue markers on each bar show the range of values of longshore transport per design per section. A detailed overview of all nourishment designs are shown in the series of Figures in Appendix D and are displayed using contour lines. The figures furthermore show the stations at which the reaches used for the Nags Head project are divided. Based on these results it seems that the overall longshore sediment transport values are similar for Alternatives 2-4, which are similar to the Before Nourishment scenario. The additional volume of sediment therefore results in similar erosion rates and creates a safer beach.

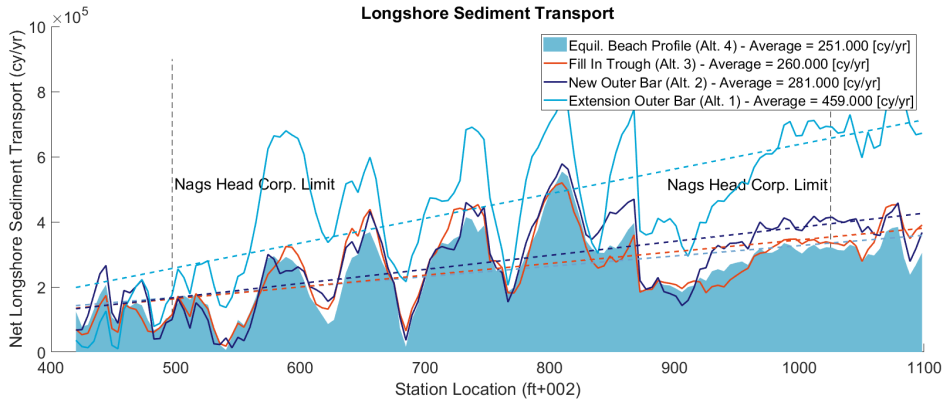

Figure 6.10: The longshore transport rates of each nourishment scenario plotted along the Nags Head project shoreline. Dashed lines indicate the linear approximation per scenario.

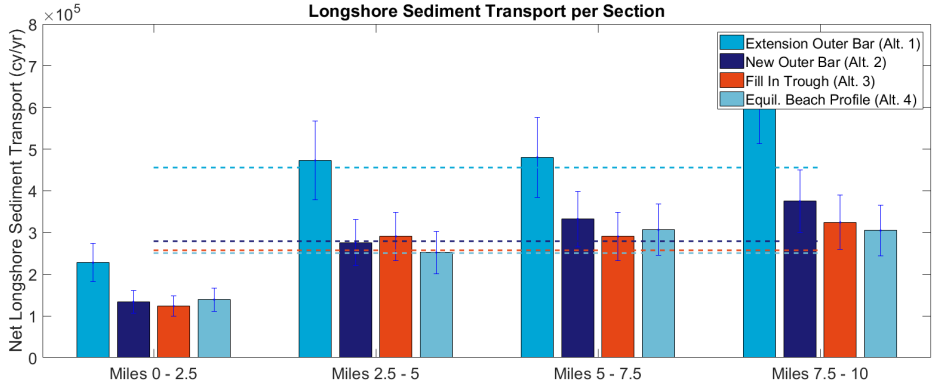

Figure 6.11: The average longshore transport rates of each nourishment scenario per section plotted along the Nags Head project shoreline.

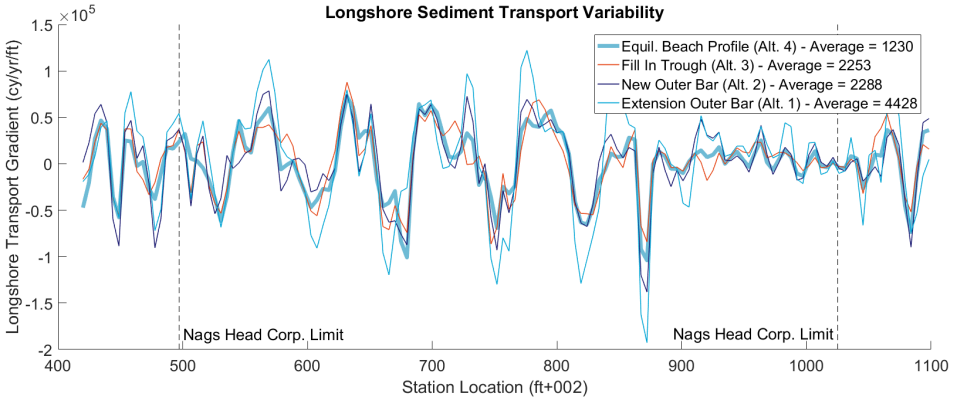

Figure 6.12: The longshore transport variability of each nourishment scenario plotted along the Nags Head project shoreline.

6.8 Discussion

The past years of research increased the accuracy of process-based modeling in three dimensional morphodynamic applications to a feasible level for nourishments impact simulations. Especially on larger scales (in the order of kilometers) morphological features like longshore transport rate computations are well represented. However, there are still some limitations in the modeling process, which will be elaborated here. On the scale of bar dynamics and shoreface nourishment designs, accurate morphodynamic predictions like beach profile evolutions seems unsuitable for a model like Delft3D (Grunnet et al., 2004). Even while including the roller model and wave-current interacting sediment transport formulations like the van Rijn model, beach profile evolution cannot be used as a criterion for shoreface nourishment design evaluation in this study. The effects nourishment have on longshore transport rates and local gradients are therefore chosen for nourishment impact evaluation to quantify the results, which are obtained by turning off the wave-related bed-load (bed_w) and suspended sediment transport (sus_w) parameters.
As a result, the model is only capable of assessing the yearly averaged longshore transport rates with a variable wave climate per nourishment design. Since the sediment transport rates are computed in Generalized Lagrangian Mean (GLM) velocities, rather than Eulerian velocities, the onshore directed Stokes drift is counterbalanced by the offshore directed return flow, resulting in a net zero cross-shore transport rate. Computations of the sediment transport rates in Eulerian velocities could give more accurate representations of beach profile evolution, even when turning off the wave-related sediment transport parameters since the net cross-shore transport rates would have a net non-zero value. This option was unfortunately not possible with the current available version of FLOW2D3D (version 6.01.07.3574).
Using a 2DH over a full 3D approach on the scale of longshore transport computations can arguably be accepted as a more feasible model application. The benefits of a 3D application prevail in the detailed representation of the real-time hydrodynamics over the vertical layer, as it does not include approximations for factors like undertow. The distribution of the flow velocities are affected using the 2DH approach, resulting in different sediment transports as well compared to a 3D model. These effects however, can be compensated by adjusting the sediment transport parameters for an accurate representation of the (larger scale) longshore transports and variability of such transport. The merits of the 2DH approach lie in the significant reduction of computational time, thereby increasing the model applicability in case of nourishment evaluation.

Nevertheless, a comparative analysis of the sediment transport formulations show that the wave energy in the model is dissipated via bottom friction using bed shear stresses and the resulting sediment transport depends on whether the generated bed shear stresses exceed the critical value. As long this critical value is not surpassed, the optimal amount of energy dissipation takes place locally. Since the dissipation and wave breaking are mostly depth dependent, this should indicate that a beach profile following the EBP (after reshaping by nourishment) is able to lower the sediment transport rates optimally as well, as the main forcing agents to shape the EBP are based on wave dissipation. The concept of using an EBP for nourishment design therefore not only holds for the design process, but is evidently integrated in the Delft3D transport formulae. This improves the model applicability for such modeling studies.

Sensitivity analysis of the morphological model show significant differences in total volume loss and longshore transport rate while adjusting the shoreline orientation and median grain size prescribed in the model, indicating that lower values for the wave angle of incidence and median grain size result in higher longshore transport rates and can significantly affect the model outcome. This indicates the strong sensitivity of the model on the input parameters, another reason why the nourishment effect quantification is based on large scale processes like longshore transport rates rather than single profile evolutions.

Conclusively, both cross-shore and longshore sediment transport processes seem to dominate coastal erosion, and especially the relation how either type of transport is affected by the other seems to be important to know in order to determine the physical processes behind coastal erosion. Separation between these two types of transports, as done in the previous two chapters gained some insight on the relative effect per transport direction. Exact determination of the coastal erosion does not seems to be possible with the current model set-up. However, nourishment impact and efficiency related to longshore transport rates and local gradients are very well represented and will be further exploited.

6.9 Summary

The primary study goal is to optimize shoreface nourishment design by maximizing nourishment longevity while using the same amount of sediment compared to other design alternatives. A 2DH version of the Delft3D process-based model is used for offshore wave transformation and to compute the nearshore hydrodynamics and morphodynamics for different shoreface nourishment designs. The computed longshore sediment transport rates and local gradients are subsequently used for nourishment efficiency quantification.

The schematized morphological tide is computed by interpolating data from nearby tidal station to force a tidal wave through the FLOW grid. The impact of the wave and tide schematization on the model outcome are negligible, as in both cases the computed data shows strong consistency with the measured data. Using the model, the predicted longshore transport rates are very similar to the measured transport rates based on yearly surveys over the past decades. The Delft3D morphological model re-creates both measured sediment transport rates along the area of interest and recognized transport patterns throughout the Nags Head project. A strong longshore increase in transport is found with rates ~2.5 times as high in the south compared to the north, with an average value of 270.000 cy/yr along the project shoreline.

Nourishment longevity and thus the nourishment efficiency of each nourishment is computed by calculating the net absolute longshore transport rates of each design after a one-year time period. The four different nourishment designs as based on the previous research question (Extension Outer Bar, New Outer Bar, Fill In Trough and EBP-design) are tested and show an average longshore transport value of; 459,000 cy/yr, 281,000 cy/yr, 260,000 cy/yr and 251,000 cy/yr respectively. Results indicate that nourishment design based on the concept of equilibrium beach profiles (EBP-design) lower the longshore transport rates most effectively, resulting in the highest longevity as well.

Another way of quantifying shoreface nourishment efficiency is to compare the local gradients in longshore transport rates per design. Lower local gradients indicate a less obstructed longshore flow, thereby decreasing the transport rates as well. An average longshore transport variability per design Alternative 1 – 4 of respectively 4,428 cy/yr/m, 2,288 cy/yr/m, 2,253 cy/yr/m and 1,230 cy/yr/m is found. Both quantitative analyses from the two previous research questions demonstrate that nourishment design based on equilibrium beach profiles decrease longshore transport rates and variability. Therefore the nourishment longevity and efficiency are strongly increased as compared to conventional nourishment designs based on guidelines. Optimizing shoreface nourishment design is therefore possible by including the beach profile forcing agents in the design process. This relation between forcing agents and beach morphology holds other interesting coastal management possibilities and will be further explored in the following research question.

7

Practical Application

Is the proposed EBP useful for predictions of the overall longshore transport gradient and longshore fill density design?

7.1 Introduction

The methodology of using the concept of equilibrium beach profiles to design shoreface nourishments is all based on an abundance of field data. Without this data, model calibration of the UNIBEST-TC model (based on variation of the cross-shore profile over time) and the Delft3D model (based on longshore transport rates) would not be possible. As explained in A - Data Collection Methodology, for ongoing projects like Nags Head on the Outer Banks, field data collection occurs (bi)-annually. Based on the changes in cross-shore profiles and compared to historical aerial photography, accurate net longshore transport rates and corresponding shoreline changes are computed.
Design of a beach or shoreface nourishment is then based on following the trend of the erosion rates over the years. In the Nags Head case, erosion and longshore transport rates at the south side are ~2.5x as high (= overall gradient) compared to profiles at the north side of the project, therefore requiring a higher nourishment fill density as well. This way, the nourishment fill density match the erosion rates, ensuring that after a certain amount of time (nourishment lifetime), the entire stretch of the project has to be renourished again, thereby optimizing the design as compared to a constant fill template.

However, one of the most urgent problems that prevents progress in nourishment design and the academic field of coastal engineering is the lack of field data. A scarcity of data implies estimations of erosion and longshore transport rates based on only aerial photography, which would drastically lower the accuracy. But what if the design process is turned around?
Based on the first Research Question, the relationship between the shape of the EBP and the site specific parameters as the forcing agents and the sediment characteristics are already known. The second and third Research Questions then applied the theory in two modeling studies, all based on the obtained knowledge of analyzing survey datasets, to see the nourishment efficiency compared to conventional nourishment designs. So now knowing that the EBP is calibrated to site specific preferences using only one-month wave data and a recent survey, could the EBP shape be used for nourishment design?

This Research Question therefore investigates how the concept of using an EBP can be applied to (preliminary) design beach or shoreface nourishments by estimating the longshore transport rates using only one dataset.

7.2 Theory

The shape of the EBP is formed by taking into account the site-specific sediment characteristics and the forcing agents (tide and waves) that acted in the nearshore environment. The same characteristics are furthermore responsible for driving sediment transport in both cross-shore and longshore direction, which indicates the first similarity between the shape of the EBP and the coastal erosion at a project site. In the previous Research Questions, the EBP shape was used to create the fill template for the 'EBP-design' shoreface nourishment. By plotting the EBP over the measured initial cross-shore profile, the deviation between the two profiles is calculated, which in term formed the nourishment fill template. The fill template per cross-shore profile shows a strong longshore variability, since a strong longshore variability of the cross-shore profile occurs as well. Chapter 5 - Cross-shore Nourishment Effects hypothesized, and proved, that the deviation between the initial and the EBP cross-shore profiles cause a difference between the equilibrium wave energy dissipation (D^*) and the wave energy dissipation of the initial profile (D), which is known to be the main driver of a net cross-shore transport rate, resulting in the case of Nags Head in coastal erosion. This also means that as the cross-shore deviations are reduced, the cross-shore erosion will be as well.

According to theory, the shape of the EBP is constant along the project site with respect to MSL. This is also based on the assumption that the wave climate is taken constant along the 10-mile project area. Nevertheless, different sediment transport and therefore erosion rates are found along the project site, even though the wave climate is not varying (the reason for these variable erosion rates are not of interest at the moment in this study and is therefore neglected for now). Since the erosion rates show this variability, and the EBP shape remains constant, even though using the same characteristics, the deviation between the initial and the EBP profile should indicate at which cross-shore profiles more erosion occurred during the same amount of time. Conclusively, the variability in longshore sediment transport and erosion rates should match the variability of the longshore variability of the fill templates.

7.3 Results

To visualize the similarity in longshore variability, two plots are shown in Figure 7.2. The top plot (*a*) shows the longshore variability in fill template, expressed as the volume difference between the initial profile and the EBP based profile, which indicates the longshore distribution of nourished sediment. The bottom plot (*b*) shows the modeled longshore transport rates. The fill density follows the measured erosion rates accordingly, with lower fill densities in the north compared to the south.

Some longshore locations, e.g. near station 625+00 and 875+00, show an above average fill density compared their surrounding average values. As the erosion rates show a strong variance, the fill density is expected to do so as well. After linearly approximating both datasets, the same longshore gradient is found, thereby demonstrating a correlation between longshore variability of the fill template and longshore sediment transport. A decreasing trend of the deviations between the linear approximations and computed data is visible. Computed data in south Nags Head (Reach 3N - 4) follow the linear approximations with decent accuracy. The longshore

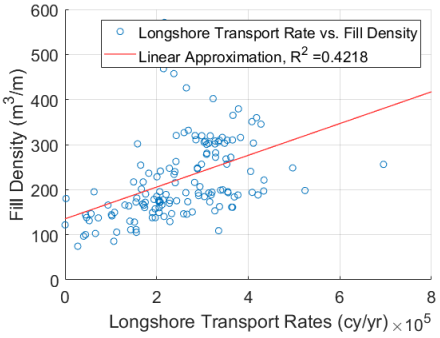

Figure 7.1: Scatter plot of the longshore transport rates compared to the fill density.

correlation between longshore transport rates and the fill density is computed so visualize the relationship between these two variants, see Figure 7.1. Results show that the predictor of longshore transport rates accounts for ~42% of all the variation in the fill density. The earlier mentioned longshore locations where the computed results are significantly higher compared to the general trend are clearly visible and account for the relative low correlation coefficient. However, for more than 90% of all data, strong correlation between the datasets is found. Furthermore, the linear approximation shows the same gradient as found in both plots in Figure 7.2, enhancing the possible relation between the two datasets. Since longshore transport rates and the resulting erosion rates are highly non-linear and are affected by several natural factors with strong unpredictability, a correlation coefficient of $R^2 = 0.4218$ is considered well within boundaries of the study domain. This suggests a correlation between longshore transport rates and fill density.

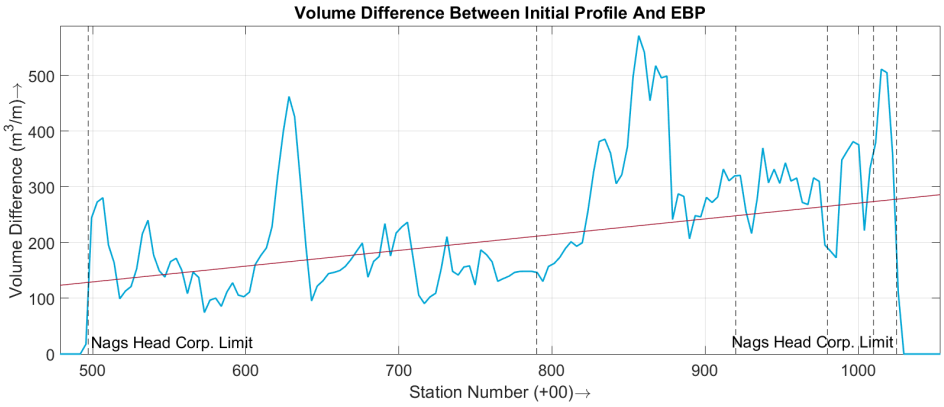

(a)

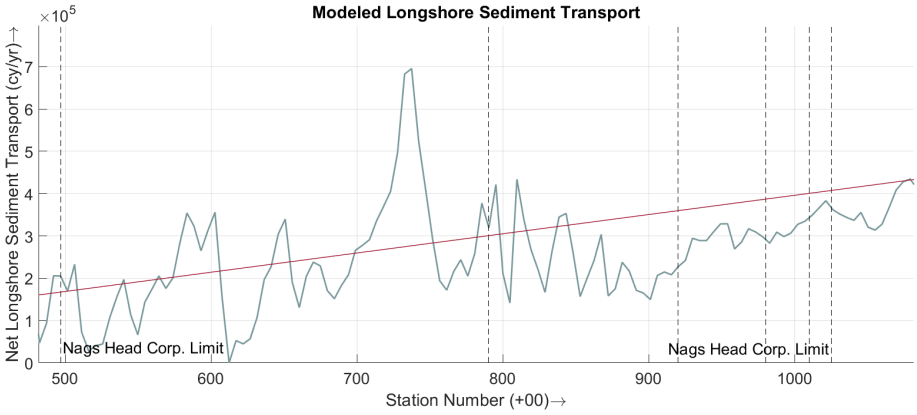

(b)

Figure 7.2: (*a*) Volume difference between the measured initial profile and the profile after dredging the nourishment based on the EBP design. (*b*) Net absolute modeled longshore sediment transport of the Before Nourishment scenario. Linear approximation of both the datasets (red) shows a similar increase of ~2.5x from north (left) to south (right), in agreement with the measured erosion rates.

7.4 Summary - Practical Application

The incoming wave climate and sediment characteristics are responsible for both the EBP shape and sediment transport resulting in coastal erosion, which is complemented with the fact that beach profile analysis between the initial profile and the EBP show that as the cross-shore deviations are reduced, the cross-shore erosion will be as well. Since the erosion rates at the project site show longshore variability, and the EBP shape remains constant, even though using the same characteristics, the deviation between the initial and the EBP profile should indicate a gradient in longshore transport rates as well, which in term could be useful for nourishment design as well, especially in remote locations. Knowing this, the longshore gradient can be estimated using only one survey dataset, which could lead to a preliminary nourishment design. Hence lowering the need for extensive and expensive surveys for longshore transport approximations. Especially in scenario's where the budget or sediment budget are limited, this approximation of longshore transport gradients could strongly improve the nourishment lifetime.

The constant longshore shape of the EBP with respect to MSL is furthermore very efficient in reducing the longshore transport gradients. Since the EBP-model is used as a template to fill in the vertical deviations between the initial profile and EBP, the longshore variabilities are spread out over the project site creating a less obstructive flow, thereby reducing longshore transport rates as well. Whereas conventional nourishment designs follow the original longshore variabilities and only enhance them, resulting in strong 3D bathymetrical features corresponding to coastal erosion as well.

8

Conclusion

The present study questioned the EBP shape as a response to dynamical parameters, the effects EBP-shaped nourishments have on either cross or longshore transport and its practical application to investigate whether shoreface nourishment design could be optimized based on the concept of EBP. Compared to conventional nourishment designs, the proposed shoreface nourishment design shows a strong reduction of both cross-shore and longshore transport rates, is most effective in counteracting coastal erosion and shows the highest nourishment longevity. A detailed conclusion of the study objective and its practical application is found by elaborating the four Research Questions separately.

How does the shape of the EBP depend on the forcing agents?
The proposed EBP shape to approximate the beach profile is based on a bi-polynomal equilibrium profile concept, representing either the surf or the shoaling profile. Each profile is formulated independently as a function of the dominating wave-energy dissipation process. The main principle of the EBP is based on the energy balance equation. The offshore limit coincides with the beach profile depth of closure, since the EBP shape depends on differences in wave fluxes. Sediment characteristics are implemented indirectly using the dimensionless fall velocity. Site-specific fitting of the EBP is therefore done using the local median grain sizes and measured hydrodynamics from the previous month. The relationships between the dimensionless fall velocity, profile morphology and the calibration coefficients are integrated in the proposed EBP and reflected in the beach morphodynamical state of being either a reflective, dissipative beach or a mix of both.
It is therefore possible, after site-specific calibration, to compute the EBP of any morphological beach state by any given beach, whilst knowing the corresponding dimensionless fall velocity to such beach state. This makes the proposed EBP useful for predictions of the beach morphology quantifications and seasonable variations as a response of the forcing agents, such as approximating longshore transport and erosion rates. Making it a possible important future tool for coastal management.

How do cross-shore transport rates lower while reshaping the cross-shore profile towards an EBP using shoreface nourishments compared with conventional nourishment designs?
The relation between the cross-shore sediment transport rates and the deviation between the equilibrium beach profile and its corresponding evolution due to such forcing agents is formulated as: $q = K(D - D^*)^n$, stating that beach profile evolution and resulting cross-shore sediment transport depend on the vertical deviation between the new profile and EBP. Where K and n are empirical coefficients and D^* is the wave energy dissipation rate corresponding to a stable cross-shore profile with a net cross-shore transport rate of zero. It is therefore known that the amount of cross-shore sediment transport depends on the distribution of wave energy dissipation, which in term has a strong dependency on the incoming wave climate and the beach profile.
Analysis of the UNIBEST-TC transport equations show that the relation between the wave climate and the non-dimensional sediment transport vectors is largely influenced in the differences between the effective and critical dimensionless shear stress ($\Theta'(t)$-Θ_{cr}), Eq 5.2. Therefore, in order to decrease the sediment transport and the stirring of sediment, the effective shear stress should

be reduced to approach the critical shear stress. This is possible by making vertical adjustments in the beach profile using nourishment, to in/decrease the near-bottom velocities by in/decreasing the bottom height.
These effects are checked by comparing three different conventional shoreface nourishment designs with a fourth design based on the concept of an EBP (the so called 'EBP-design', Alt. 4) to see which design lowers the cross-shore transport rates the most efficient. The conventional alternatives are designed by; extension of the outer bar (Alt. 1), creating a new outer bar (Alt. 2) and filling in the trough (Alt. 3). Results shows that the EBP-design shows a strong reduction of cross-shore transport rates compared to conventional shoreface nourishments. The average in/decrease in cross-shore sediment transport rates of the four nourishment designs compared to the before dredging scenario is +15.6%, +13.1%, -4.4% and **-5.6%** compared to Alternative 1-4 respectively. Further analysis of the results concluded that the strongest changes in net cross-shore transport rates occur at locations where dissipation of wave energy differs most considerably from the equilibrium rate. This increase in cross-shore transport might result in coastline retreat, which might harm vulnerable structures or dunes.

How do longshore transports and local gradients in sediment transport lower by using the concept of EBP during nourishment design?
Analogous guideline based conventional nourishment designs as described in Research Question 2 are compared to an EBP-based design in a coastal flow model. Model results show a similar outcome as compared to the cross-shore profile model, where the EBP-design produces the lowest longshore transport rates, thus the highest nourishment longevity. The average longshore transport rates for Alternative 1 – 4 are respectively 459.000 cy/yr, 281.000 cy/yr, 260.000 cy/yr and **251.000 cy/yr**, concluding that an EBP-based design in like manner reduces the longshore transport rates as well, thus optimizing nourishment longevity. An average longshore transport variability per design Alternative 1 – 4 of respectively 4,428 cy/yr/m, 2,288 cy/yr/m, 2,253 cy/yr/m and 1,230 cy/yr/m is found. Both quantitative analyses from the two previous research questions demonstrate that nourishment design based on equilibrium beach profiles decrease longshore transport rates and variability. Large local transport gradients are known to dominate coastal change at nourishment scales, thereby substantiating this Research Question's hypothesis that EBP-based designs are most efficient for shoreface nourishment design in terms of longevity and efficiency.

Is the proposed EBP useful for predictions of the overall longshore transport gradient and longshore fill density design?
Erosion rates at the project site show longshore variability, while the EBP shape remains constant, even though using the same morphodynamic characteristics. The deviation between the initial and EBP profile therefore indicates a gradient in longshore transport rates as well. After linearly approximating the longshore transport rates and fill density datasets, the same longshore gradient is found, thereby demonstrating that longshore variability of the fill template and longshore sediment transport are correlated to each other. Now, longshore transport gradients along the project site won't have to be estimated by annual survey data but only requires one bathymetry survey. Which in turn makes nourishment design only dependent on project budget for nourishment fill density design, possibly reducing the overall project costs especially in remote areas with a scarcity of beach profile data.
Finally, the constant longshore shape of the EBP is efficient in reducing the longshore transport variability. As the EBP-model is used as a template to fill in the vertical deviations between the initial profile and EBP, the longshore variabilities are spread out over the project site creating a less obstructive flow (i.e. - a divergence of non-linear local sediment transport rates over the coastal zone), thereby reducing longshore transport rates as well. Whereas conventional nourishment designs follow the original longshore variabilities and only enhance them.

9

Recommendations

This study has provided more insight into the morphodynamics and general properties of shoreface nourishment design. The modeling studies have shown how changes in nourishment design could influence the coastal erosion, but certain aspects during the nourishment design process remain uncertain or could be optimized. This chapter focuses on recommendations for study improvements regarding shoreface nourishment design. Modeling approaches and applications are disregarded consequently.

Selection Equilibrium Beach Profiles
The starting point of this study was to resemble beach profiles using empirical approximations such as the Dean 1977 profile. The main advantage of using this approach compared to dynamic equilibrium beach profiles is the longshore uniformity and uncomplicated applicability for nourishment design, since the only necessity is one bathymetric survey. However, dynamic EBP inspects the beach profile envelope over a certain period of time which is a direct indicator of beach morphology. Therefore, nourishment design based on this approach might be more efficient in counteracting coastal erosion as it is directly linked to this phenomenon, rather than a theoretical-based design. Another problem encountered using empirical EBPs, is the time scale of the morphodynamics around the shoreline cannot keep up with the high variability of the hydrodynamics, resulting in a net averaged sediment transport. The mean profile calculated from the dynamic EBP envelope possibly gives a better representation of these short-term shoreline morphodynamics and possibly redistributes the nourishment more efficiently over the longshore and cross-shore profile. Nonetheless, the empirical EBP assets and conveniences outweigh the advantages of a dynamic EBP in the current project scope and is chosen in this study accordingly.

Geotechnical aspects with respect to EBP calibration
The shape of the EBP and its corresponding nourishment design (Alternative 4) are highly dependent on the beach sediment characteristics. Small changes in the mean grain size strongly influences the nourishment design, and thus its efficiency. The sediment distribution plots in Appendix A - Data Collection Methodology show large variations between grab sample locations in the median grain size and standard deviation which should be reflected in the nourishment design as well. In the current application, a constant grain size diameter is used throughout the project. Major improvement in nourishment design will be realized when the beach profiles are divided in increments following the grab sample locations. Longshore and cross-shore interpolation of the sediment characteristics and corresponding nourishment design will then reflect these variations and should improve the nourishment efficiency as well. Likewise as mentioned previously, the order of the morphological timescales changes from months-years at the outer bar to hours-days when approaching the shoreline. The current application of the EBP uses constant hydrodynamic data over the project area and incorporates the seasonal variability by averaging the wave data from the previous month to calibrate the EBP model. This method of monthly-averaging wave data is accurate at cross-shore locations in which the order of the morphological timescales can be approximated with this wave data. However, the nearshore morphodynamics

are directly affected by the hydrodynamics which in the current application are still represented using monthly-averaged wave data. Reducing the averaging period from months to weeks or days allows the waves to more accurately interact with the nearshore morphodynamics, which increases the efficiency of the EBP-based nourishment design.

Modeling Limitations
The study methodology is divided into a cross-shore and longshore approach to point out the significance in Feeder and Lee effects respectively (Van Duin et al., 2004). The beach profile model UNIBEST-TC is useful to clarify the relative difference in nourishment impact compared to the Before Dredging scenario. Its simplicity results in relative accurate computations of bar morphodynamics, without the necessity for simplifications like wave climate schematization. However, since the model is only applicable in one beach profile, no coupling with longshore processes is possible. And it is especially this coupling, the interaction how cross-shore processes affect longshore transport rates and gradients, that could dominate nourishment efficiency.
It was therefore chosen to set-up an additional model, Delft3D, while knowing the limitations that the model poorly represents nearshore cross-shore phenomena like bar migration and thus nourishment impact. In order to more accurately capture the nourishment impact on longshore transport rates, the wave-related bed-load bed_w and suspended sediment transport sus_w parameters were turned off. As a result, the longshore processes were decoupled from cross-shore direction, thereby only allowing computations of yearly averaged longshore transport rates using a variable wave climate. Cross-shore transport rate induced gradients in longshore transport rates can therefore not be computed either.
For future studies, it would be interesting to set-up a model that accurately captures the above-mentioned model restriction and adaptations to the Delft3D model possibly makes this possible. Mass fluxes and transports are now computed using GLM velocities, therefore in 2DH mode by turning off bed_w and sus_w, no net cross-shore transport rates are allowed. Later versions of the FLOW-module (FLOW2D3D version 6.02.08.00000) allows hydro- and morphodynamic computations using Eulerian velocities, resulting in a non-zero net transport. Moreover (when sufficient calibration data is provided), a full 3D model application would give more insight in the vertical distribution of transport rates and would thereby compute nourishment impact more accurately.

Shoreface nourishment evaluation
Nourishment impact evaluation in this study is based on quantifying the lee and feeder effect. Both effects are quantified by investigating the averaged decrease in significant wave height and offshore sediment transport. Seasonal fluctuations and storm-impact events are accurately incorporated in the feeder effects, as the impact is based on changes in the total volume of sediment transport. However, by averaging the yearly significant wave height the strong variations during these fluctuations and impacts are lost. The wave height reduction between the four nourishment design scenarios during e.g. a storm impact shows more information of the lee effect. Since these storm impacts have a strong contribution in sediment transport rates and therefore the coastal erosion, nourishment efficiency would benefit from inclusion of these results.
Finally, considerable differences in all model results in this study were unanticipated as the applied wave climate is roughly constant in each simulation. However, different study sites possible influence the model outcomes. Applicability of the proposed EBP might vary along beaches with offbeat sediment characteristics, as will the shoreface nourishment impact per design scenario. Expansion of this study over additional particular study areas with different wave climates and sediment characteristics helps gaining knowledge and confidence in the applicability using the concept of EBP to optimize shoreface nourishment design.

References

Aragonés, L., Serra, J. C., Villacampa, Y., Saval, J., Tinoco, H., 2016. New methodology for describing the equilibrium beach profile applied to the valencia's beaches. Geomorphology 259, 1–11.

Baart, F., Den Bieman, J., Van Koningsveld, M., Luijendijk, A., Parteli, E., Plant, N., Roelvink, J., Storms, J., de Vries, S., van Thiel de Vries, J., et al., 2012. An integrated coastal model for aeolian and hydrodynamic sediment transport. In: EGU General Assembly Conference Abstracts. Vol. 14. p. 12842.

Bagnold, R. A., 1966. An approach to the sediment transport problem from general physics. US government printing office.

Baquerizo, A., Losada, M. A., 1998. Longitudinal current induced by oblique waves along coastal structures. Coastal engineering 35 (3), 211–230.

Battjes, J. A., Janssen, J., 1978. Energy loss and set-up due to breaking of random waves. In: Coastal Engineering 1978. pp. 569–587.

Bernabeu, A., Medina, R., Vidal, C., 2003. A morphological model of the beach profile integrating wave and tidal influences. Marine Geology 197 (1), 95–116.

Board, M., et al., 1995. Beach nourishment and protection. National Academies Press.

Booij, N., Ris, R., Holthuijsen, L. H., 1999. A third-generation wave model for coastal regions: 1. model description and validation. Journal of geophysical research: Oceans 104 (C4), 7649–7666.

Bosboom, J., Aarninkhof, S., Reniers, A., Roelvink, J., Walstra, D., 1997. Unibest-tc 2.0. Overview of model formulations. Delft Hydraulics report H 2305, 42.

Bosboom, J., Aarninkhof, S., Reniers, A., Roelvink, J., Walstra, D., 2000. Unibest-tc 2.0, overview of model formulations. WL Delft Hydraulics.

Briere, C., Giardino, A., van der Werf, J., 2011. Morphological modeling of bar dynamics with delft3d: the quest for optimal free parameter settings using an automatic calibration technique. Coastal Engineering Proceedings 1 (32), 60.

Bruins, R., 2016. Morphological behaviour of shoreface nourishments along the dutch coast: Data analysis of historical shoreface nourishments for a better understanding and design.

Bruun, P., 1954. Coast erosion and the development of beach profiles. Vol. 44. US Beach Erosion Board.

Coelho, C., Silva, R., Veloso-Gomes, F., Taveira Pinto, F., 2006. A vulnerability analysis approach for the portuguese west coast. Risk Analysis V: Simulation and Hazard Mitigation. 1, 251–262.

CSE, 2006. Preliminary coastal engineering analyses for large-scale beach restoration at nags head. technical report for town of nags head (nc).

CSE, 2011a. Coastal engineering & geotechnical analyses for beach nourishment, nags head, north carolina. final design report for town of nags head, nc.

CSE, 2011b. Coastal Erosion and Solutions A Primer.

CSE, 2017. Littoral processes, beach renourishment at nags head, dare county, north carolina.

Dean, R. G., 1977. Equilibrium beach profiles: US Atlantic and Gulf coasts. Department of Civil Engineering and College of Marine Studies, University of Delaware.

Dean, R. G., Chen, R., Browder, A. E., 1997. Full scale monitoring study of a submerged breakwater, palm beach, florida, usa. Coastal Engineering 29 (3-4), 291–315.

Dean, R. G., Dalrymple, R. A., 2004. Coastal processes with engineering applications. Cambridge University Press.

Eagleson, P. S., Glenne, B., Dracup, J., 1963. Equilibrium characteristics of sand beaches. Journal of the Hydraulics Division 89 (1), 35–57.

Emery, K., 1961. A simple method of measuring beach profiles. Limnology and oceanography 6 (1), 90–93.

Giardino, A., Broekema, Y., van der Werf, J., van Rooijen, A., 2016. Physical and numerical modelling of different nourishment desigins.

Giardino, A., Van der Werf, J., Van Ormondt, M., Brière, C., Walstra, D., 2009. Modelling and observations of a shoreface nourishment at egmond (netherlands). In: Proceedings of the RCEM Conference, Santa Fè, Argentina.

González, M., Medina, R., Losada, M., 2010. On the design of beach nourishment projects using static equilibrium concepts: Application to the spanish coast. Coastal Engineering 57 (2), 227–240.

Grunnet, N. M., Ruessink, B., 2005. Morphodynamic response of nearshore bars to a shoreface nourishment. Coastal Engineering 52 (2), 119–137.

Grunnet, N. M., Walstra, D.-J. R., Ruessink, B., 2004. Process-based modelling of a shoreface nourishment. Coastal Engineering 51 (7), 581–607.

Hanson, H., Brampton, A., Capobianco, M., Dette, H., Hamm, L., Laustrup, C., Lechuga, A., Spanhoff, R., 2002. Beach nourishment projects, practices, and objectives?a european overview. Coastal engineering 47 (2), 81–111.

Hartog, W. M., Benedet, L., Walstra, D.-J. R., Van Koningsveld, M., Stive, M. J., Finkl, C. W., 2008. Mechanisms that influence the performance of beach nourishment: a case study in delray beach, florida, usa. Journal of Coastal Research, 1304–1319.

Hasselmann, K., 1973. Measurements of wind wave growth and swell decay during the joint north sea wave project (jonswap). Dtsch. Hydrogr. Z. 8, 95.

Houwman, K. T., Ruessink, G., 1997. Cross-shore sediment transport mechanisms in the surfzone on a timescale of months to years. In: Coastal Engineering 1996. pp. 4793–4806.

Hubertz, J., 1992. The wave information studies (wis) wave model, version 2.0 (user's guide). Tech. rep., Coastal Engineering Research Center Vicksburg MS.

Hydraulics, D., 2000a. Physical formulations swan and data for validation. Tech. Rep. H3528.

Hydraulics, W. . D., 2000b. Modification first-guess swan and bench mark tests for swan. Tech. rep., WL | Delft Hydraulics.

Iglesias, G., López, I., Carballo, R., Castro, A., 2009a. Headland-bay beach planform and tidal range: A neural network model. Geomorphology 112 (1), 135–143.

Iglesias, G., López, I., Castro, A., Carballo, R., 2009b. Neural network modelling of planform geometry of headland-bay beaches. Geomorphology 103 (4), 577–587.

Inman, D. L., Elwany, M. H. S., Jenkins, S. A., 1993. Shorerise and bar-berm profiles on ocean beaches. Journal of Geophysical Research: Oceans 98 (C10), 18181–18199.

Kana, T. W., 1995. Signatures of coastal change at mesoscales. In: Coastal Dynamics' 95. ASCE, pp. 987–997.

Komar, P. D., 1998. Beach processes and sedimentation.

Kraus, N. C., Isobe, M., Igarashi, H., Sasaki, T. O., Horikawa, K., 1982. Field experiments on longshore sand transport in the surf zone. In: Coastal Engineering 1982. pp. 969–988.

Kriebel, D. L., Dean, R. G., 1985. Numerical simulation of time-dependent beach and dune erosion. Coastal Engineering 9 (3), 221–245.

Larson, M., Kraus, N. C., Wise, R. A., 1999. Equilibrium beach profiles under breaking and nonbreaking waves. Coastal Engineering 36 (1), 59–85.

Lesser, G., Roelvink, J. v., Van Kester, J., Stelling, G., 2004. Development and validation of a three-dimensional morphological model. Coastal engineering 51 (8-9), 883–915.

Luijendijk, A., 2001. Validation, calibration and evaluation of delft3d-flow model with ferry measurements.

Medina, R., Bernabeu, A., Vidal, C., Gonzalez, M., 2001. Relationship between beach morphodynamics and equilibrium profiles. In: Coastal Engineering 2000. pp. 2589–2601.

NCDENR, 1998. Long-term average annual shoreline change study and setback factors.

Ojeda, E., Ruessink, B., Guillen, J., 2008. Morphodynamic response of a two-barred beach to a shoreface nourishment. Coastal Engineering 55 (12), 1185–1196.

Pape, L., Kuriyama, Y., Ruessink, B., 2010. Models and scales for cross-shore sandbar migration. Journal of Geophysical Research: Earth Surface 115 (F3).

Plant, N. G., Edwards, K. L., Kaihatu, J. M., Veeramony, J., Hsu, L., Holland, K. T., 2009. The effect of bathymetric filtering on nearshore process model results. Coastal Engineering 56 (4), 484–493.

Ranasinghe, R., Swinkels, C., Luijendijk, A., Roelvink, D., Bosboom, J., Stive, M., Walstra, D., 2011. Morphodynamic upscaling with the morfac approach: Dependencies and sensitivities. Coastal engineering 58 (8), 806–811.

Rector, R. L., 1954. Laboratory study of equilibrium profiles of beaches. Tech. rep., Coastal Engineering Reseacch Center Vicksburg MS.

Reniers, A. J., Roelvink, J., Thornton, E., 2004. Morphodynamic modeling of an embayed beach under wave group forcing. Journal of Geophysical Research: Oceans 109 (C1).

Ribberink, J. S., 1998. Bed-load transport for steady flows and unsteady oscillatory flows. Coastal Engineering 34 (1), 59–82.

Roelvink, J., 2006. Coastal morphodynamic evolution techniques. Coastal Engineering 53 (2), 277–287.

Roelvink, J., Walstra, D.-J., 2004. Keeping it simple by using complex models. Advances in hydroscience and engineering 6, 1–11.

Ruessink, B., Kuriyama, Y., 2008. Numerical predictability experiments of cross-shore sandbar migration. Geophysical Research Letters 35 (1).

Ruessink, B., Kuriyama, Y., Reniers, A., Roelvink, J., Walstra, D., 2007. Modeling cross-shore sandbar behavior on the timescale of weeks. Journal of Geophysical Research: Earth Surface 112 (F3).

Ruggiero, P., Walstra, D., Gelfenbaum, G., Van Ormondt, M., 2009. Seasonal-scale nearshore morphological evolution: Field observations and numerical modeling. Coastal Engineering 56 (11), 1153–1172.

Saville Jr, T., 1958. Wave run-up on composite slopes. In: Proc. 6th Int. Conf. Coastal Eng., ACE, 1958.

Sun, B., 2004. Validation of hydrodynamic and morphodynamic modelling on a shoreface nourishement at egmond, the netherlands. IHE.

Sutherland, J., Peet, A., Soulsby, R., 2004. Evaluating the performance of morphological models. Coastal engineering 51 (8), 917–939.

Thornton, E. B., Guza, R., 1983. Transformation of wave height distribution. Journal of Geophysical Research: Oceans 88 (C10), 5925–5938.

Tolman, H. L., et al., 2009. User manual and system documentation of wavewatch iii tm version 3.14. Technical note, MMAB Contribution 276, 220.

Ton, A., 2017. Process-based modelling of hydro-and morphodynamics around the anmok submerged breakwater.

Tracy, B. A., Cialone, A., 2006. Comparison of gulf of mexico wave information studies (wis) 2-g hindcast with 3-g hindcasting. Tech. rep., ENGINEER RESEARCH AND DEVELOPMENT CENTER VICKSBURG MS COASTAL AND HYDRAULICS LAB.

USACE, 2000. Final feasibility report and environmental impact statement on hurricane protection and beach erosion control: Dare county beaches (bodie island portion), dare county, north carolina.

Van der Spek, A., Kruif, A., Spanhoff, R., 2007. Richtlijnen onderwatersuppleties. Rapportnr.: 2007.012.

Van der Werf, J., Giardino, A., van Ormondt, M., Walstra, D., Ramaekers, G., 2010. Detailed morphodynamic simulations of shoreface nourishment scenarios. In: Proceedings of the sixth IAHR Symposium on River, Coastal and Estuarine Morphodynamics (RCEM), Santa Fe, Argentina. pp. 953–957.

Van Duin, M., Wiersma, N., Walstra, D., Van Rijn, L., Stive, M., 2004. Nourishing the shoreface: observations and hindcasting of the egmond case, the netherlands. Coastal Engineering 51 (8), 813–837.

Van Enckevort, I., Ruessink, B., Coco, G., Suzuki, K., Turner, I., Plant, N. G., Holman, R. A., 2004. Observations of nearshore crescentic sandbars. Journal of Geophysical Research: Oceans 109 (C6).

Van Rijn, L., 2011. Coastal erosion and control. Ocean & Coastal Management 54 (12), 867–887.

Van Rijn, L., Roelvink, J., Horst, W. t., 2001. Approximation formulae for sand transport by currents and waves and implementation in delft-mor. Z3054.

Van Rijn, L., Walstra, D., Grasmeijer, B., Sutherland, J., Pan, S., Sierra, J., 2003. The predictability of cross-shore bed evolution of sandy beaches at the time scale of storms and seasons using process-based profile models. Coastal Engineering 47 (3), 295–327.

Vandever, J., Miller, H., 2003. How efficient is mother nature at oregon inlet, north carolina? Coastal Sediments, pp 515–516.

Walstra, D., Hoekstra, R., Tonnon, P., Ruessink, B., 2013. Input reduction for long-term morphodynamic simulations in wave-dominated coastal settings. Coastal Engineering 77, 57–70.

Walstra, D.-J., Ruessink, G., Aagaard, T., Deigaard, R., Fuhrman, D., 2017. Recent insights into inter-annual sandbar dynamics.

Wang, P., Kraus, N. C., 2005. Beach profile equilibrium and patterns of wave decay and energy dissipation across the surf zone elucidated in a large-scale laboratory experiment. Journal of Coastal Research, 522–534.

Waters, C. H., 1939. Equilibrium slopes of sea beaches. University of California, Berkeley.

Wijnberg, K. M., Aarninkhof, S. G., Spanhoff, R., 2007. Response of a shoreline sand wave to beach nourishment. In: Coastal Engineering 2006: (In 5 Volumes). World Scientific, pp. 4205–4217.

Wright, L., Short, A. D., 1984. Morphodynamic variability of surf zones and beaches: a synthesis. Marine geology 56 (1-4), 93–118.

Wu, X., Voulgaris, G., Kumar, N., 2017. Parameterization of synoptic weather systems in the south atlantic bight for modeling applications. Ocean Dynamics 67 (10), 1231–1249.

List of Figures

List of Tables

Appendices

A

Data Collection Methodology

A brief introduction into the applied methodology for data collection is listed below and are according to CSE (2006). Detailed explanations are found in the aforementioned report.

Over the past 40 years, the methodology and approach for beach surveys has evolved from fairly crude methods (eg - Emery (1961)) to highly sophisticated data collection systems involving global positioning system (GPS) satellite navigation in three dimensions (coordinates and elevations with respect to common horizontal and vertical datums). Prior to the late 1990s, rod-and-level, theodolite, or sled surveys through the surf zone were favored because they were the most accurate, consistent, and cost-effective methods of data collection; these methods follow recommendations of the National Academy of Science (Board et al., 1995). No corrections are required for water depth by these methods, because the measurements involve placement of a rod or prism directly on the bottom.

Reliable land survey techniques are simply extended offshore by this method. This method is favored over boat surveys using fathometers because the latter require uncertain corrections for tide, waves, boat motion, and acoustic drift. Many of the problems associated with historical surveys can be traced to these imprecisions (Board et al., 1995). In recent years with the availability of real-time-kinematic (RTK) GPS x-y-z positioning (post 1999), it is now possible to reduce (but not completely eliminate) the errors associated with boat surveys.

The present standard of practice for beach monitoring, and one that is consistent with nearly all historical profile surveys, is single-beam bathymetric surveys using a linked RTK-GPS receiver. Data collected by boat over water are combined with land portions to yield a comprehensive profile of the active littoral zone (foredune to deep water). Following are a brief description of data collection methods and analysis for the present study.

Hydrographic data collection methodology followed procedures set forth in the USACE Hydrographic Surveying Manual. The datum for the surveyed profiles was standard North Carolina state plane coordinates (NAD'83) and vertical datum (NGVD'29[1] for the 2005 and 2006 surveys, NAVD'88 for surveys thereafter), consistent with USACE 1994 surveys. All profile data were converted to NAVD'88 for the present analysis. A detailed explanation of the data collection

Figure A.1 illustrates the various relationships among key reference datums for a station on the ocean at Duck (NC) 15 miles north of the project area. Measurements over subaerial portions of Nags Head extended to low-tide wading depth.

[1]NGVD: National Geodetic Vertical Datum of 1929, which is 0.5 ft below present mean sea level. NAVD: North American Vertical Datum of 1988, which is 0.5 ft above present mean sea level and 1.0 ft above NGVD'29.]

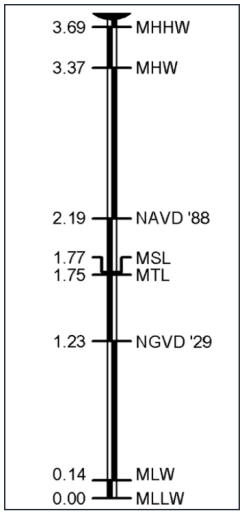

Figure A.1: Various relationships among key reference datums (ft) for a station on the ocean at Duck, North Carolina, 24 kilometer north of the project area

Offshore profiles were collected at 10 Hz or less at high tide overlapping the wading-depth measurements. The raw data were then filtered to eliminate spikes and to provide a 5–7 point floating average. Smoothed inshore data were edited to a manageable size and merged with subaerial data. The onshore and offshore data sets were merged and filtered to reduce the number of data points. Additionally, offshore points were smoothed using a 7-point floating-point average, and the data were checked for anomalies. Data collected in x-y-z format were used directly for purposes of developing a digital terrain model (DTM), which provides a three-dimensional picture of the beach, the longshore bar, and the offshore zone.

A.1 Beach Profiles

Although sediment transport and morphology changes in the nearshore are three-dimensional, it is customary in beach analysis to separately consider the cross-shore and planform (i.e. – longshore) evolution. Survey data (collected in x-y-z format) were converted to x-z (distance-elevation) pairs for purposes of comparing beach conditions among profile lines. A representative profile per reach of all reaches from the November 2010 (before the 2011 project) and June 2016 surveys (Year 5 after the 2011 nourishment project) are shown in the series of Figures A.3a-A.5.

A.2 Sediment Characteristics

The design of the EBP shape and its application in either the UNIBEST-TC or the Delft3D model are all based on uniform sediment characteristics along the Nags Head project site. Different sediment layers could be applied in both models, but a detailed representation of the local characteristics was unattainable. Sediment grab samples were performed and analyzed at 16 different cross-shore locations for each beach station to obtain the cross-shore variability in sediment characteristics, see Figure A.2. To accurately depict this cross-shore variability, the grain size distribution for station number 500+00 and 950+00[2] is shown in the series of Figures A.6-A.17.

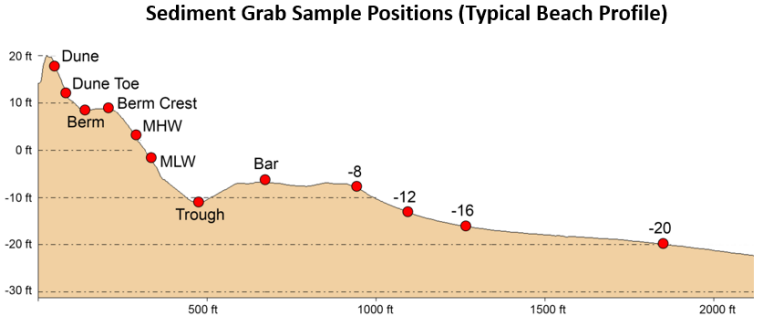

Figure A.2: Averaged profile comparison of each reach and all reaches for the Nags Head project area before the 2011 project and five years after the 2011 project. (After (CSE, 2017))

[2]Sediment grab samples are taken every 5.000 feet, therefore grab sample positions don't coincide with the beach stations

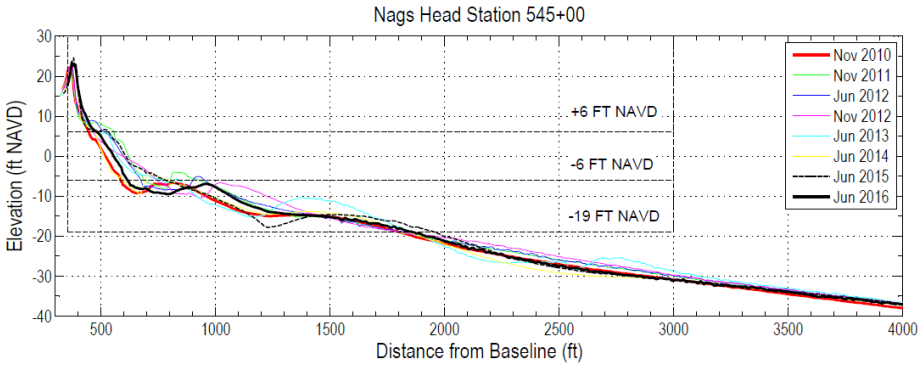

Unit Volume from the Face of Dune to Indicated Depth Contour (CY/FT)

Date	To +6 FT	To -6 FT	To to -19 FT
Nov 2010	23.8	95.9	484.4
Nov 2011	30.5	153.3	588.6
Jun 2012	30.9	140.1	573.0
Nov 2012	29.1	136.6	589.4
Jun 2013	33.8	137.7	596.7
Jun 2014	30.2	105.3	526.8
Jun 2015	32.1	151.2	564.4
Jun 2016	35.9	123.6	540.8

(a)

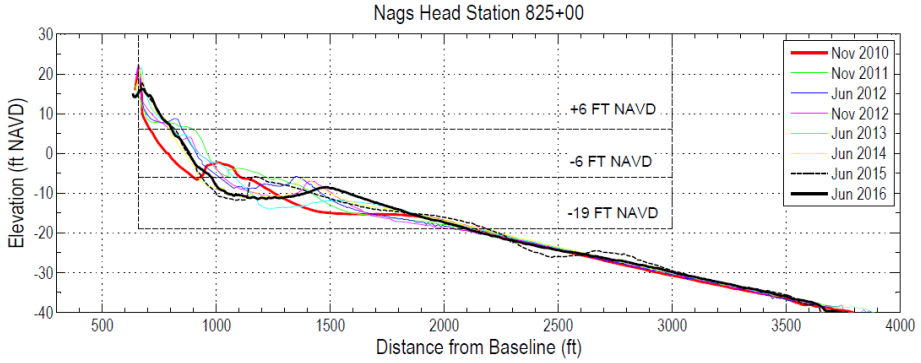

Unit Volume from the Face of Dune to Indicated Depth Contour (CY/FT)

Date	To +6 FT	To -6 FT	To to -19 FT
Nov 2010	9.8	84.9	483.5
Nov 2011	18.3	163.8	598.0
Jun 2012	24.2	139.5	567.8
Nov 2012	21.7	141.7	550.0
Jun 2013	31.4	157.8	569.0
Jun 2014	32.9	122.8	557.7
Jun 2015	32.3	129.2	569.5
Jun 2016	31.7	131.6	565.7

(b)

Figure A.3: Representative beach profiles for Reach 1 (a) and Reach 2 (b). The plotted profiles are obtained from beach surveys between November 2010 and June 2016. Unit volume analysis for the beach profile per survey is listed to show the sediment fluxes along the profile.

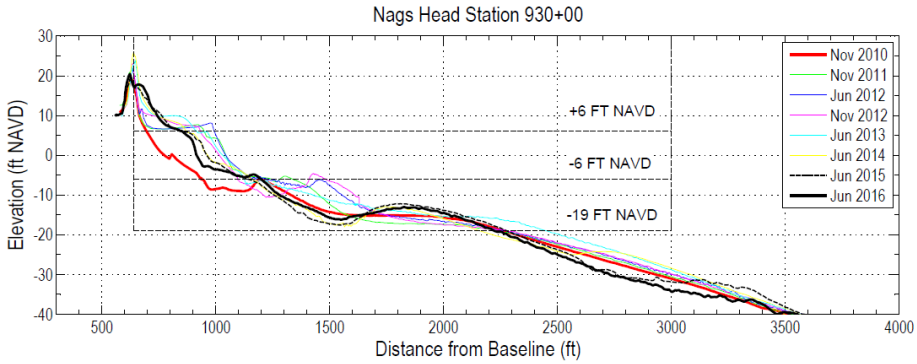

Unit Volume from the Face of Dune to Indicated Depth Contour (CY/FT)

Date	To +6 FT	To -6 FT	To to -19 FT
Nov 2010	9.6	81.5	514.8
Nov 2011	19.9	203.0	657.7
Jun 2012	24.1	209.4	717.2
Nov 2012	35.8	204.5	692.0
Jun 2013	50.1	226.0	748.9
Jun 2014	45.5	203.5	627.5
Jun 2015	39.7	191.2	640.9
Jun 2016	40.1	177.9	634.9

(a)

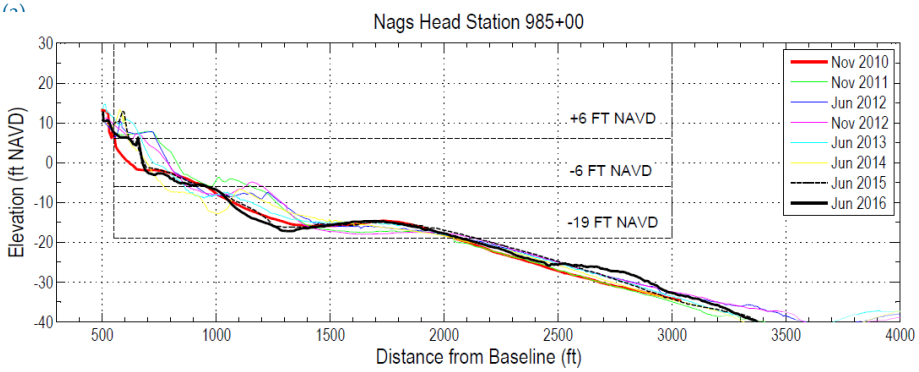

Unit Volume from the Face of Dune to Indicated Depth Contour (CY/FT)

Date	To +6 FT	To -6 FT	To to -19 FT
Nov 2010	0.1	59.1	440.8
Nov 2011	9.4	143.7	550.9
Jun 2012	11.4	122.5	534.5
Nov 2012	6.4	110.8	505.8
Jun 2013	16.1	104.0	500.4
Jun 2014	11.0	73.9	458.7
Jun 2015	10.8	91.4	479.2
Jun 2016	1.4	73.6	438.8

(b)

Figure A.4: Representative beach profiles for Reach 3N (a) and Reach 3S (b). The plotted profiles are obtained from beach surveys between November 2010 and June 2016. Unit volume analysis for the beach profile per survey is listed to show the sediment fluxes along the profile.

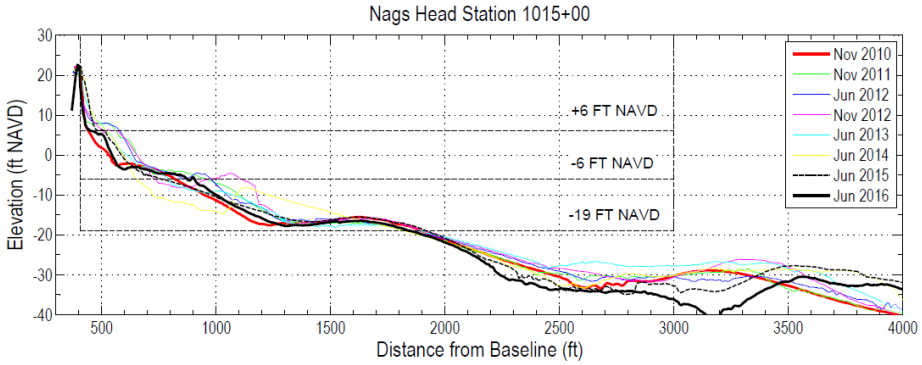

Unit Volume from the Face of Dune to Indicated Depth Contour (CY/FT)

Date	To +6 FT	To -6 FT	To to -19 FT
Nov 2010	6.4	80.7	436.6
Nov 2011	13.3	135.4	533.4
Jun 2012	17.2	136.8	537.1
Nov 2012	13.2	126.4	557.2
Jun 2013	21.0	119.4	488.5
Jun 2014	24.1	106.3	488.7
Jun 2015	19.8	104.7	491.2
Jun 2016	5.1	86.6	450.1

Figure A.5: Representative beach profiles for Reach 4. The plotted profiles are obtained from beach surveys between November 2010 and June 2016. Unit volume analysis for the beach profile per survey is listed to show the sediment fluxes along the profile.

Station 500+00

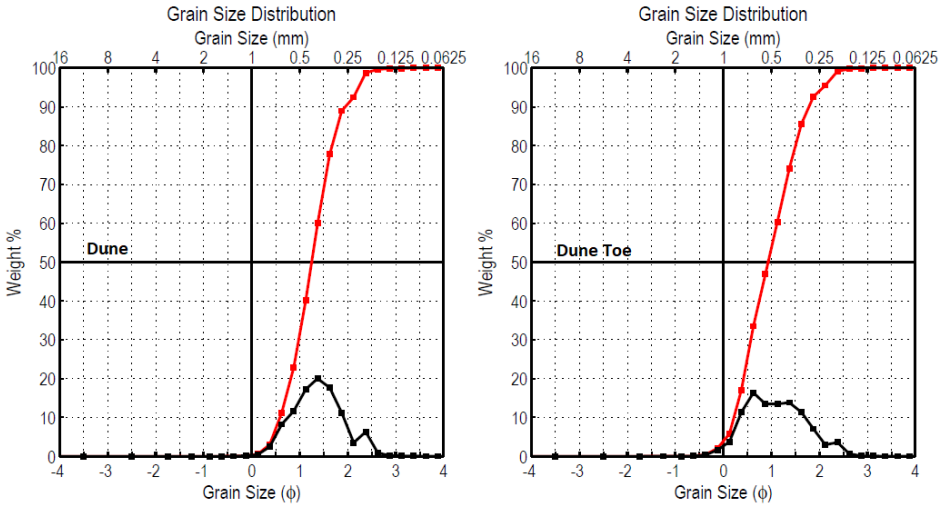

Figure A.6: Grain size distribution for profile 520+00 sampled at the dune with a mean size of 0.382 mm and a standard deviation of 0.699 mm (left) and at the dune toe with a mean size of 0.469mm and a standard deviation of 0.656 mm (right).

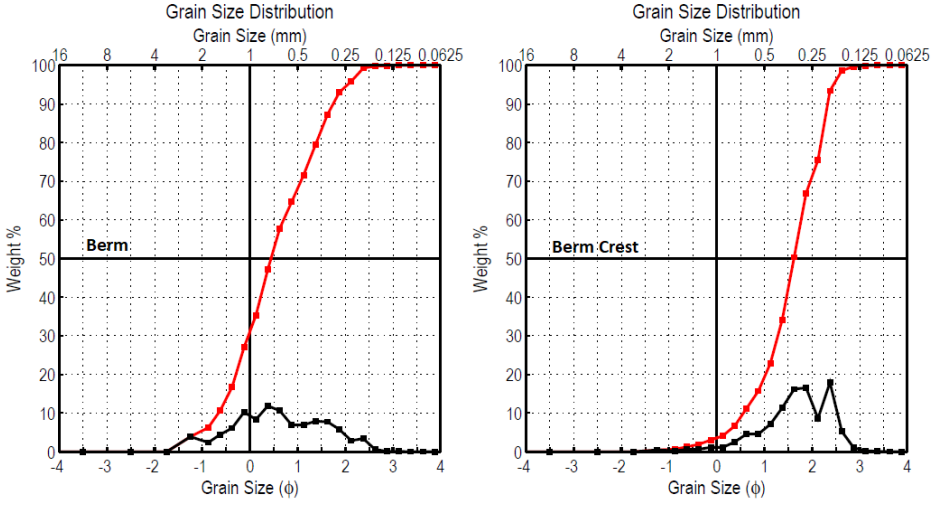

Figure A.7: Grain size distribution for profile 520+00 sampled at the berm with a mean size of 0.646 mm and a standard deviation of 0.530 mm (left) and at the berm crest with a mean size of 0.317 mm and a standard deviation of 0.610 mm (right).

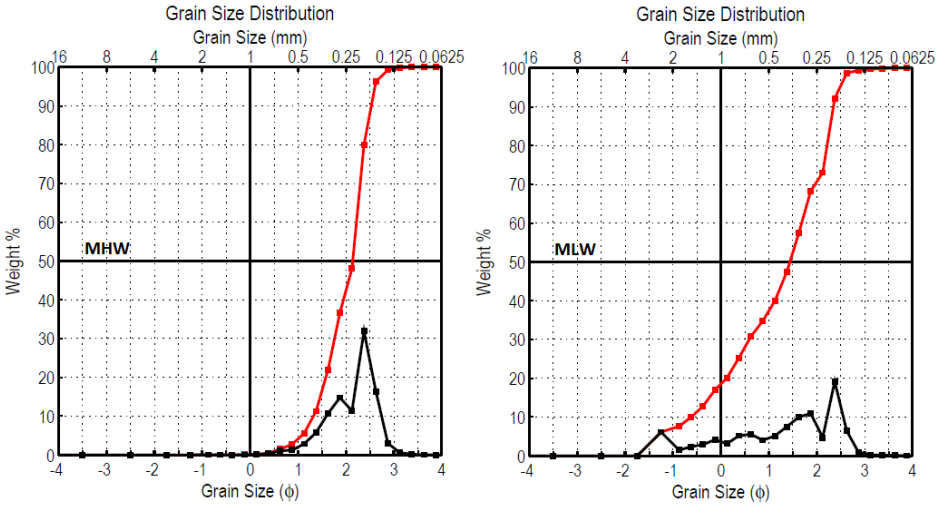

Figure A.8: Grain size distribution for profile 520+00 sampled at MHW with a mean size of 0.231 mm and a standard deviation of 0.711 mm (left) and at MLW with a mean size of 0.416 mm and a standard deviation of 0.454 mm (right).

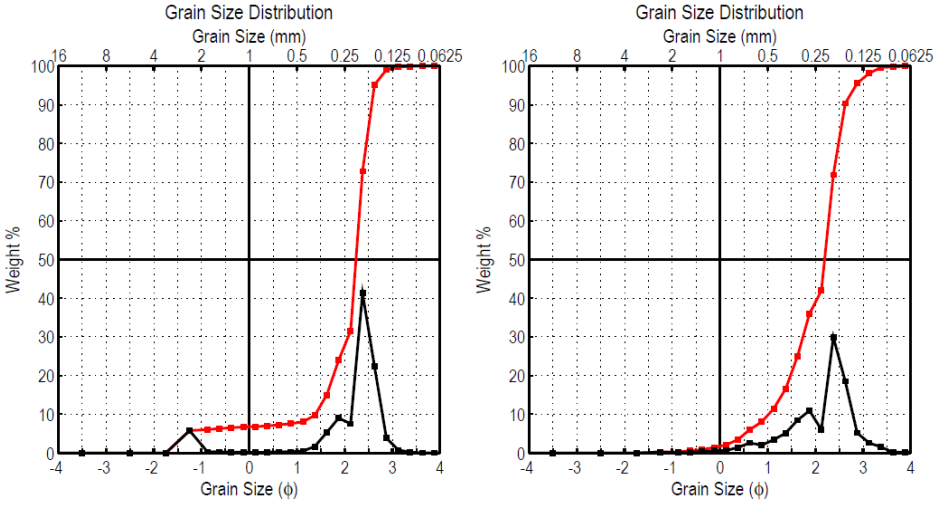

Figure A.9: Grain size distribution for profile 520+00 sampled at the trough with a mean size of 0.236 mm and a standard deviation of 0.520 mm (left) and at the bar with a mean size of 0.233 mm and a standard deviation of 0.613 mm (right).

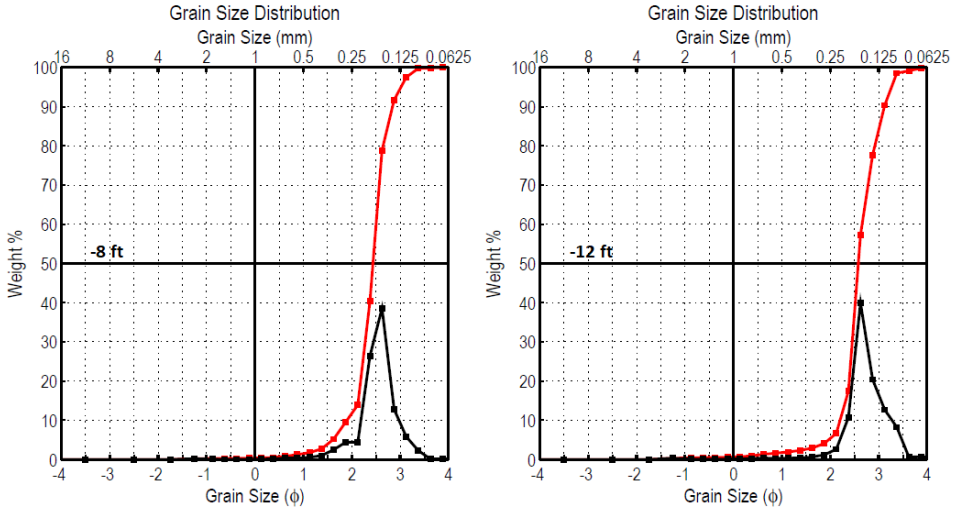

Figure A.10: Grain size distribution for profile 520+00 sampled at -8 ft with a mean size of 0.175 mm and a standard deviation of 0.731 mm (left) and at -12 ft with a mean size of 0.153 mm and a standard deviation of 0.703 mm (right).

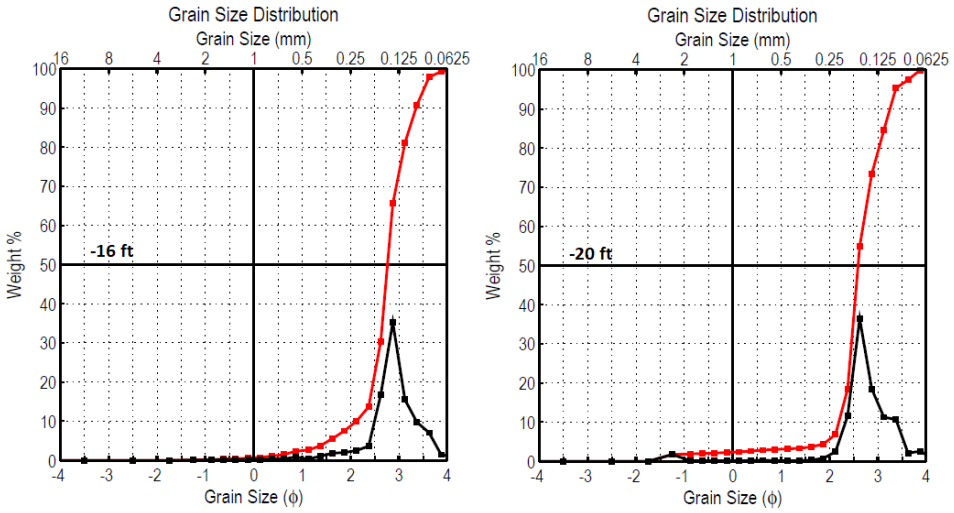

Figure A.11: Grain size distribution for profile 520+00 sampled at -16 ft with a mean size of 0.140 mm and a standard deviation of 0.655 mm (left) and at -20 ft with a mean size of 0.153 mm and a standard deviation of 0.604 mm (right).

Station 950+00

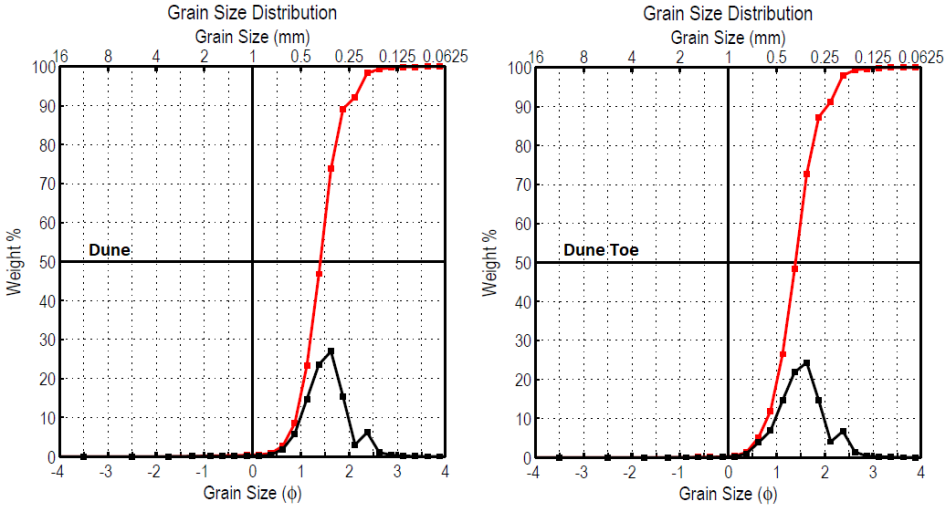

Figure A.12: Grain size distribution for profile 930+00 sampled at the dune with a mean size of 0.345 mm and a standard deviation of 0.73 5mm (left) and at the dune toe with a mean size of 0.349 mm and a standard deviation of 0.720 mm (right).

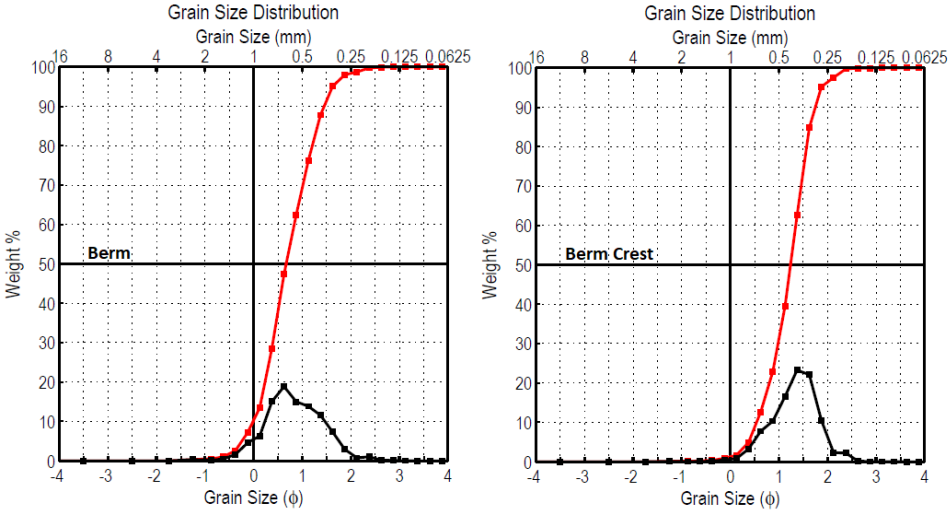

Figure A.13: Grain size distribution for profile 930+00 sampled at the berm with a mean size of 0.563 mm and a standard deviation of 0.669 mm (left) and at the berm crest with a mean size of 0.401 mm and a standard deviation of 0.718 mm (right).

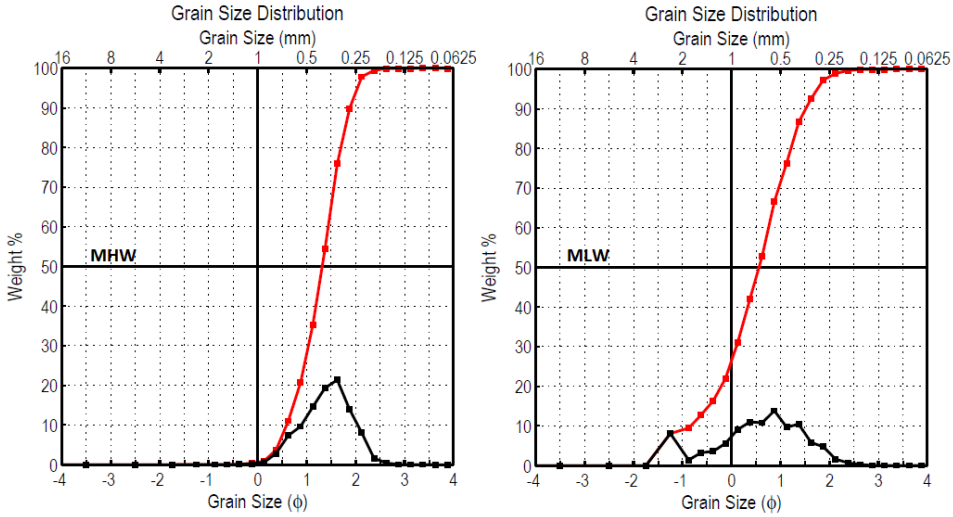

Figure A.14: Grain size distribution for profile 930+00 sampled at MHW with a mean size of 0.378 mm and a standard deviation of 0.712 mm (left) and at MLW with a mean size of 0.667 mm and a standard deviation of 0.54 6mm (right).

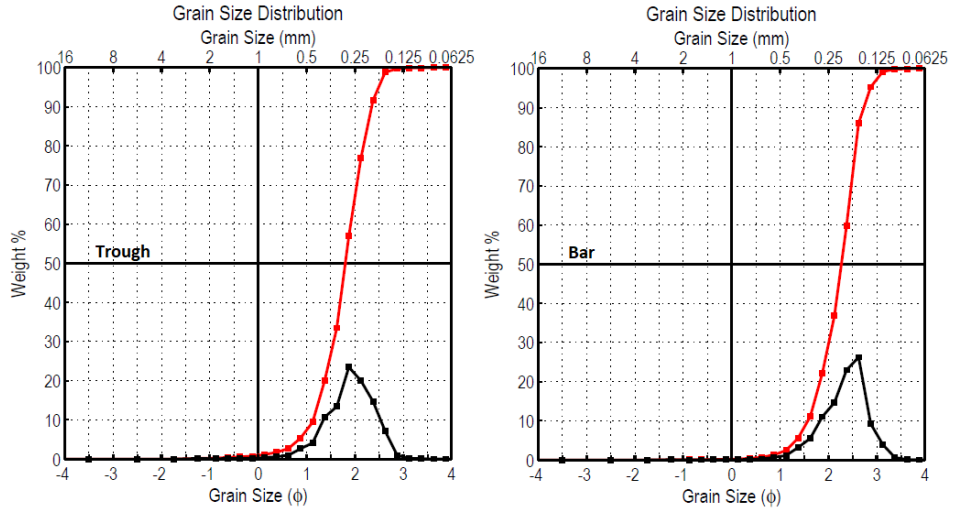

Figure A.15: Grain size distribution for profile 930+00 sampled at the trough with a mean size of 0.273 mm and a standard deviation of 0.694 mm (left) and at the bar with a mean size of 0.200 mm and a standard deviation of 0.716 mm (right).

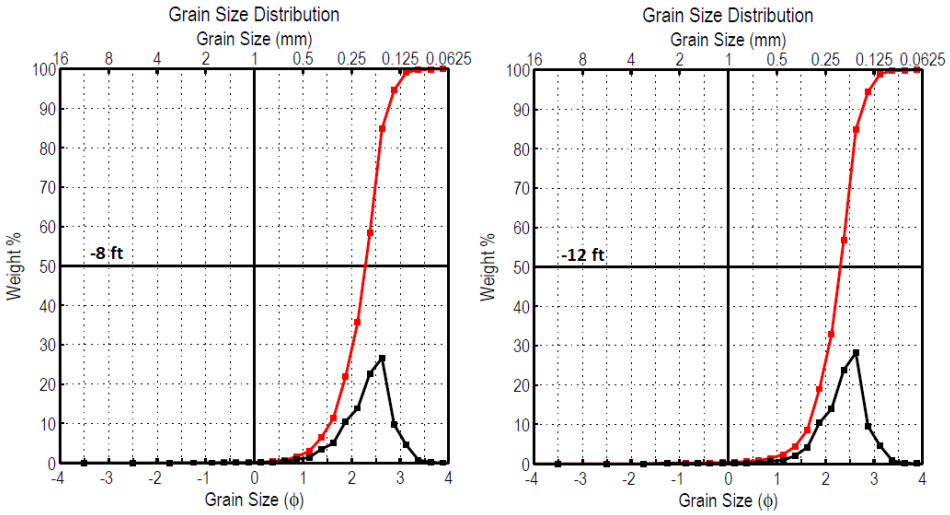

Figure A.16: Grain size distribution for profile 930+00 sampled at -8 ft with a mean size of 0.199 mm and a standard deviation of 0.710 mm (left) and at -12 ft with a mean size of 0.195 mm and a standard deviation of 0.713 mm (right).

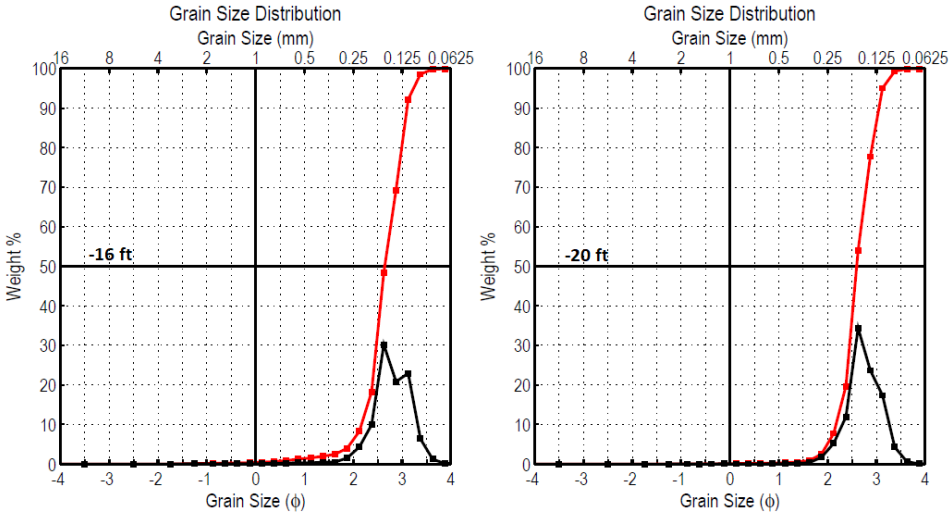

Figure A.17: Grain size distribution for profile 520+00 sampled at -16 ft with a mean size of 0.148 mm and a standard deviation of 0.720 mm (left) and at -20 ft with a mean size of 0.151 mm and a standard deviation of 0.779 mm (right).

B

Equilibrium Beach Profiles

Each reach of the Nags Head project is represented by two cross-shore beach profiles. After calibration, the corresponding equilibrium beach profile according to Chapter 3 Study Area is plotted against the measured beach profile (serie of Figures B.1-B.5). The vertical cutoff depth of the equilibrium beach profiles is at the depth of closure of the corresponding measured profile.

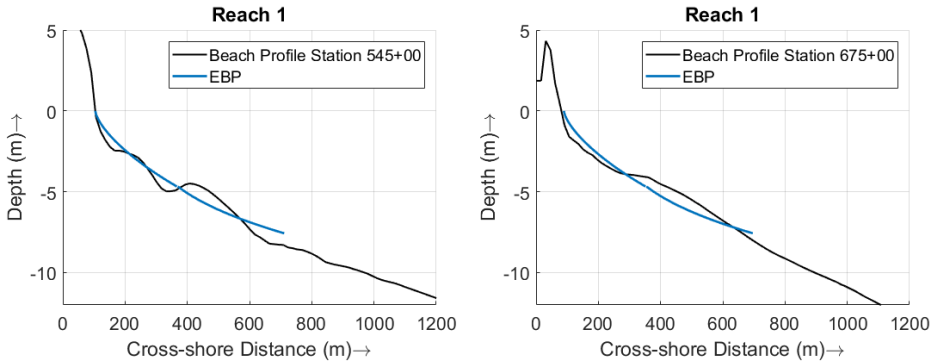

Figure B.1: Two representative beach profiles of the current reach with its corresponding Equilibrium Beach Profile. The EBP starts at MSL and has a vertical cutoff depth at the depth of closure.

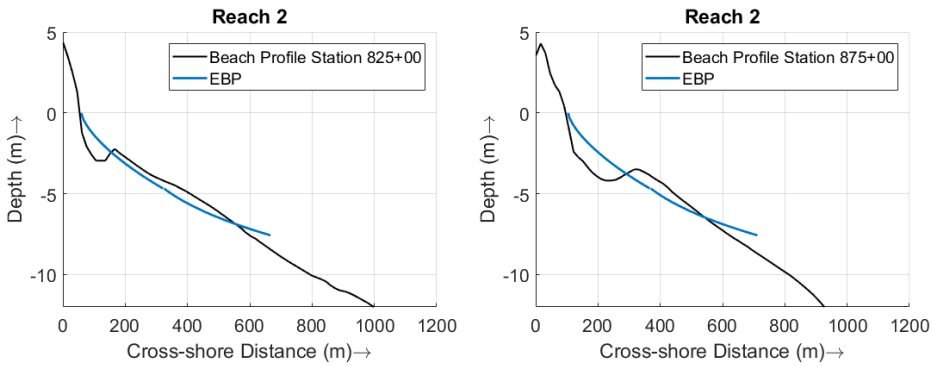

Figure B.2: Two representative beach profiles of the current reach with its corresponding Equilibrium Beach Profile. The EBP starts at MSL and has a vertical cutoff depth at the depth of closure.

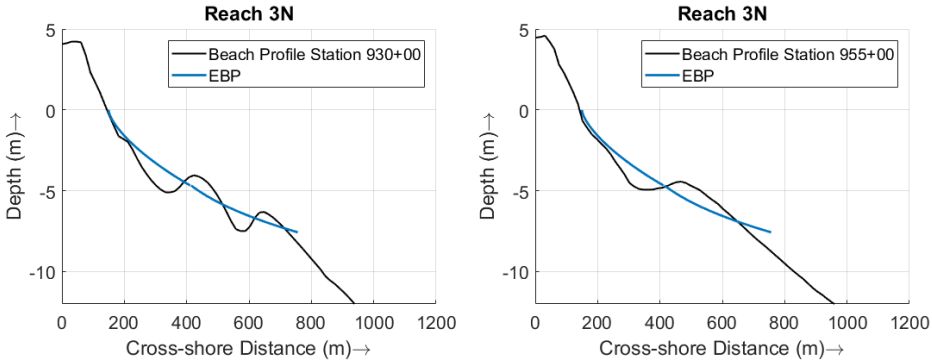

Figure B.3: Two representative beach profiles of the current reach with its corresponding Equilibrium Beach Profile. The EBP starts at MSL and has a vertical cutoff depth at the depth of closure.

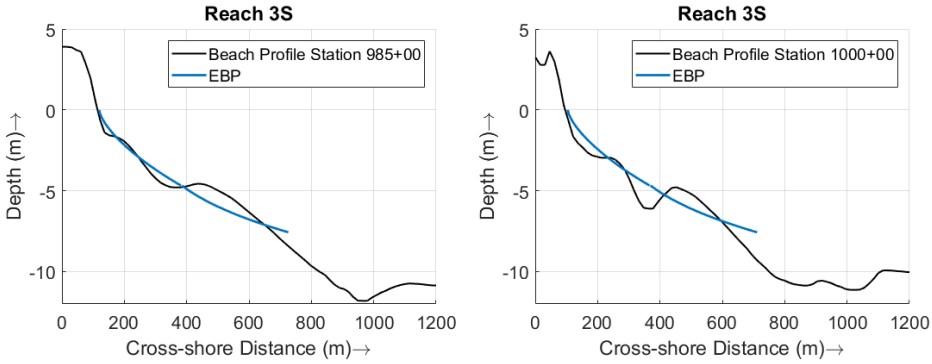

Figure B.4: Two representative beach profiles of the current reach with its corresponding Equilibrium Beach Profile. The EBP starts at MSL and has a vertical cutoff depth at the depth of closure.

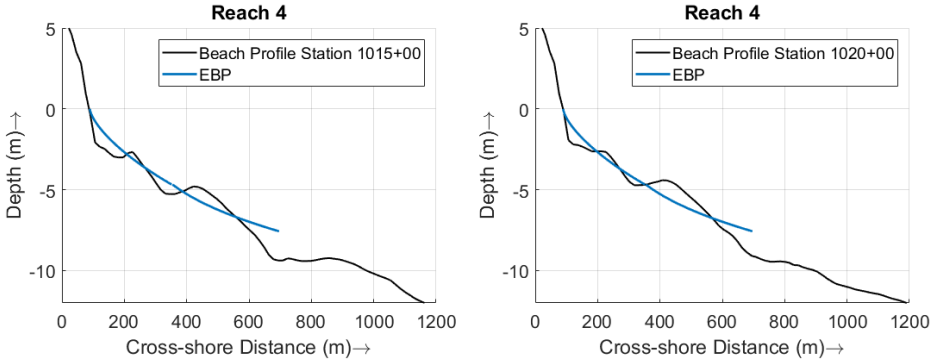

Figure B.5: Two representative beach profiles of the current reach with its corresponding Equilibrium Beach Profile. The EBP starts at MSL and has a vertical cutoff depth at the depth of closure.

C

Sensitivity Analysis

C.1 Delft3D

To evaluate the Delft3D performance and how the model responds to several parameter settings, a sensitivity analysis is performed. Previous sensitivity studies regarding Delft3D show that the morphological results are most influenced by wave input parameters (Plant et al., 2009). A study by Luijendijk (2001) regarding calibration of a Delft3D model showed that the model results are only minorly influenced by the grid size, time step, and type of boundary conditions (as long as not all boundaries are water-level boundaries). The sensitivity analysis consisted of several stages. First, several runs with the default parameter settings were made and the output was evaluated to check the general performance of the model. After these initial computations, several runs were made with different parameter settings to see how these parameters influence the results. The settings that were modified were the wave climate dataset, the angle of wave incidence, median grain size, and the profile of the groin. Finally, Table C.1 holds an overview of the main input parameters of the Delft3D model. The following are excerpts from the input files used in the calibrated model simulations. For brevity, this list is not intended to be all inclusive. It contains general model setup information, parameters which are typically modified for calibration purposes, as well as, details regarding model features beyond the default settings which were employed.

Wave Climate Dataset: Various wave hindcast models are available for wave climate schematization and input to numerical simulation models. In the present analysis, the WIS hindcast waves were compared with the WAVEWATCH III modeled waves. A previous study comparing these two types of hindcast wave datasets concluded that the WIS results tend to slightly over-predict wave height and the WAVEWATCH III model tends to under-predict waves (Tracy and Cialone, 2006). The first step in this sensitivity analysis was to re-run the UNIBEST-TC model using the WAVEWATCH III data to see the differences in cross-shore distribution of the averaged, yearly net longshore transport rates (Figure C.1).

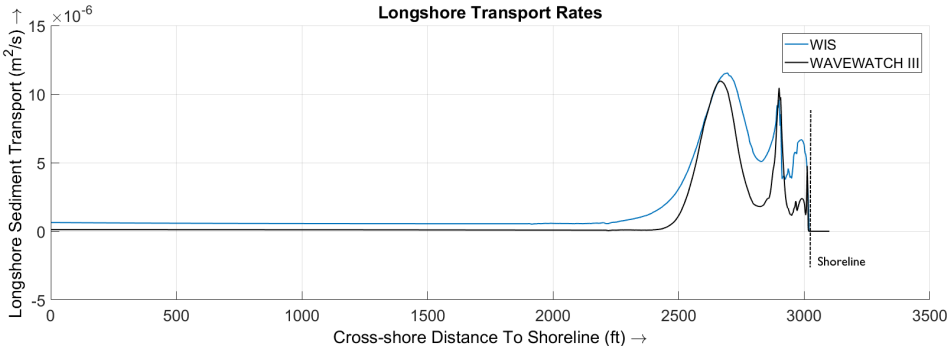

Figure C.1: Averaged yearly net longshore transport rates for the real-time WAVEWATCH III hindcast data (blue) and the WIS hindcast data (red).

Figure C.1 shows a measurable difference between the averaged, yearly net longshore transport rates for the two datasets with the WIS hindcast data yielding greater transport compared with the WAVEWATCH III hindcast data. This finding supports the conclusion of Tracy and Cialone (2006); over-prediction of the wave height using the WIS model and under-prediction using the WAVEWATCH III model.

Angle of Wave Incidence: The wave climate schematization using UNIBEST-TC is based on using one cross-shore profile with a shore-normal azimuth of 68°, which is obtained by averaging the azimuths of all five reaches. The actual shoreline azimuths reach by reach along Nags Head vary ~6° from north to south. The longshore sediment transport rates will therefore change from north to south as well, since these are highly dependent on the shore angle. The effect that the changes in shoreline azimuths have on the sediment transport and, thereby, the morphological changes were computed by changing the angle of wave incidence by ±3°. By adding +3° to the angle of wave incidence, the waves will approach the shoreline more perpendicular, expecting a lower longshore transport rate. By adding -3°, the opposite effect is expected.

The results of both simulations are summarized in Figure C.2. As expected, with increasing angles of wave incidence, the longshore transport rates throughout the project decrease. The net average longshore transport rate shows a significant drop compared to the original model, as does the opposite occurs while lowering the angle of wave incidence. According to previous studies to simulate longshore transport rates at Nags Head using a one-line model (CSE, 2011a); the influence of wave energy strongly influenced the total transport rates. Changing the wave hindcast station even changes the net direction of the longshore transport. Therefore, these strong changes between the wave angle of incidence only indicate the Delft3D model is capable of transforming the offshore wave data and properly computing longshore transport rates in response to changes in nearshore bathymetry.

Median Grain Size: The sensitivity of Delft3D is checked for sediment grain sizes typical for the area. Before the first large nourishment project occurred in 2011, geotechnical studies showed that the median grain-size diameter along Nags Head was ~0.35 millimeters (mm). Following the nourishment projects, the grain size has become coarser with a present median diameter around 0.420 mm. Furthermore, the grain sizes throughout the littoral zone and in the project areas are variable. A sensitivity check was performed on the grain-size diameter to see if there were significant differences in net sediment transport under coarser sand.

Lowering the median grain size from 0.420mm to 0.350mm increases the net averaged longshore transport rate by a factor 1.35, which indicates that the transport rate is highly dependent on the sediment grain size (Figure C.3). The variability in longshore transport rates, however, shows hardly any influence. Therefore, by changing the sediment characteristics, only the magnitude of sediment transport is affected, not the corresponding variability. Which means that the overall differences in erosion rates are unaffected as well.

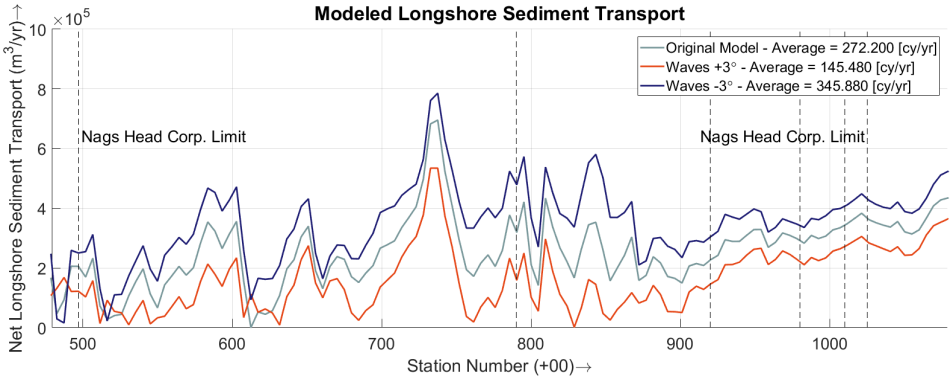

Figure C.2: Results of the two simulations with changes in the angle of wave incidence. Lower longshore transport rates are found by increasing the wave angle with 3° (orange) and higher rates are found by lowering the wave angle with 3° (purple), as compared to the original Nags Head model (grey)

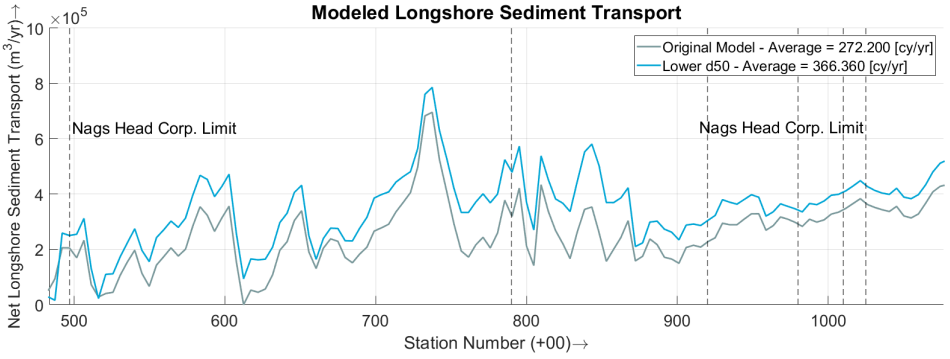

Figure C.3: Results of the simulation with changes in the median grain size (cyan) compared to the original model run (grey). Results show, as expected, higher longshore transport rates as the median grain size lowers.

Table C.1: Delft3D model parameters

Roughness		
Bottom roughness formula		Chezy
Horizontal roughness		65
Stress formulation due to wave forces		Fredsoe
Viscosity		
Horizontal eddy viscosity	m2/s	0.01
Horizontal eddy diffusivity	m2/s	0.1
Sediment		
Reference density for hindered settling	kg/m3	1600
Specific density	kg/m3	2650
Dry bed density	kg/m3	1600
Median sediment diameter	mm	0.42
Morphology		
Spin-up before morphological changes	s	1440
Miminum depth for sediment calculation	m	0.1
Streamwise bed gradient factor for bed load transport		1
Transverse bed gradient factor for bed load transport		1.5
Factor for erosion of adjacent dry cells		0.6
Multiplication factor for suspended sediment reference concentration		1.4
Multiplication factor for bed-load transport vector magnitude		1
Wave-related suspended transport factor		0
Wave-related bed-load transport factor		0
Additional parameters		
Cstbnd		#YES#
Roller		#YES#
Fwee		0
F_lam		0
Betarol		0.1
Gamdis		0.55

C.2 UNIBEST-TC

The net / gross direction and magnitude of the cross-shore transport rates area highly dependent on the grain size distribution. Using lower grain sizes allows for higher concentrations of suspended sediment and because of the undertow higher offshore transport rates as well. To visualize these effects, the median grain size diameter is selected to match the grain size of the outer bar. Results show an over-prediction of offshore directed cross-shore transport.

The results of lowering the median grain size are furthermore compared with the initial results in Figure C.8 for a quantitative comparison. The bars show the total absolute integrated cross-shore transport rates, comparable to Figure 5.11. Results are in agreement with the previous Figures, indicating that a lowering of the median grain size will increase the offshore transport rates.

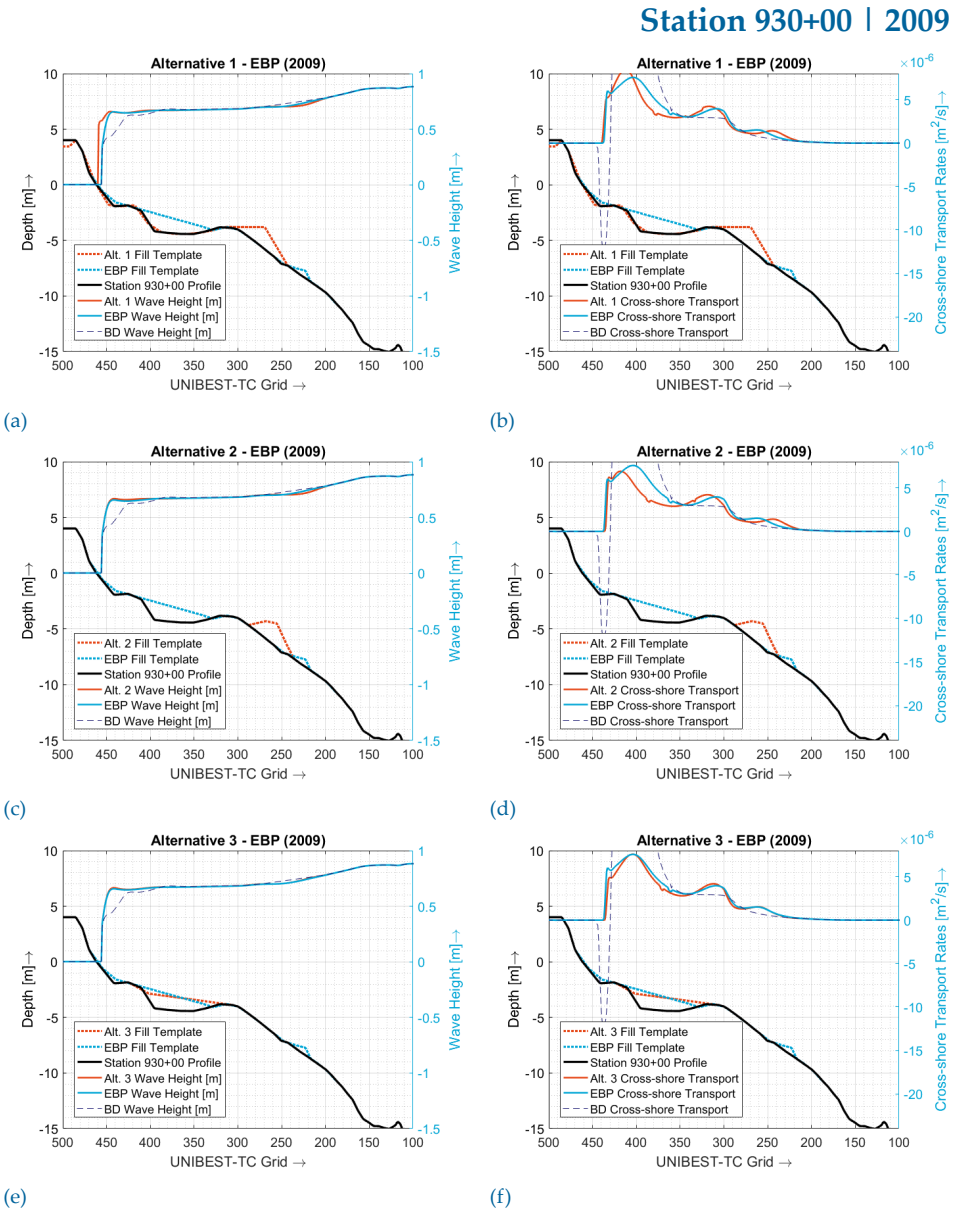

Figure C.4: *left:* the distribution of the significant wave height over the cross-shore profile for each of the conventional nourishment designs (Alternative 1, 2 and 3) plotted against the results of the 'EBP-design' (Alternative 4). *right:* the net averaged cross-shore transport rates distributions plotted over the profile. *Using* d_{50}*=0.200 mm,* d_{90}*=0.280 mm and* d_{ss}*=0.190 mm.*

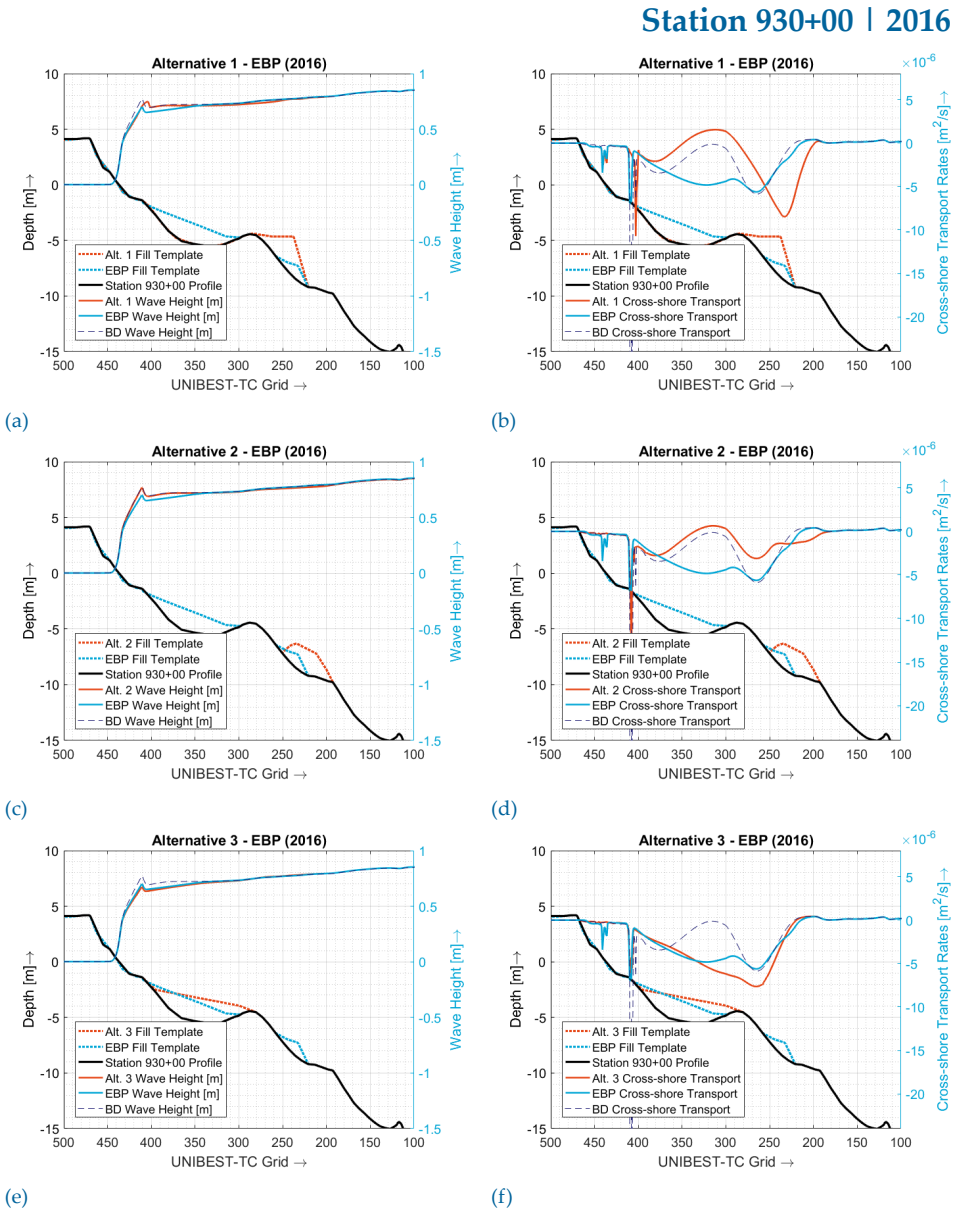

Figure C.5: *left:* the distribution of the significant wave height over the cross-shore profile for each of the conventional nourishment designs (Alternative 1, 2 and 3) plotted against the results of the 'EBP-design' (Alternative 4). *right:* the net averaged cross-shore transport rates distributions plotted over the profile. *Using* d_{50}*=0.200 mm,* d_{90}*=0.280 mm and* d_{ss}*=0.190 mm.*

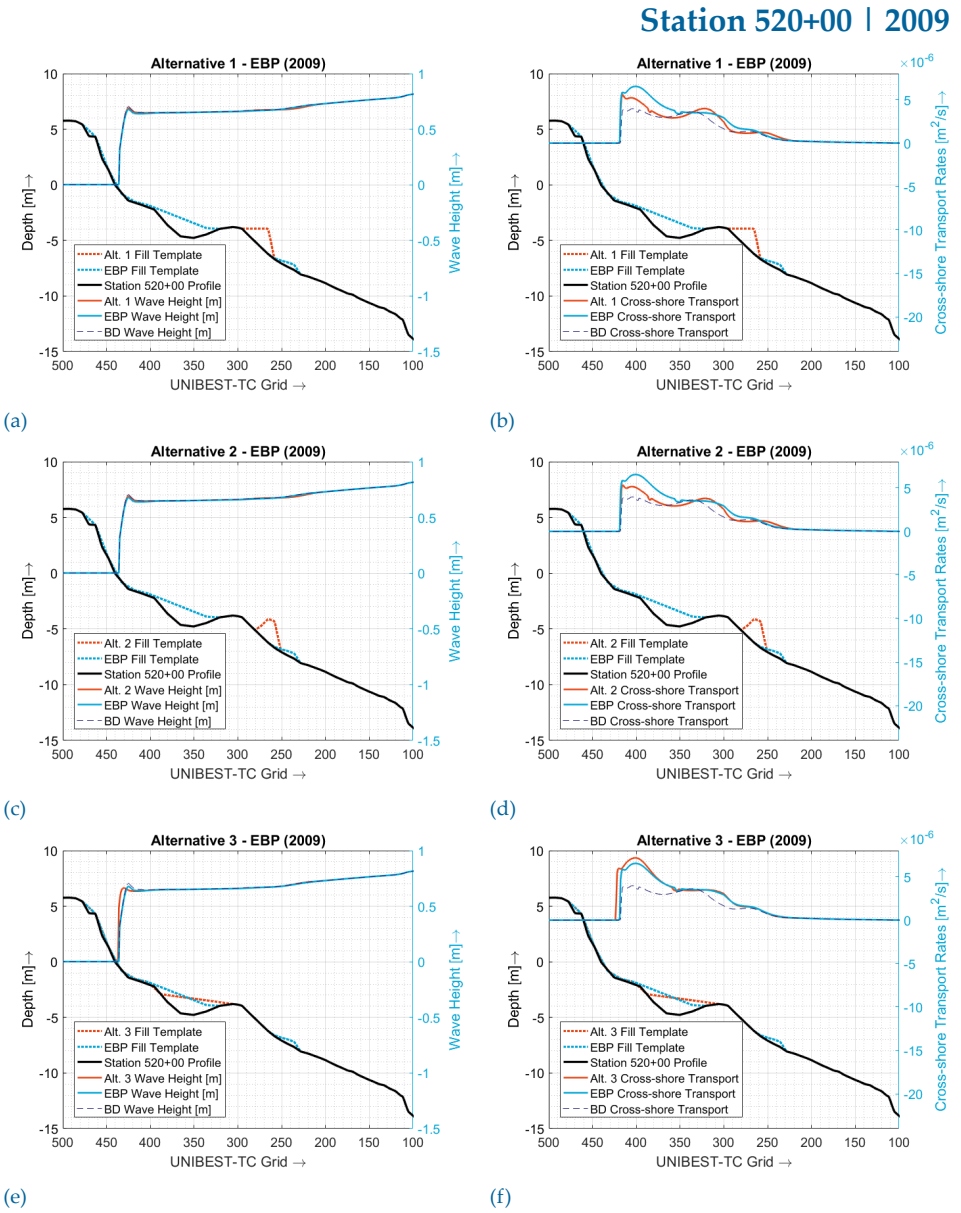

Figure C.6: *left:* the distribution of the significant wave height over the cross-shore profile for each of the conventional nourishment designs (Alternative 1, 2 and 3) plotted against the results of the 'EBP-design' (Alternative 4). *right:* the net averaged cross-shore transport rates distributions plotted over the profile. *Using* d_{50}*=0.200 mm,* d_{90}*=0.280 mm and* d_{ss}*=0.190 mm.*

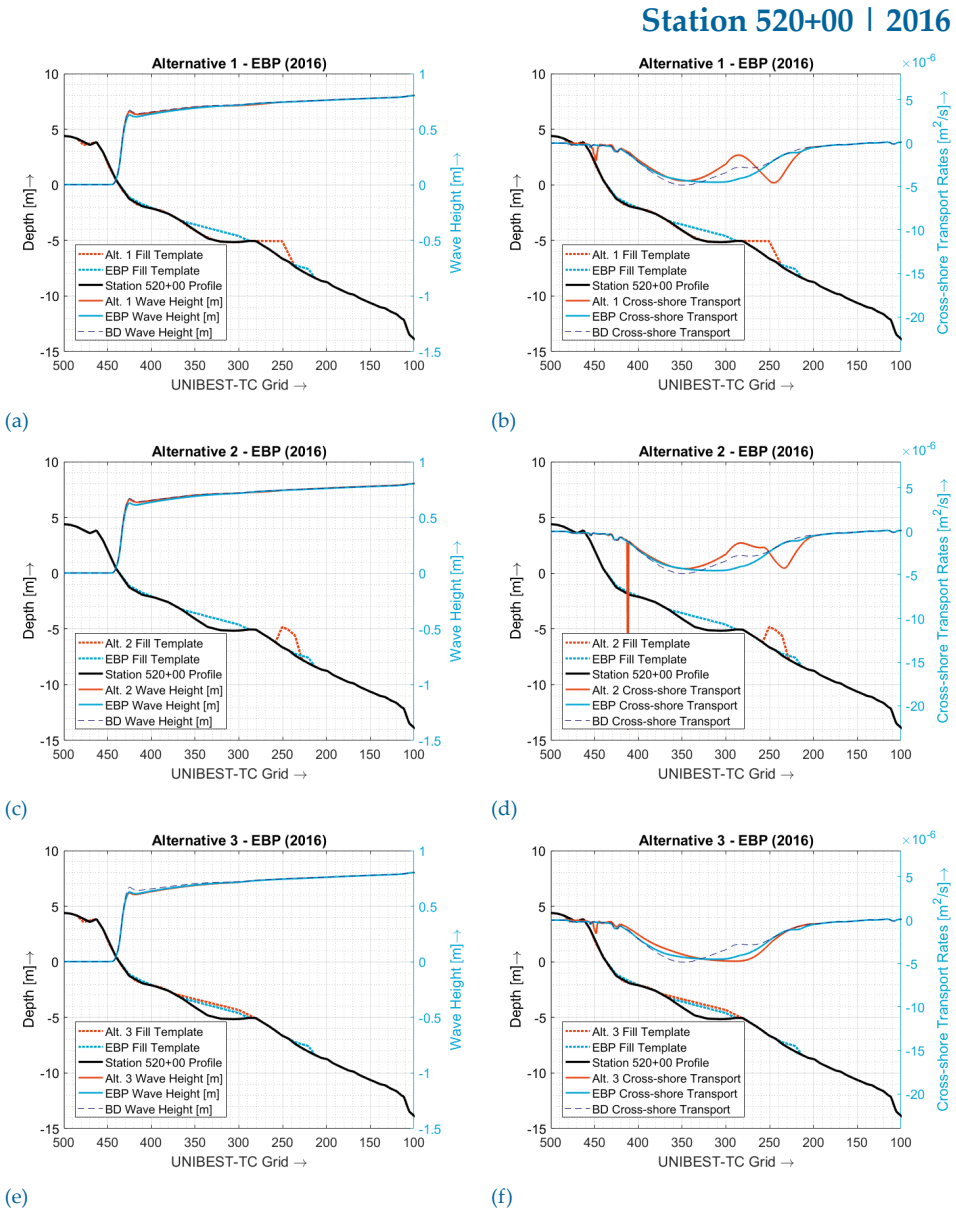

Figure C.7: *left:* the distribution of the significant wave height over the cross-shore profile for each of the conventional nourishment designs (Alternative 1, 2 and 3) plotted against the results of the 'EBP-design' (Alternative 4). *right:* the net averaged cross-shore transport rates distributions plotted over the profile. *Using* d_{50}*=0.200 mm,* d_{90}*=0.280 mm and* d_{ss}*=0.190 mm.*

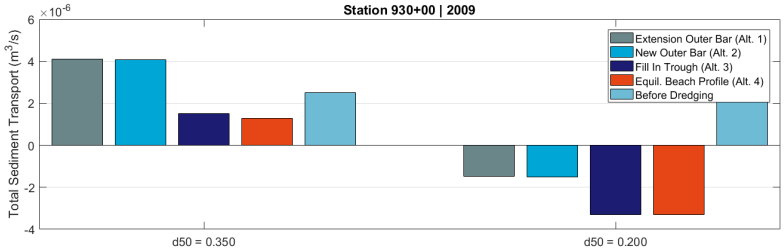

(a)

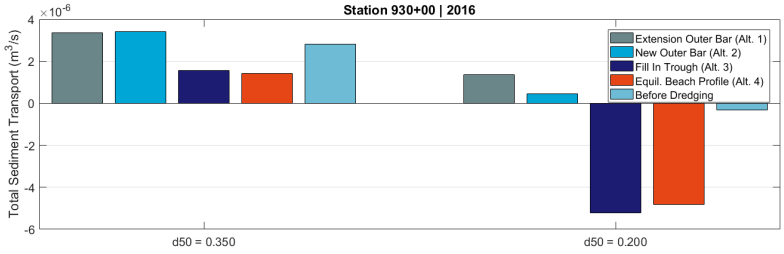

(b)

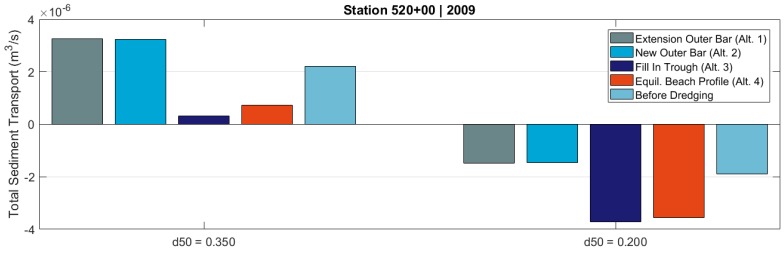

(c)

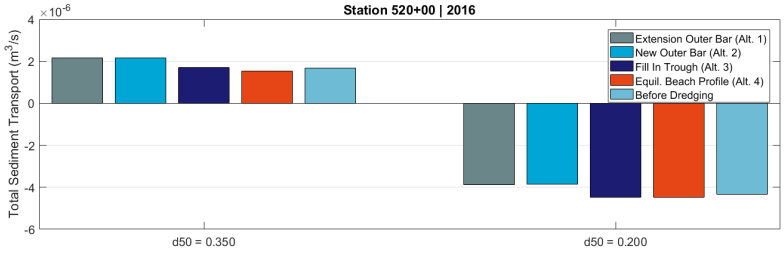

(d)

Figure C.8: Sensitivity analysis of the influence of the median grain size to the total volume of cross-shore sediment transport. Left barplots show the total transport used in the report with a d_{50} of 0.350mm and the right plot shows the results for a d_{50} of 0.200mm. *a:* Station 930+00 in 2009, *b:* Station 930+00 in 2016, *c:* Station 520+00 in 2009,*d:* Station 520+00 in 2016.

D

Overview Nourishment Locations and Delft3D Results

This appendix is intended to give an overview of the design of all four different shoreface nourishment designs along the Nags Head project site and their effects on the coastline morphology after a year of modeling. After preforming the Delft3D runs for the four different nourishment scenario's, all results were analyzed to see the impact the different nourishments have on the beach morphology. The shoreline is divided into four equally spaced 2.5 mile sections in order to better compare the results.

For each section, the bed level changes of the four difference scenarios after the one-year morphological study are compared with each other and plotted over the existing shoreline. In each figure, the bed level changes occurring at the beach face are shown to highlight the shoreline response due to nourishment. Note that the wave related sediment transport calibration parameters bed, w and sus, w are both turned off. Since the flow and sediment transport computation are performed using GLM velocities, there is hardly any net cross-shore transport. Meaning that the onshore driven stokes drift and offshore driven return flow cancel each other out. Therefore the main interest of this appendix is the shoreface nourishment location per design. The possible (vertically limited) beach profile changes using computed after yearly averaged longshore transport rates with variable wave climate are then only an indication of the possible morphological effects. To highlight the effects individual nourishments have on the shallow nearshore (up to 200m offshore) the cumulative sedimentation and erosion patterns of the first grid cells are included per figure. The shoreline changes can later possibly be connected to the variations of the local longshore transport gradients as proposed by Ruggiero et al. (2009), which has to be done with a model suited for such applications, i.e. include cross-shore variation in sediment transport rates.

Nourishment design is also displayed in the figures using contour lines. The figures furthermore show the stations at which the reaches used for the Nags Head project are divided. All the results are summarized in Table D.1 which gives a brief description the effects of each nourishment per section. These effects only indicate the morphological changes of the coastal zone and are not to be used for an assessment of the real-life occurring morphodynamics.

Table D.1: Nourishment effect per beach section

Alternative	Section	Effect - Changes
Ext. Outer Bar (Alt .1):	Mile 0 – 2.5	· Bar widening · Minor onshore transport · Little change visible beach
New Outer Bar (Alt. 2):	Mile 0 – 2.5	· Minor onshore transport · Little change visible beach
Fill In Trough (Alt. 3):	Mile 0 – 2.5	· Average onshore transport · Average change visible beach
EBP-Design (Alt. 4):	Mile 0 – 2.5	· Average onshore transport · Decrease alongshore variability · Average change visible beach
Ext. Outer Bar (Alt .1):	Mile 2.5 – 5.0	· Bar widening · Minor onshore transport · Little change visible beach
New Outer Bar (Alt. 2):	Mile 2.5 – 5.0	· Minor onshore transport · Little change visible beach
Fill In Trough (Alt. 3):	Mile 2.5 – 5.0	· High onshore transport · Average change visible beach
EBP-Design (Alt. 4):	Mile 2.5 – 5.0	· Average onshore transport · Decrease alongshore variability · Average change visible beach
Ext. Outer Bar (Alt .1):	Mile 5.0 – 7.5	· Bar widening · Average onshore transport · Little change visible beach
New Outer Bar (Alt. 2):	Mile 5.0 – 7.5	· Average onshore transport · Little change visible beach
Fill In Trough (Alt. 3):	Mile 5.0 – 7.5	· Average onshore transport · Average change visible beach
EBP-Design (Alt. 4):	Mile 5.0 – 7.5	· High onshore transport · Decrease alongshore variability · Average change visible beach
Ext. Outer Bar (Alt .1):	Mile 7.5 – 10.0	· Bar widening · Average onshore transport · Little change visible beach
New Outer Bar (Alt. 2):	Mile 7.5 – 10.0	· Average onshore transport · Little change visible beach
Fill In Trough (Alt. 3):	Mile 7.5 – 10.0	· High onshore transport · Average change visible beach
EBP-Design (Alt. 4):	Mile 7.5 – 10.0	· High onshore transport · Decrease alongshore variability · Average change visible beach

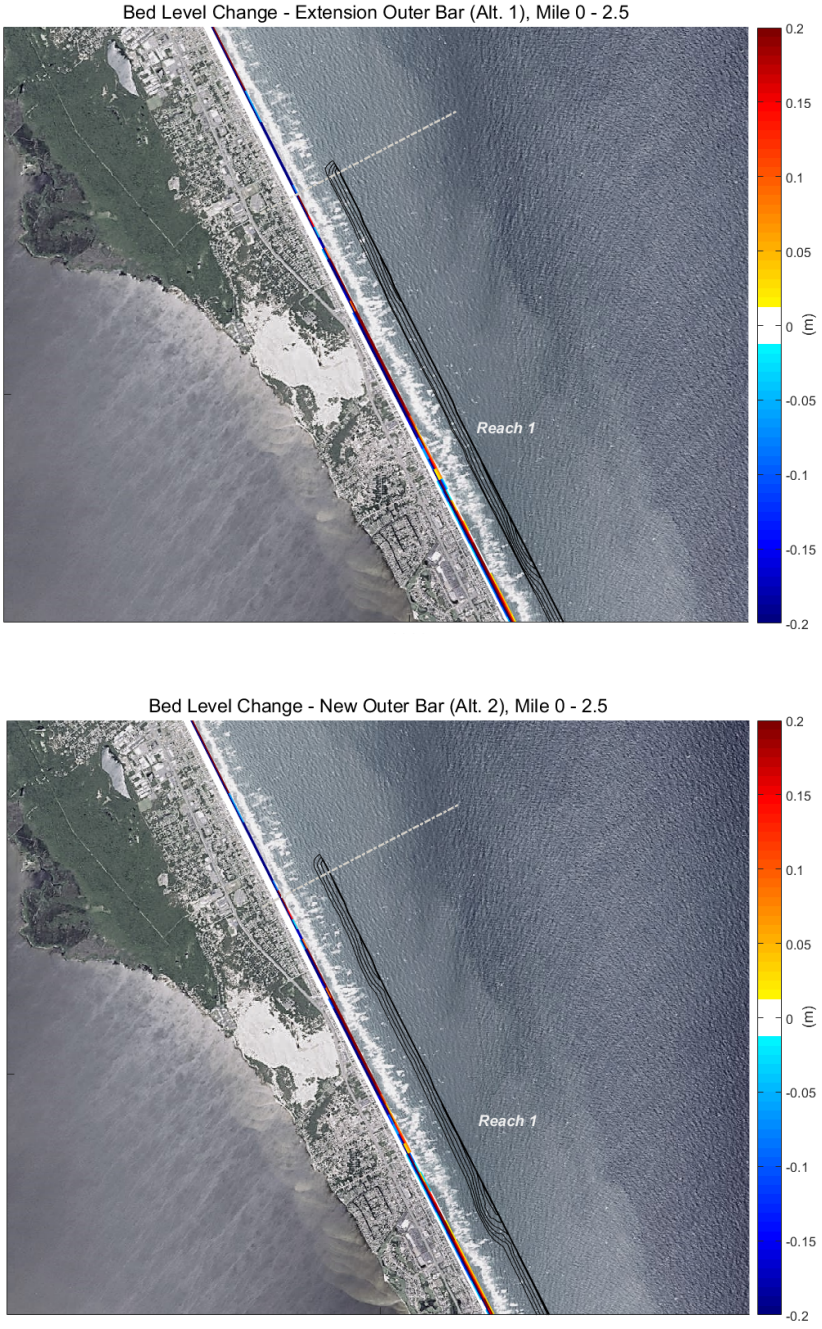

Figure D.1: Shoreface nourishment locations of alternatives 1 and 2 in mile 0 - 2.5 and its effect on the shoreline morphology

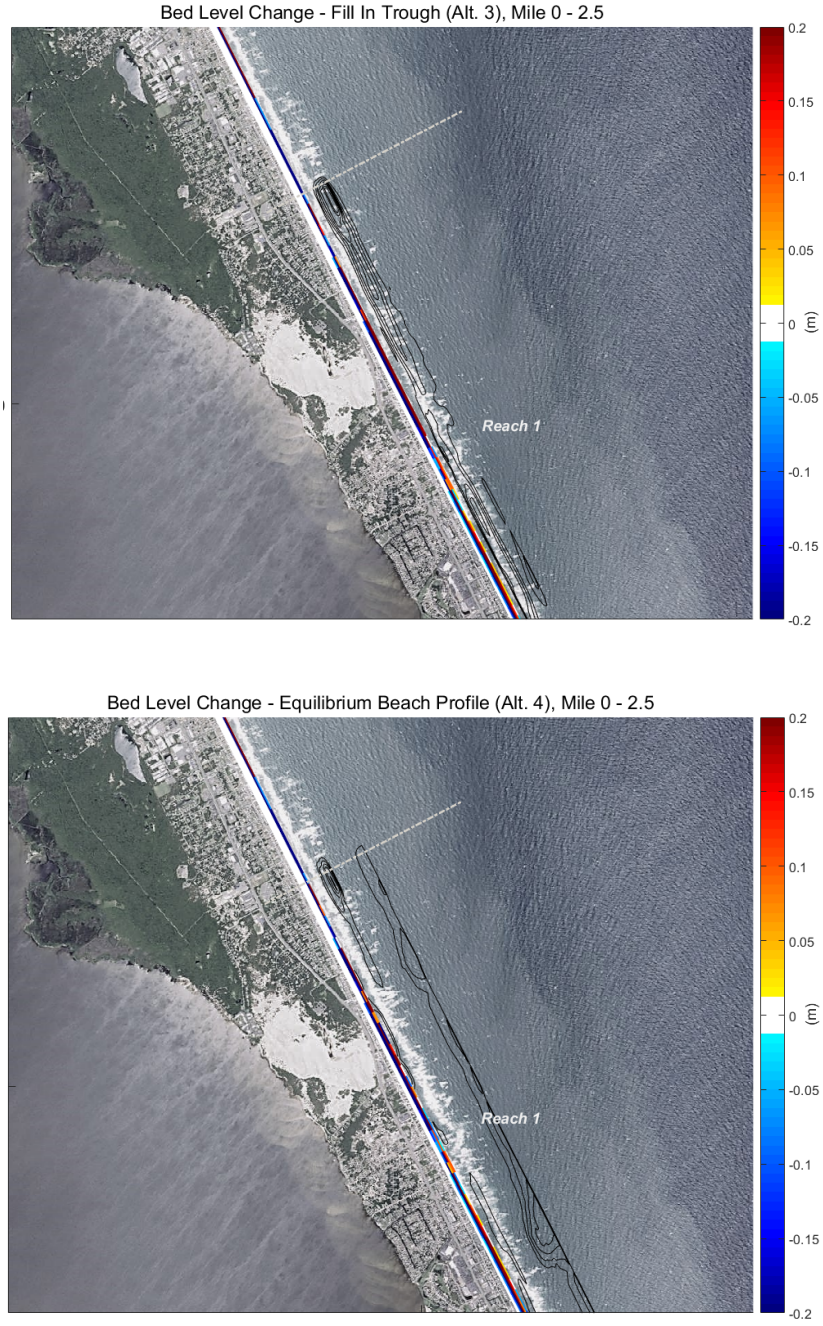

Figure D.2: Shoreface nourishment locations of alternatives 3 and 4 in mile 0 - 2.5 and its effect on the shoreline morphology

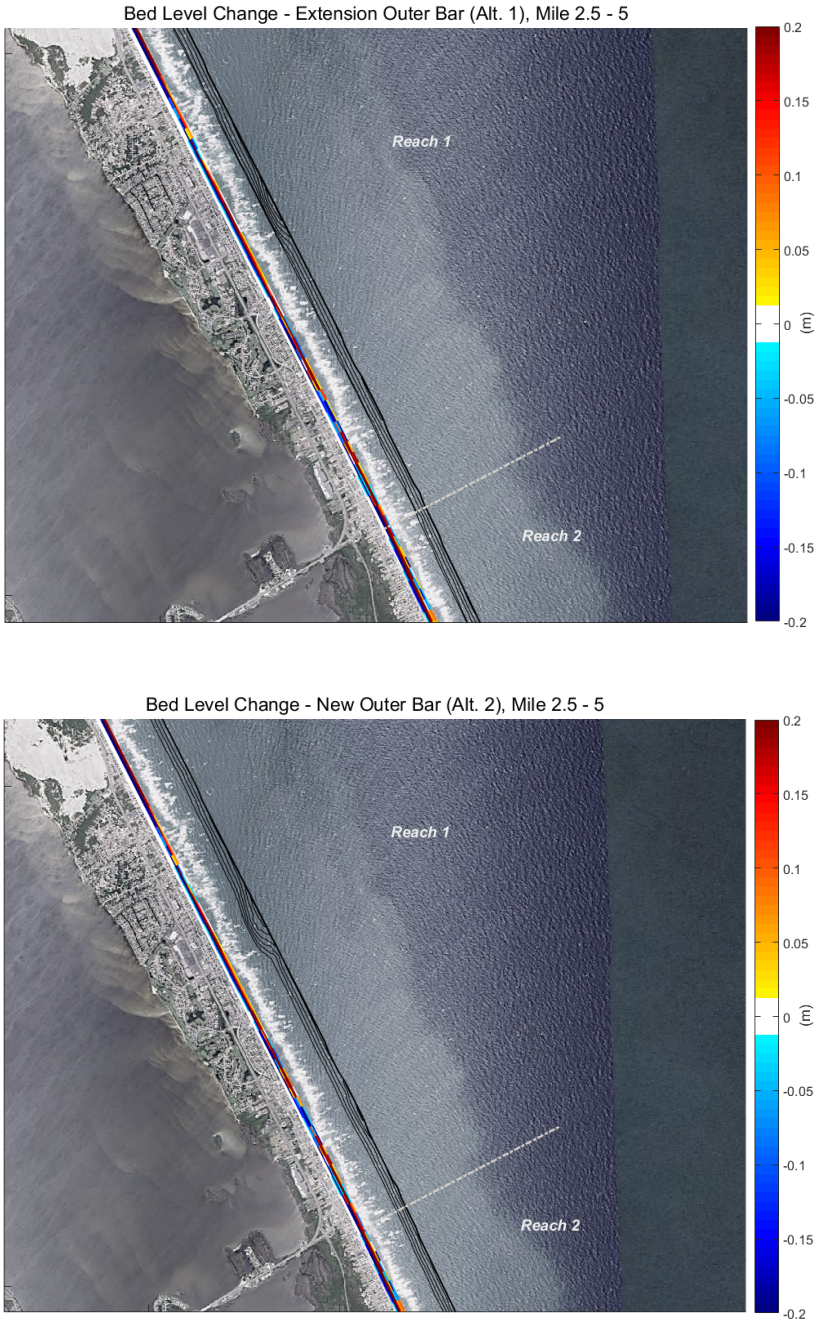

Figure D.3: Shoreface nourishment locations of alternatives 1 and 2 in mile 2.5 - 5 and its effect on the shoreline morphology

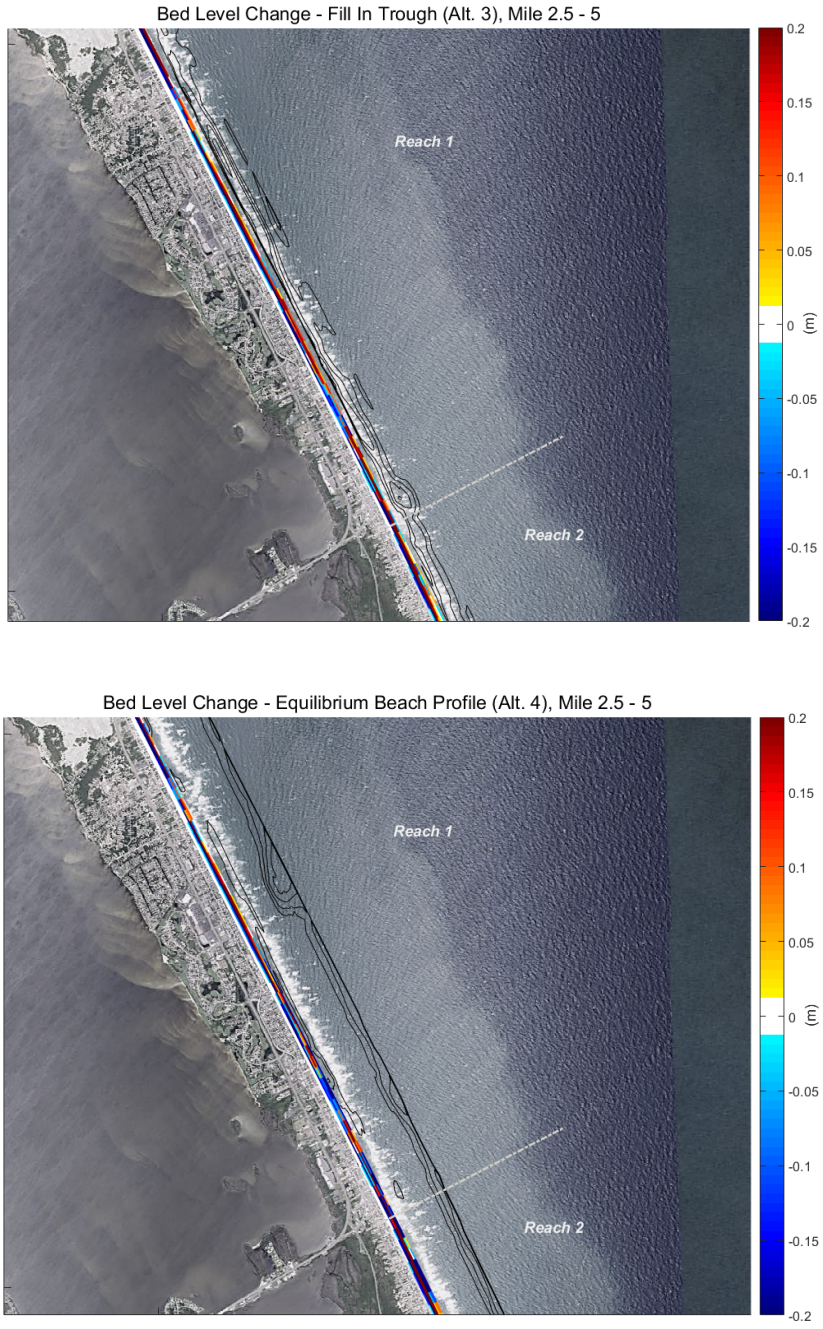

Figure D.4: Shoreface nourishment locations of alternatives 3 and 4 in mile 2.5 - 5 and its effect on the shoreline morphology

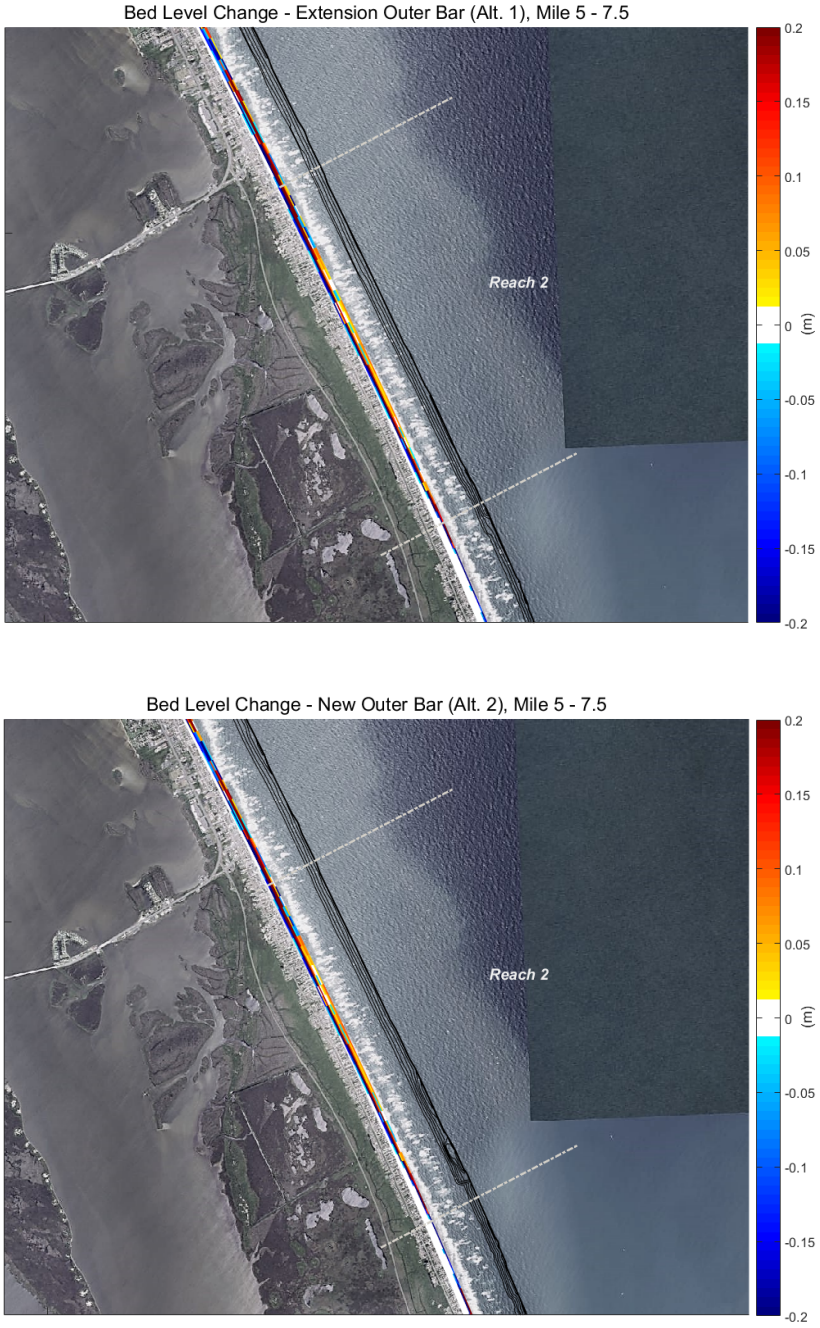

Figure D.5: Shoreface nourishment locations of alternatives 1 and 2 in mile 5 - 7.5 and its effect on the shoreline morphology

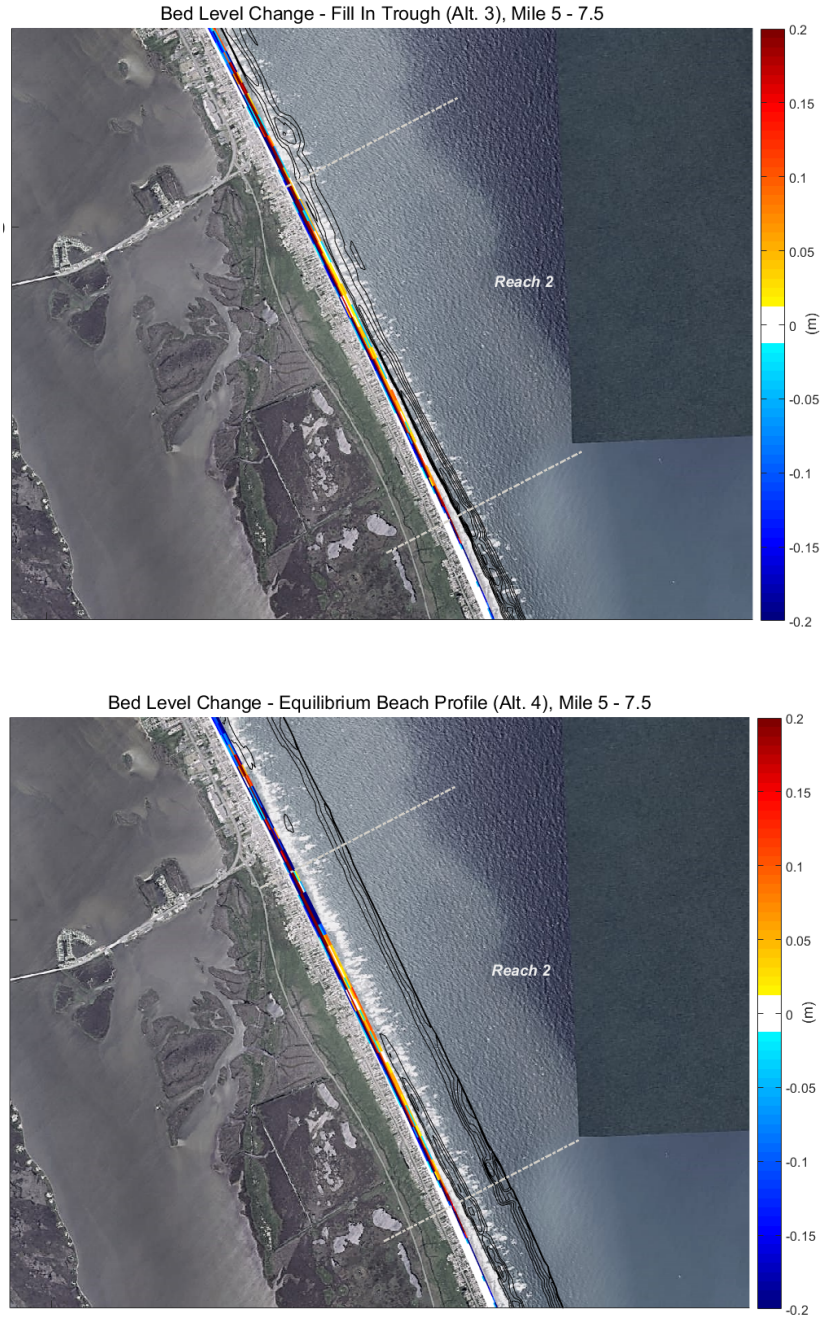

Figure D.6: Shoreface nourishment locations of alternatives 3 and 4 in mile 5 - 7.5 and its effect on the shoreline morphology

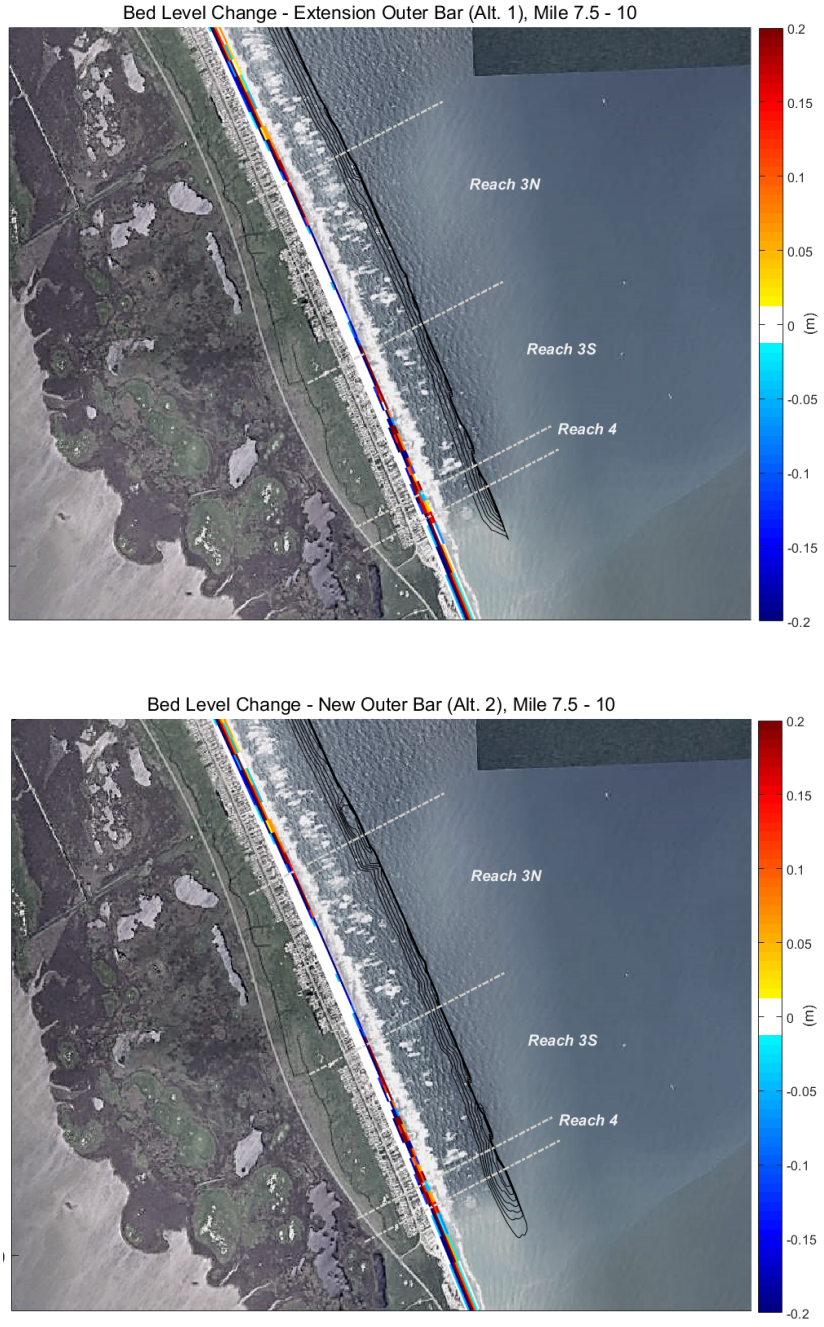

Figure D.7: Shoreface nourishment locations of alternatives 1 and 2 in mile 7.5 - 10 and its effect on the shoreline morphology

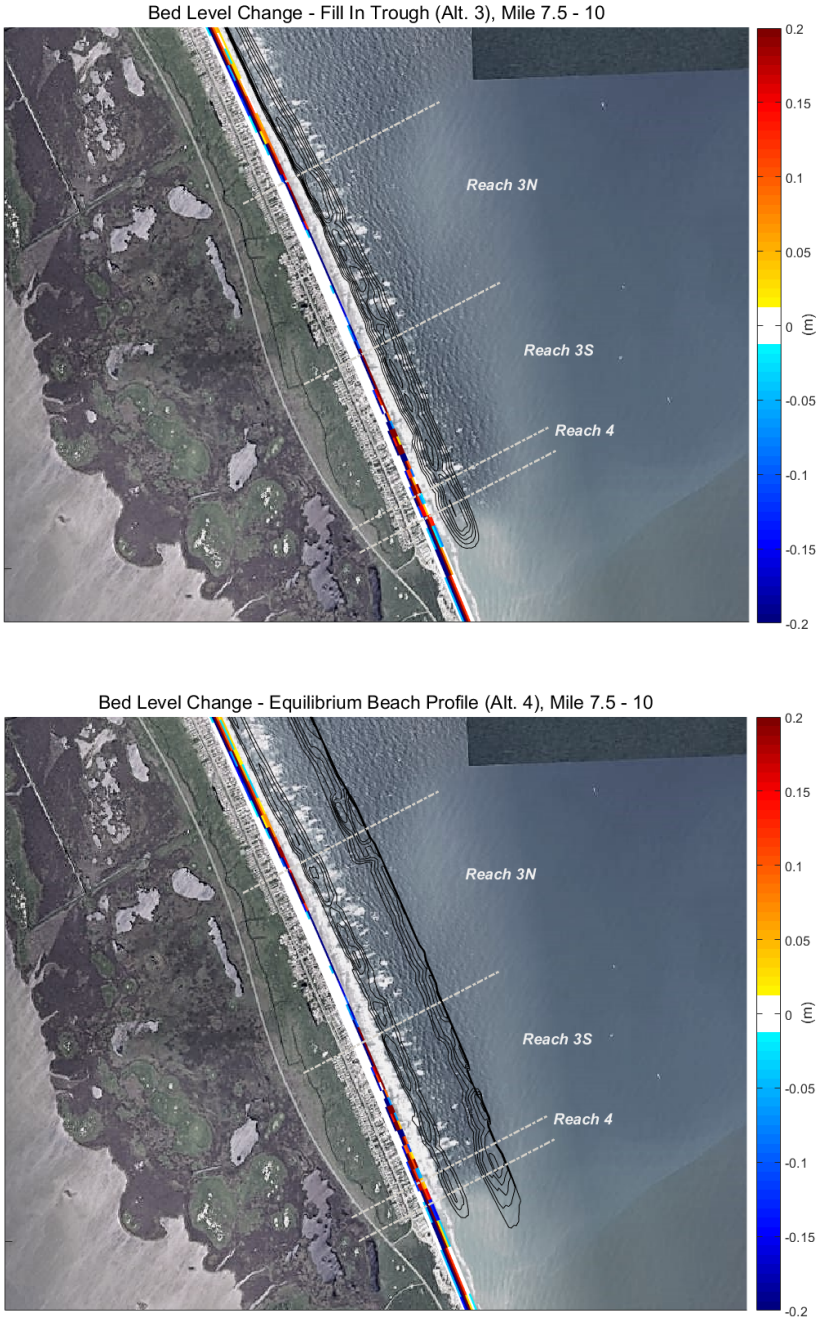

Figure D.8: Shoreface nourishment locations of alternatives 3 and 4 in mile 7.5 - 10 and its effect on the shoreline morphology